

University of Louisville

## ThinkIR: The University of Louisville's Institutional Repository

---

Electronic Theses and Dissertations

---

12-2014

### Development of a thin-film porous-microelectrode array (p-mea) for electrical stimulation of engineered cardiac tissue.

Hiren Vrajlal Trada 1977-  
*University of Louisville*

Follow this and additional works at: <https://ir.library.louisville.edu/etd>



Part of the [Cardiology Commons](#), and the [Therapeutics Commons](#)

---

#### Recommended Citation

Trada, Hiren Vrajlal 1977-, "Development of a thin-film porous-microelectrode array (p-mea) for electrical stimulation of engineered cardiac tissue." (2014). *Electronic Theses and Dissertations*. Paper 1736. <https://doi.org/10.18297/etd/1736>

This Doctoral Dissertation is brought to you for free and open access by ThinkIR: The University of Louisville's Institutional Repository. It has been accepted for inclusion in Electronic Theses and Dissertations by an authorized administrator of ThinkIR: The University of Louisville's Institutional Repository. This title appears here courtesy of the author, who has retained all other copyrights. For more information, please contact [thinkir@louisville.edu](mailto:thinkir@louisville.edu).

DEVELOPMENT OF A  
THIN-FILM POROUS-MICROELECTRODE ARRAY (P-MEA) FOR  
ELECTRICAL STIMULATION OF ENGINEERED CARDIAC TISSUE

By

Hiren Vrajlal Trada  
B.E., University of Mumbai, India, 1999  
M.S. University of Louisville, KY, USA, 2004

A Dissertation  
Submitted to the Faculty of the  
J. B. Speed School of Engineering of the University of Louisville  
in Partial Fulfillment of the Requirements  
for the Degree of

Doctor of Philosophy

Department of Electrical and Computer Engineering  
University of Louisville  
Louisville, Kentucky

December 2014



DEVELOPMENT OF A  
THIN-FILM POROUS-MICROELECTRODE ARRAY (P-MEA) FOR  
ELECTRICAL STIMULATION OF ENGINEERED CARDIAC TISSUE

By

Hiren Vrajlal Trada  
B.E., University of Mumbai, India, 1999  
M.S. University of Louisville, KY, USA, 2004

A Dissertation Approved on

December 1<sup>st</sup>, 2014

by the following Dissertation Committee:

---

Dissertation Director: Kevin M. Walsh, Ph.D.

---

Dissertation Co-Director: Bradley B. Keller, M.D.

---

John F. Naber, Ph.D.

---

Shamus McNamara, Ph.D.

## DEDICATION

This dissertation is dedicated to my family:

to my father Vrajlal, who emphasized the importance of education in life;

to my mother Remma, who instilled in me a love of books from a young age; and

to my wife Kunisha, for patiently waiting all these years while

I fumbled my way through this long journey.

## ACKNOWLEDGEMENTS

‘It takes a village to raise a child’ and in my case it was never truer. I would like to express my sincere gratitude to my advisor and dissertation chair, Dr. Kevin Walsh who has shown the patience of a saint while I worked my way through this program. He was one of my first teachers here at the University of Louisville when I started as a graduate student.

Dr. Bradley Keller who has become a valued mentor, is owed another debt of gratitude for the support he has shown me the last few years. It was a fortunate day for me when he came to Belknap Campus looking to collaborate with Dr. John Naber on a project. I sat in on that initial meeting and was inspired by his talk and ideas to create something that gradually turned into the focus of this dissertation.

Thank you to Dr. John Naber and Dr. Shamus McNamara for agreeing to be on my dissertation committee and providing guidance and mentoring when I needed it the most. Most of all I appreciate the time taken by them during their break and vacation time to work on my dissertation.

I would like to thank Michael Martin and Mark Crain for taking me under their wings and teaching me the ropes of microfabrication; Don Yeager for helping me with a smile whenever I needed him in the cleanroom and the machine shop.

Regarding this project work, it would never take off the ground if Joseph Tinney wasn't around to isolate cells and create ECTs for me; I gratefully acknowledge his expertise with the project and in the lab. I would like to thank Dr. Fangping Yuan for performing histological staining and analysis on the numerous samples we churned out and Dr. William Kowalski for writing an algorithm that made my work easier. Thanks to Doug Jackson, from whom I learned interfacing, harness making, component selection and numerous other things; his lab is a play area for adults who like to tinker around. Thanks also goes to Venkat Vendra for teaching me electrochemical analysis methods and to Dr. Mahendra Sunkara for the use of his facilities; Dr. Cindy Harnett for the use of the laser engraver for this project and Yehya Senousy & Evgeniya Moiseeva for teaching me how to use it.

Last but not the least, I would like to acknowledge the staff and the Department of Electrical and Computer Engineering at the University of Louisville; Lisa Bell, Susan Cunningham – thank you for helping me over the years.

I am grateful for the financial support provided by the Department Of Electrical and Computer Engineering over the years as a teaching assistant and later with a doctoral fellowship. Thanks to Dr. Walsh for supporting me as his TA & RA. Thanks to Dr. Keller and the Kosair Charities Pediatric Heart Research Program for their financial support. I'm grateful and humbled to have it. Dr. Walsh & Dr. Keller, both have supported me financially and in every way a graduate student requires. Hopefully, someday I can be in a position to repay these debts.

## ABSTRACT

### DEVELOPMENT OF A THIN-FILM POROUS-MICROELECTRODE ARRAY (P-MEA) FOR ELECTRICAL STIMULATION OF ENGINEERED CARDIAC TISSUE

Hiren Vrajlal Trada

December 1<sup>st</sup>, 2014

Electrical stimulation has been increasingly used by research groups to enhance and increase maturation of cells in an engineered cardiac tissue (ECT). Current methods are based on using off-the-shelf wires or electrodes to deliver a stimulus voltage to the in-vitro tissue in culture medium. A major issue with this approach is the generation of byproducts in the medium due to the voltage levels required, which are typically in the range of 5V-10V. No solution currently exists that can accomplish electrical stimulation of cells in an ECT at a low voltage level. Therefore, in this study a novel, porous, thin-film, microelectrode array (PMEA) device is proposed. The primary advantage of this device is the ability to successfully function at a very low voltage thus minimizing any undesirable oxidative byproducts in the culture environment or cell injury. This was achieved by designing and fabricating a thin device capable of being embedded in the ECT to deliver voltage. The P-MEA device is essentially a thin-film cable i.e. a conducting wire encapsulated with an insulating material; in this case thin-film gold electrodes sandwiched between two layers of insulating polyimide.

Major features of the P-MEA include overall dimensions of 10mm width and 82mm length, four arms to allow movement of the individual sensor pads within ECTs, each embedded electrode arm incorporates eight 100 $\mu$ m x 200 $\mu$ m rectangular pores surrounding a 950 $\mu$ m x 340 $\mu$ m exposed electrode, large pads on either side of the porous embedded sensor to function as return electrodes, suture holes to aid in-vivo suturing and stabilization and eight electrode connector pads.

Average thickness of the device was 16 $\mu$ m, with an average electrode film thickness of 0.4 $\mu$ m. Electrode resistance ranged from 69.45 $\Omega$  to 78.52 $\Omega$ . Electrochemical impedance spectroscopy was performed on the P-MEA electrodes and it confirmed that the P-MEA successfully operates in the 0.01V to 1.0V range with favorable charge transfer characteristics. Proof of principle experiments confirmed the ability of the P-MEA to effectively embed within the ECT and electrically stimulate it during chronic, in-vitro culture. Histology imaging shows that the embedding of the device has no adverse effects on the ECT and the cardiomyocytes are aligned within the tissue. Experiments are ongoing to evaluate the role of electrical stimulation on the maturation and function of ECTs which are made of stem cells and other sources.

In summary, this device is capable of safe low-voltage electrical stimulation of engineered cardiac tissues (ECTs); it has been designed, fabricated, and its ability to function as a low-voltage stimulus device has been validated using electrochemical tests and in-vitro culture experiments. The design and fabrication of the device went through three major iterations. A final manufacturing process was refined and successfully transferred to the UofL MNTC staff for subsequent manufacturing.

## TABLE OF CONTENTS

	PAGES
ACKNOWLEDGEMENTS.....	iii
ABSTRACT.....	v
LIST OF TABLES.....	ix
LIST OF FIGURES.....	x
I. INTRODUCTION	
1.1 Cardiac Injury, Remodeling and Repair.....	1
1.2 Objective Statement.....	7
1.3 Hypothesis.....	7
1.4 Specific Aims.....	8
1.5 Background.....	9
II. DESIGN	
2.1 Initial design.....	14
2.2 Version 2.....	18
2.3 Version 3.....	21
III. FABRICATION	
3.1 Materials.....	25
3.2 Process Flow.....	27
3.3 Fabrication Process.....	29
IV. ELECTRICAL AND ELECTROCHEMICAL TESTING	
4.1 Device integrity testing.....	45
4.2 Equivalent Electrode Model.....	47
4.3 Electrochemical Impedance Spectroscopy (EIS).....	49

V.	ENGINEERED CARDIAC TISSUE	
	5.1 Cell isolation and implant creation.....	58
	5.2 Electrical Stimulation.....	62
	5.3 Histological and Immunofluorescence Staining.....	68
	5.4 Contractile Force Measurement.....	74
VI.	CONCLUSION	
	6.1 Device success and shortcomings.....	76
	6.2 Current and Future work.....	82
	6.3 Pending Outcomes.....	84
	REFERENCES.....	85
	APPENDIX.....	93
	CURRICULUM VITAE.....	95

## LIST OF TABLES

Table	Page
3.1 Spin parameters for deposition of Polyimide PI-2611 on Si wafer. Two steps are used to spread the polyimide and evenly coat the surface.....	30
3.2 Spin parameters for coating photoresist S1827; total time was 18.7 seconds.....	35
4.1 Equivalent circuit parameters for an idealized P-MEA. R1 & C1 form the working electrode (small pads), R2 & C2 form the counter electrode (large pads) and Rs is the solution resistance.....	57
5.1 (a) Intrinsic beat rates for Control ECTs (all values in bpm).....	63
(b) Intrinsic beat rates for Sham ECTs (all values in bpm).....	64
(c) Intrinsic beat rates for Sensor-paced ECTs (all values in bpm).....	64
5.2 Maximum pacing rates for sensor-paced ECTs (all values in bpm).....	66
5.3 Minimum threshold voltages (in volts) for sensor-paced ECTs at 120bpm.....	67

## LIST OF FIGURES

Figure	Page
1.1 Chart detailing the cost in billions of dollars of the burden of heart disease; the estimated cost of all CVD is beyond \$1 trillion. (from <i>Heart Disease and Stroke Statistics - 2014 Update</i> ; Chapter 24, Pg. e283 [ref. 1]; HPB indicates High Blood Pressure; CHD, Coronary Heart Disease, and CHF, Congestive Heart Failure).....	2
1.2 Typical setup used by most research groups to achieve electrical stimulation. More often than not it involves two conducting rods (platinum or carbon) to carry the electrical signal from a stimulator.....	5
1.3 Electrical conduction system of the heart. [3].....	9
1.4 Typical setup used by most groups for electrical stimulation of ECT. Scaffolds seeded with cells are suspended between carbon or steel rods connected with platinum wires [24-27].....	12
2.1 6-well culture plate used for ECT creation. The well on the top-left has a mock wooden ECT between the end tabs. The well on the right has the paper mock-up....	15
2.2 P-MEA-S device, Version 1. A section of the porous feature is shown in the blow-up. The ‘rectangle’ denotes the placement of the ECT.....	17

2.3 P-MEA device, Version 2. . Thin-film metal conductor sandwiched between two layers of insulating polymer material.....	18
2.4 P-MEA, Version 2 shown with separated layers. (a) Top insulating polymer layer. (b) Metal electrode layer running the entire length of the device.....	19
2.5 The porous mesh section of the device. This mesh section is embedded in the tissue; the exposed areas of the electrodes are noted by the brighter shade of red color.....	22
2.6 (a) Representative design of a P-MEA device. The red section represents the gold electrodes while the blue represents the polyimide layer. The feature in green is representative of an embedded ECT.....	22
(b) Blown-up view of the main device area. The small pads were embedded inside the ECT, while the big pads are in the culture medium.....	22
(c) Close-up view of one of the embedded pads. The porous feature is highlighted by the 8 rectangular openings on either side of the small pad. The area in shaded red indicates the electrode portion covered by the polyimide.....	22
(d) Contact area with the connection pads.....	22
2.7 Supporting board and connecting circuit board for making connections to the P-MEA device. (a) laser-cut acrylic board, (b) circuit board with spring-probe connectors and custom wiring harness, (c) circuit board to run parallel connections to multiple devices at the same time.....	24
3.1 (a) PMEA device. Green arrow lines show the approximate location of the cross-sectioning. The device design used for the example is Version 3.....	27
(b) Left column shows the cross-sectional view of the (cut shown by the green arrow lines in 3.1.a).....	28

(c) Right column shows the flowchart for the processing steps.....	28
3.2 (a) PI2611 bottle stored in refrigerator.....	30
(b) Spin-coating PI-2611 on a silicon wafer.....	30
3.3 PI cure vacuum oven from Yield Engineering Systems. Wafers (up to 6” in diameter) are loaded vertically and nitrogen gas flows in a perpendicular direction (to the chamber), across the surface of the wafer. (Image source: company website).....	31
3.4 Temperature profile of a seven hour thermal curing process for the polyimide PI-2611 in a YES vacuum oven with heating and cooling ramp rates of 100°C/hour.....	32
3.5 Mask aligner model MA/BA6 from SÜSS MicroTec AG. The mask is upside down and the wafer is in contact or close proximity to the surface. The alignment is performed using the optics and computer system. (Image source: company website).....	33
3.6 Photoresist lift-off process flow. The toluene soak hardens the top of the resist, leaving overhanging edges at the sidewalls of the resist.....	34
3.7 PVD 75 sputter deposition system from KJL. The double doors hide the main process chamber on the left while the controlling computer and power supplies are on the right. The process chamber usually contains four 3” targets but can be customized to unique needs (MNTC PVD75 has two 3” and one 4” targets). (Image source: company website).....	36
3.8 A 4” silicon wafer with a sputter-coated layer of Ni/Au on a polyimide layer. Note the faint lines visible under the surface; they are the electrodes etched in photoresist....	37
3.9 Acetone solvent soak for the lift-off process. Photoresist dissolves readily in acetone and the patterned photoresist was removed along with the metal on top of it. Note the	

gold particles floating in the acetone in the left beaker. The right beaker shows a lift-off process in progress with the Ni/Au layer partially removed.....	38
3.10 Wafer with completed gold electrodes after a lift-off process and DI water rinse cleaning. (version 2 of the P-MEA shown in fabrication).....	39
3.11 Second layer of polyimide – soft bake on hotplate prior to vacuum curing.....	39
3.12 Aluminum coating on top of the cured polyimide layer. The aluminum film was used as a mask for the polyimide etch.....	40
3.13 P-MEA device pattern in photoresist S1827 layer; the resist is seen in the yellow colored pattern over the shiny aluminum coating. The PI layer is visible around the periphery of the wafer under the aluminum layer.....	41
3.14 The wafer with the etched aluminum layer. This aluminum layer now has the pattern from Mask 2.....	42
3.15 The silicon wafer containing the P-MEA devices (version 2) after the completed etch process. Note the residue on the exposed gold pads; the shinier traces of the metal are sandwiched between the two polyimide layers.....	43
3.16 Version 3 of the P-MEA devices on a 4” silicon wafer. The devices were squeezed together to increase the number of devices to six (from five in version 2).....	44
4.1 Cascade probe station for testing device electrode integrity and resistance.....	45
4.2 Probe testing the electrodes. Probe on the left is on the embedded pad and was positioned underneath the lens, while the probe on the right is on the connecting pad.....	46
4.3 (a) An ECT embedded with a P-MEA device. The four big pads were tied together (externally) and the four small embedded pads were tied together.....	48

(b) Equivalent circuit model for the P-MEA device in culture medium (DMEM). R1 & C1 represent the interface between the embedded pads & DMEM; R2 & C2 represent the interface at the large pads & DME, and RS represents the solution resistance.....	48
4.4 Representative Nyquist plot for a single time constant interface. Nyquist plots don't contain any frequency information, they only represent impedances.....	51
4.5 Model 273A, Potentiostat/Galvanostat (Princeton Applied Research, Oak Ridge, TN); used for the EIS experiments and measurements.....	52
4.6 'EIS Spectrum Analyser' is a free software available from Belarusian State University for EIS analysis.....	52
4.7 Experimental setup for EIS and other electrochemical tests. The P-MEA is being tested for electrochemical performance in culture medium.....	53
4.8 (a) Nyquist plots for individual EIS tests on P-MEA-S in DMEM media at 0.01, 0.1, 1, and 2 volts. Note the downward shift in the EIS plot at 2 volts consistent with irreversible reactions.....	54
(b) Expanded scale of the individual EIS plot at 2 volts.....	54
4.9 Individual EIS phase plots for P-MEA-S in DMEM media at 0.01, 0.1, 1, and 2 volts. Note the downward shift in the phase plot at 2 volts consistent with the loss of capacitive performance.....	56
5.1 (a) Embryos being removed from fertile day-7 incubated chick eggs.....	59
(b) Heart excised from day-7 embryos.....	59
5.2 (a-d) (clockwise from top left): (a) Positioning the P-MEA device (ver. 2) in a tissue culture plate. (b) Culture plate on the tissue train base plate. (c) Depositing the chick	

cardiac cell derived ECT gel construct. (d) The chick ECTs after polymerization, note the vacuum-created trough in the empty wells. (e) (Ver. 3) P-MEA embedded ECT filled with culture medium and an ECT without an embedded P-MEA.....	61
5.3 The pacing protocol and the electrical stimulus applied across the ECT. Biphasic pulse of 1ms (negative and positive each) with a 2 $\mu$ s pulse gap. Initial stimulation frequency was 2Hz and was varied depending on the experiment.....	63
5.4 Chart comparing intrinsic beat rates for all three groups. P-MEA embedded ECTs have higher beat rates than control ECTs.....	65
5.5 Chart showing maximum pacing rates of chronically stimulated ECTs. Max rates peak at Day 7 and decline thereafter.....	66
5.6 Minimum threshold voltage for ECT capture at 120bpm; well below 0.5V.....	67
5.7 (a-c) ECT myofiber cellular distribution for Control ECT at day 10. Cardiac Troponin-T (TnT-Green). Nuclei (DAPI-blue). Proliferating cells (EdU – red). (all images at 40x magnification, scale bar represents 50 $\mu$ m).....	71
(d-f) ECT myofiber cellular distribution for Sham ECT at day 10. Cardiac Troponin-T (TnT-Green). Nuclei (DAPI-blue). Proliferating cells (EdU – red). (all images at 40x magnification, scale bar represents 50 $\mu$ m).....	72
(g-i) ECT myofiber cellular distribution for Sensor-paced ECT at day 10. Cardiac Troponin-T (TnT-Green). Nuclei (DAPI-blue). Proliferating cells (EdU – red). (all images at 40x magnification, scale bar represents 50 $\mu$ m).....	73
5.8 A sensor embedded ECT under force measurement. The remnants of the P-MEA can be seen in the still-embedded pads in the ECT. The left hook is attached to a force transducer and the right anchor is movable to stretch the ECT.....	74

5.9 ECT force recordings. Passive and active total force generated by the ECT paced at 2 and 4 Hz (all force values in mN). (Sham ECT referred as Sensor Non-Paced).....	75
6.1 Evolution of the P-MEA design over three major iterations (not to scale); (a) Version 1, (b) Version 2, (c) Version 3.....	77
6.2 Electrode deterioration in Ver. 2 of P-MEA; undesirable byproducts released into the medium leading to cell death and tissue necrosis (encircled dark/shadowed region).	78
6.3 (a) Splayed effect caused by embedment of the P-MEA (b) Thinning of ECT resulted in the ECT being separated from the pad (c) ECT encapsulated around one arm of the P-MEA.....	81
6.4 A P-MEA device implanted onto the surface of an adult rat heart. This particular device was sutured on the infarcted myocardium and placed for a duration of three weeks.....	83

# CHAPTER 1

## INTRODUCTION

### 1.1 Cardiac Injury, Remodeling, and Repair

Cardiovascular Disease (CVD) is the leading cause of mortality in the United States (and indeed worldwide). The American Heart Association (AHA), working in conjunction with other government health agencies, releases an annual report titled '*Heart Disease and Stroke Statistics*', detailing the statistics relating to heart disease in the United States [1]. In their '*2014 Update*' the AHA reveals that Cardiovascular Diseases account for more than 30% of all deaths in the United States.

While this number is large, the rate has been steadily declining over the last decade. However, even with the declining rate, the burden of CVD remains very high with total annual costs in excess of \$650 billion. Projected estimates have this number crossing an unsustainable \$1 trillion in the next 20 years (see chart shown in Figure 1.1). The AHA lays out target goals to reduce this burden by emphasizing healthy lifestyles and habits. Heart disease can be prevented to a certain extent by a healthy lifestyle, but not completely eliminated.

One fundamental cause for the large financial and health burdens of heart disease is the inability of the heart to replace damaged heart cells following injury. The heart tissue is made up of multiple cells types including cardiomyocytes (CM), fibroblasts, and endothelial cells within a complex extra-cellular matrix [2, 3]. The human heart consists

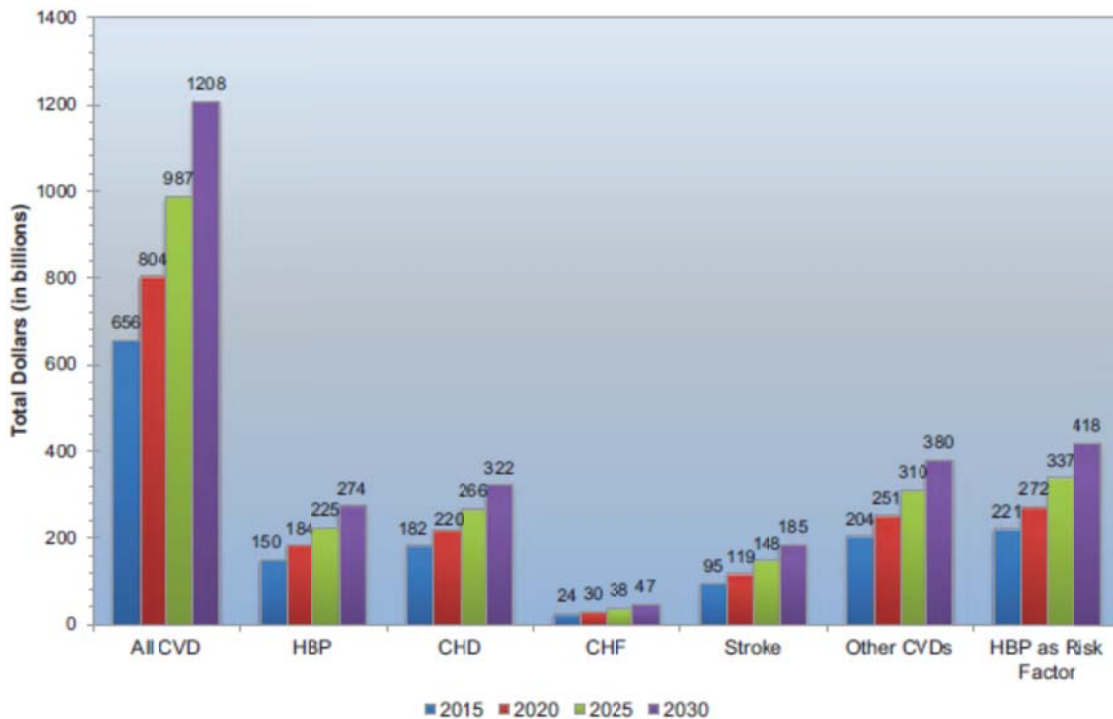


Figure 1.1: Chart detailing the cost in billions of dollars of the burden of heart disease; the estimated cost of all CVD is beyond \$1 trillion. (from *Heart Disease and Stroke Statistics - 2014 Update*; Chapter 24, Pg. e283 [ref. 1]; HBP indicates High Blood Pressure; CHD, Coronary Heart Disease, and CHF, Congestive Heart Failure).

of billions of contractile CM which beat in unison. The heart can suffer damage due to a wide range of causes, a chief example being Myocardial Infarction (MI), which occurs due to a sudden decrease in blood flow and oxygen delivery to the myocardium, resulting in irreversible cell death and variable degrees of cardiac dysfunction. Tissue damage due to cell death is an irreversible process since mature CM cannot proliferate after birth. The myocardial adaptive response to injury is to remodel tissues using fibroblasts and scar formation to maintain structural integrity despite CM loss. However, this scar tissue

has negative impacts on cardiac muscle performance by increasing tissue stiffness, altering contractile properties, and introducing barriers to efficient tissue electrical depolarization and mechanical shortening.

It seems logical that the damage caused due to a loss of CM could be reversed by an influx of new cells. For this to occur, the cardiac tissue needs to be supplied with new functional, healthy CM to repair the damaged area. This can be accomplished in two ways; stimulation of in situ CM proliferation or implantation of new CM via various methods. To date, no effective methods to trigger the proliferation of in situ mature CM has been validated, as thus, this approach is not a current pre-clinical or clinical option. However, there have been various approaches to implant a wide range of cells and cell formulations into preclinical models of cardiac injury and into patients with cardiac injury. One strategy to stimulate cardiac repair is the direct injection of cells into damaged regions of the heart with the goal of regenerating healthy myocardium. However, this method of direct injection is not reliable since the implanted cells uniformly die within 30 days [4]. There are various theories as to the etiology of cell death for these implanted cells including a hostile microenvironment (hypoxia, inflammation), abnormal cell-cell interactions, and abnormal cell-matrix interactions.

An alternate approach is the generation of 3-dimensional engineered cardiac tissues (ECTs) that can be implanted onto the heart in order to restore cardiac tissue and function. The focus of this thesis is the development of a strategy and device for the electrical stimulation of engineered cardiac tissues, and so the majority of the following text focuses on that application of cellular repair of the damaged heart.

The field of Tissue Engineering, more specifically, Cardiac Tissue Engineering, uses scaffolds to create tissue made of cardiac cells. Engineered Cardiac Tissue (ECT) made from such cells can be used as in-vitro models for research studies on myocardial function, pharmacology, and diseases. The overarching goal of Cardiac Tissue Engineering is to develop cardiac tissues in-vitro with the same morphological and functional properties as native in vivo myocardium. The engineered tissues can be implanted onto a diseased or an infarcted heart wall, which can no longer perform its cardiac functions, with the purpose of repairing the area and to introduce some sort of functionality back to the damaged area.

To be feasible for implantation, an in-vitro engineered cardiac tissue needs to have similar properties to its native in vivo target tissue. During embryo development the growing heart consists of cells that differentiate and proliferate into cardiac tissues. These cardiomyocytes are subject to mechanical loading and electrical stimulus to drive their development; as the cells mature, the heart forms. Soon after birth, the cells lose the ability to proliferate and we are born with all the cardiac cells that we will ever have in a lifetime.

Cardiac tissue can be engineered from a variety of cell sources; however mature cells do not have the ability to proliferate and are therefore less desirable to form and remodel ECTs. Immature cells from embryonic sources have the ability to differentiate and proliferate if they are subjected to the mechanical and electrical conditions found in native tissue. A 2-dimensional structure cannot mimic a native biological environment; hence the need arises to create a bio-mimetic 3-dimensional structure to simulate native tissue. Despite 3D geometries, the maturation of in-vitro ECTs can be delayed relative to

native in vivo immature myocardium, leading to the use of various conditioning protocols to accelerate ECT maturation [5]. In-vitro cyclic mechanical loading has been shown to accelerate ECT CM proliferation and functional maturation similar to the biologic effects of mechanical load in vivo [6]. Electrical stimulation has also been used to accelerate the maturation of proliferating stem cell derived CM within ECTs using adjacent electrodes to connect with the engineered tissue [7-9]. These electrode arrays can be used to quantify cardiac tissue maturation via the voltage thresholds required to simulate CM contraction and record depolarization and conduction.

Most research groups accomplish in-vitro stimulation of excitable tissue, such as ECTs, using readily available, off-the-shelf components to achieve in-vitro electrical field stimulation. These are primarily wires made from platinum, stainless steel electrodes or carbon rods as shown in the layout in figure 1.2 [7, 9-12].

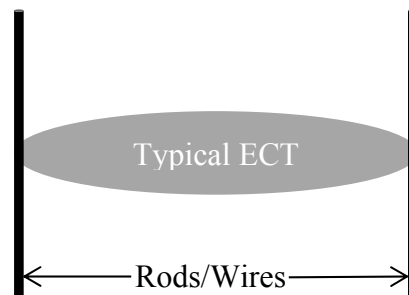


Figure 1.2: Typical setup used by most research groups to achieve electrical stimulation. More often than not it involves two conducting rods (platinum or carbon) to carry the electrical signal from a stimulator.

A simple rod electrode may not be ideally suited to the task due to the high voltage required to initiate tissue depolarization and pacing (usually 5V to 10V). However, these voltages far exceed the water electrolysis threshold voltage of 1.23V [13] and can produce gas bubbles in the culture medium which may impede nutrient stability, delivery, and cause cell injury. Another confounding variable is the high-glucose content of standard ECT culture media. Electrical voltages in the range of 4V to 5V (and above) cause redox reactions in the media, reducing and oxidizing glucose to form sorbitol and gluconate respectively [14, 15]. The negative consequences of released gases, compounds and substrate oxidation can also lead to undesirable shifts in culture media pH. A solution which has been designed solely for the purpose of investigating cardiac tissue does not exist.

In this dissertation, a novel device is presented that was designed and fabricated to accomplish the tasks of stable, in-vitro, acute and chronic ECT electrical stimulation at much lower threshold voltages via direct contact and coupling to cells embedded within ECT. This was achieved by designing and fabricating a thin-film, porous, multiple electrode array (P-MEA) that could be embedded within the ECT at the time of ECT formation.

## 1.2 Objective Statement

The objective of this study is to develop a thin-film microelectrode array that can be embedded into an engineered cardiac tissue for the purpose of electrical stimulation.

## 1.3 Hypothesis

*A microfabricated thin-film device embedded into an engineered cardiac tissue can achieve efficient electrical stimulation of cells at a much lower voltage compared to existing methods.*

Corollary 1:

*Embedding a thin-film device will not cause adverse effects or reactions in the tissue.*

Corollary 2:

*Electrical stimulation of ECT with the aid of this device can be achieved at 1V or less (compared to 5V or more for existing methods).*

Corollary 3:

*Electrical stimulation of ECT (using said device) can aid in the functional maturation of the ECT.*

## 1.4 Specific Aims

### *Specific Aim 1:*

To design and develop a P-MEA device via an iterative design process for use in ECT experiments. This includes designing and fabricating a custom macro-micro interface for electrical coupling to pacing and/or recording systems.

### *Specific Aim 2:*

To develop the fabrication process flow, and in subsequent iterations, to refine the process to obtain high yield suitable for repetitive manufacturing.

### *Specific Aim 3:*

To perform electrochemical characterization of the device to determine safe operating limits. This includes data analysis and computer simulation of the device using an equivalent electrochemical model.

### *Specific Aim 4:*

To accomplish in-vitro electrical stimulation of Engineered Cardiac Tissue (ECT), including comparison of three groups of ECTs: [1] Control (non-embedded ECTs), [2] Sham ECTs (embedded but non-stimulated), and [3] Device ECTs (embedded and stimulated).

- (a) Acute Pacing - data generation and collection of threshold voltages, intrinsic beat rates and maximum pacing rates.
- (b) Chronic Pacing – effects of electrical stimulation on threshold voltages, beat rates, and on tissue morphology, proliferation, and maturation.

### *Specific Aim 5:*

Validate the findings through peer-reviewed publications.

## 1.5 Background

The heart is the first major organ of the human body to develop and form in a growing embryo. It is the engine which drives the circulatory system of the body to distribute blood and nutrients to the tissues and organs. The heart is made up of cardiac cells known as cardiomyocytes (CM) which typically contract (in unison) about 3 billion times in an average human lifespan [3, 4]. This mechanical ability of the cardiomyocytes to contract in unison allows the heart to function as a mechanical pump to generate pressure and deliver blood. The mechanical contraction is caused by the change in electrical potential of the cell membranes due to the flow of ions across the membrane. Electrically speaking, 99% of the CMs are used for mechanical contraction and 1% of the cells behave as the pacemaker of the heart to initiate an action potential. These ‘pacemaker’ cells can be found in (1) the sinoatrial (SA) node, (2) the atrioventricular (AV) node (3) the bundle of His (atrioventricular bundle), and (4) Purkinje fibers (Figure 1.3). The SA node is the place where the action potentials are initiated and thus is the primary pacemaker of the heart. The ventricular and atrial cells perform the mechanical pumping based on the electrical signals from the SA node.

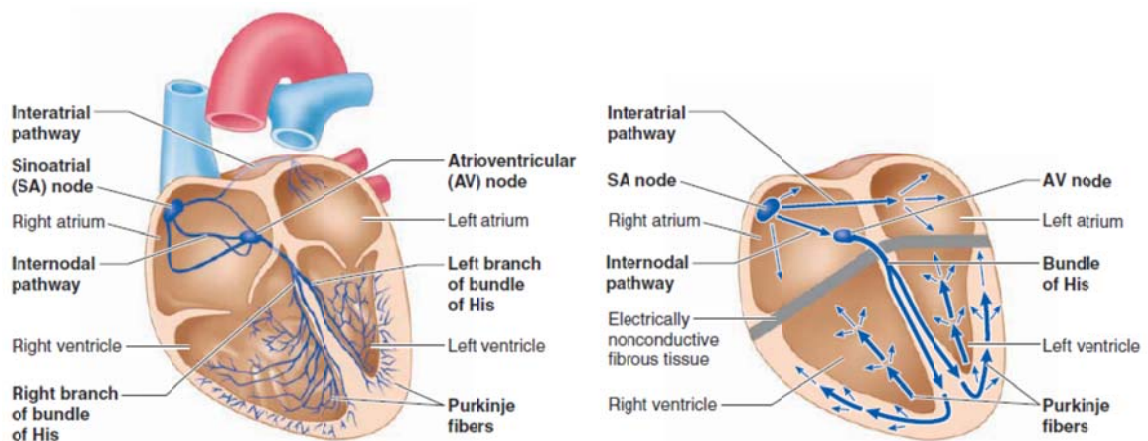


Figure 1.3: Electrical conduction system of the heart. [3].

Blood flows through the heart without stopping; the atrium receives it and pushes it to the ventricles which send it out of the heart. If the blood flow decreases or stops for any reason, the heart suffers a myocardial infarction (MI). Cells start dying in the affected area and a healing response is initiated. However, adult cardiac cells cannot divide and proliferate to replace the ones that are lost. Scar tissue forms over the affected area which results in diminished capacity of the heart.

Strategies for repair of a diseased heart have had two approaches; (a) direct injection of cells into the diseased site, (b) grafting a cardiac patch on to the affected area [5, 32]. The issue with direct injection of cells into the damaged tissue is that nearly 90% of the cells die out within 2-4 weeks of application [5]. The second approach is the focus of cardiac tissue engineering. Interest in tissue engineering by numerous research groups in the past decade or so has generated a wealth of knowledge about the field [6, 7, 12, 13, 15, 21, 37, 39, 41-48].

To repair the damage caused due to a MI, a cardiac patch has been suggested, which can be grafted on to the scar tissue to render back a degree of functionality. A cardiac patch is essentially a scaffold made of collagen or similar natural polymer with cardiac cells seeded on to the scaffold. The cells for such patches can be obtained from a variety of sources such as; embryonic or neonatal cardiomyocytes, embryonic stem cells (ESC) and induced pluripotent stem cells (IPS) among others. A novel method was presented by Hirose et. al. where they used human aortic endothelial cells (HAECs) to create a sheet of a monolayer of cells, called cell sheets [16]. These cell sheets are seeded on temperature sensitive tissue culture dish surfaces which change to hydrophilic when their temperature is lowered to 32°C from the normal culture temperature of 37°C. This

causes the sheets to detach from the culture dish without the use of digestive enzymes. Shimizu et al were successful in creating multiple layers of electrically coupled cell sheets and grafting on rat hearts [17-20].

The goal of cardiac tissue engineering is to generate functional 3D tissues that can be implanted in-vivo to facilitate cardiac repair and regeneration. An engineered tissue comprises cellular and extracellular components, undergoes remodeling and maturation during in vitro culture, and requires both structural and functional integration for successful in vivo implantation and survival [37]. In general, successful integration of engineered tissues requires that the implanted biomaterials have both biologic and biomechanical compatibility with the target tissues and microenvironment [38]. These general principles are relevant to the generation of 3D engineered cardiac tissues (ECTs) and various approaches have been used to generate in vitro functional cardiac tissues from a variety of stem, embryonic, fetal, and neonatal cell types [39-44], various biomaterial formulations [45-48], with successful in vivo implantation [49-51].

Cardiac cells in their natural biological environment are subjected to dynamically changing mechanical and electrical forces during development and in response to injury [52]. Standard 2D cell cultures do not mimic this dynamic environment, hence 3D environments are required for immature cardiomyocytes (CM) to proliferate, differentiate, and form functional tissues. These 3D formulations are designed to provide realistic mechanical loading conditions with adequate nutrient support to facilitate tissue maturation.

Despite 3D geometries, the maturation of in vitro ECTs can be delayed relative to native in vivo immature myocardium, leading to the use of various

conditioning protocols to accelerate ECT maturation [10]. Cyclic mechanical loading has been shown to accelerate ECT CM proliferation and functional maturation [54]. Electrical stimulation has also been used to accelerate the maturation of proliferating stem cell derived CM within ECTs using adjacent electrodes to connect with the engineered tissue [11, 28, 29, 55].

Most research groups, focusing on in-vitro stimulation of ECT, use off-the-shelf components to achieve in-vitro field electrical stimulation such as carbon rods and platinum wires. The voltages associated with such a setup is usually in the range of 5V and above. Radisic et al used two 1/4-inch-diameter carbon rods placed 1 cm apart and connected to a stimulator with platinum wires [10, 22]. Tandon and Cannizzaro used a similar setup for their experiments with scaffolds suspended between carbon rods (Figure 1.4) [24-27].

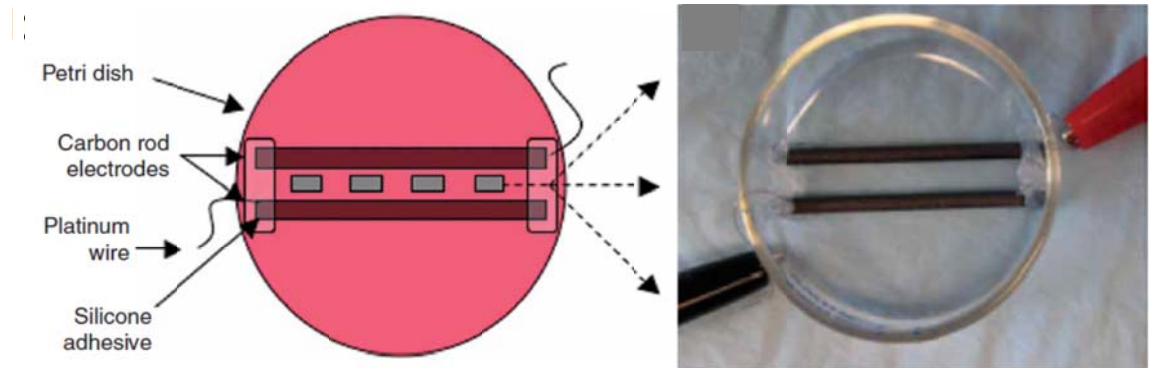


Figure 1.4: Typical setup used by most groups for electrical stimulation of ECT. Scaffolds seeded with cells are suspended between carbon or steel rods connected with platinum wires [24-27].

The issue with using an off-the-shelf rod or electrode is the high value of voltages required to stimulate the tissues with reported values ranging from 5V-10V [10, 22, 24, 27]. These voltages far exceed the water electrolysis threshold voltage of 1.23V and can

produce gas bubbles in the culture medium which may impede nutrient stability and delivery [30]. Another variable is the high-glucose content of standard ECT culture media. Electrical voltages in the range of 5V cause redox reactions in the media, reducing and oxidizing glucose to form sorbitol and gluconate respectively [31-34]. The negative consequences of released gases, compounds and substrate oxidation can also lead to undesirable shifts in culture media pH. Moreover, electrical stimulation at high voltages can cause direct damage to the tissue by local heating and/or over-stimulation [35]. To eliminate these problems the stimulation voltage should be kept as low as possible, ideally less than the water electrolysis voltage level of 1.23V.

The thin-film porous microelectrode array presented in this dissertation, aims to eliminate the problems associated with current methods by embedding an electrode inside the ECT. The device would be encapsulated by the tissue and make direct contact with the cells during electrical stimulation. This would allow the use of low voltage levels to accomplish safe in-vitro pacing of ECT. To the best of knowledge, with an investigation of past and present published work, such a device does not exist for electrical stimulation of engineered cardiac tissue. A successful P-MEA device would be a unique contribution to the field of cardiac tissue engineering.

## CHAPTER II

### DESIGN

#### 2.1 Initial Design

The ECT utilized in this research are small, 3-dimensional, cylindrical, gelatinous structures primarily comprised of collagen, matrigel and cardiac cells; approximately 15mm in length and 2mm in diameter [40]. The ECT was grown inside a commercially available 6 culture well plate (Tissue Train Plate, FlexCell, International) that includes two anchor end tabs in each well. The microelectrode array had to interface with the ECT and provide an external electrical connection. To determine the optimal device dimensions for embedding the device in the 3D ECT, paper mock-ups were used inside the culture well (Figure 2.1). This allowed the determination of device features that were essential to the primary function as well as additional convenience features.

The following key design areas were identified using the mock setup: the embedded portion, the dimensions of the device, and the contacts for external connections. The embedded portion was the most critical area of the device since the cells in the tissue interact with exposed pads in the device. This required a metal electrode region with maximum contact surface area possible within the tissue area as well as a relatively strong physical connection. Since the tissue comprises of cardiac cells it has native beating which results in physical movement of the ECT.

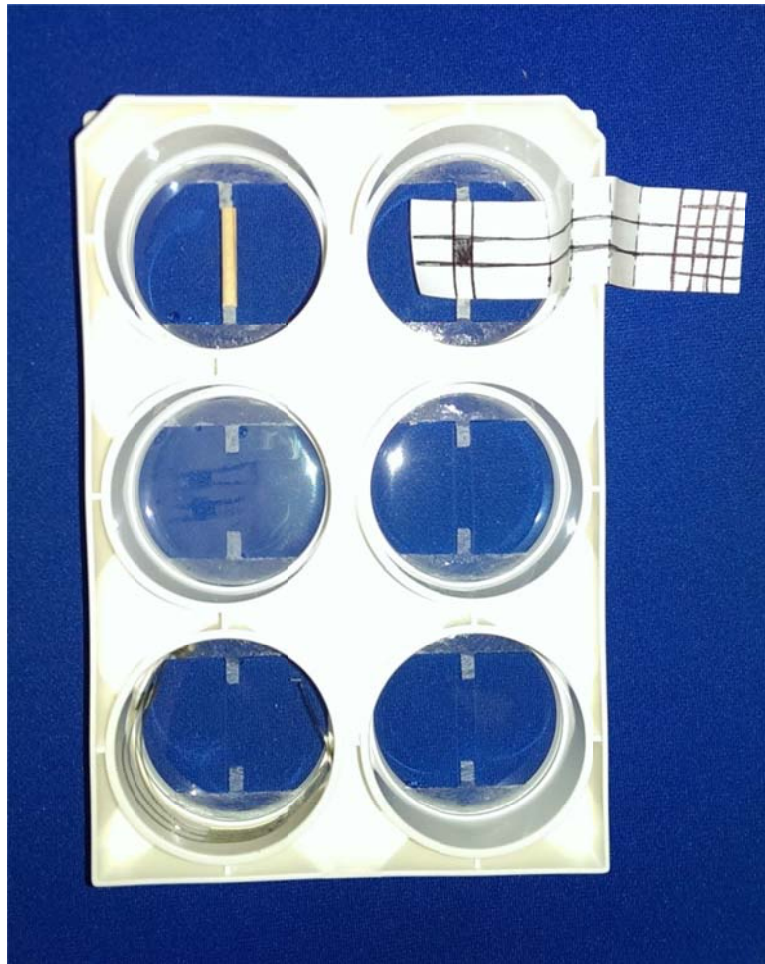


Figure 2.1: 6-well culture plate used for ECT creation. The well on the top-left has a mock wooden ECT between the end tabs. The well on the top right has the paper mock-up device. The base of each well is covered by a deformable silicone membrane.

To aid mechanical retention of the device inside the ECT and to prevent the device from becoming dislodged during in-vitro culture and in-vivo implant, it was decided to incorporate a ‘porous’ feature in the device. Furthermore, to help minimize any adverse effect the embedded device may have on the material properties of the ECT, the embedded portion of the device was split into four separate arms distributed along the width of the device. The decreased surface area created with the porous design enhances/optimizes cell viability and also allows for free natural movement by the ECT

during in-vitro culture. A exposed metal electrode in each embedded arm makes contact with the cells. The porosity of the structure increases retention of the device in the tissue. The device has to feed over the top edge of the covered culture plate to an external connector, requiring a relatively long conductive connector element. Using the initial mock-up, approximate dimensions for the device were determined.

- (a) Composite length between 50mm and 90mm.
- (b) Width of 20mm.
- (c) Total of 4 arms with porous features in each “arm” for embedment.
- (d) Porous features should allow 2-4 exposed electrodes in each arm.

A design based on these criteria was created and is featured in Figure 2.2. Total dimensions of the device are 50mm x 20mm, the four arms are ‘10mm x 2mm’ separated by a distance of 4mm each. Each individual arm consists of a porous grid of 5 x 25 openings and each opening is 200 $\mu$ m x 200 $\mu$ m in size. Spacing between each porous opening is also 200 $\mu$ m in each direction. The green rectangle represents an ECT and is used to depict the approximate positioning of the ECT within the device.

The design was fabricated using standard microfabrication techniques and several prototypes were created using a single layer of polymer material. The purpose of the design was to study the physical effects of embedding the device into the ECTs and material bioeffects on the engineered tissues. To achieve this goal, it was not necessary to include electrodes in the prototype. Hence, version 1 of the P-MEA device does not feature any metal electrodes or connection pads. The initial idea was to include space for four electrodes in each arm for a total of sixteen electrodes in each device.

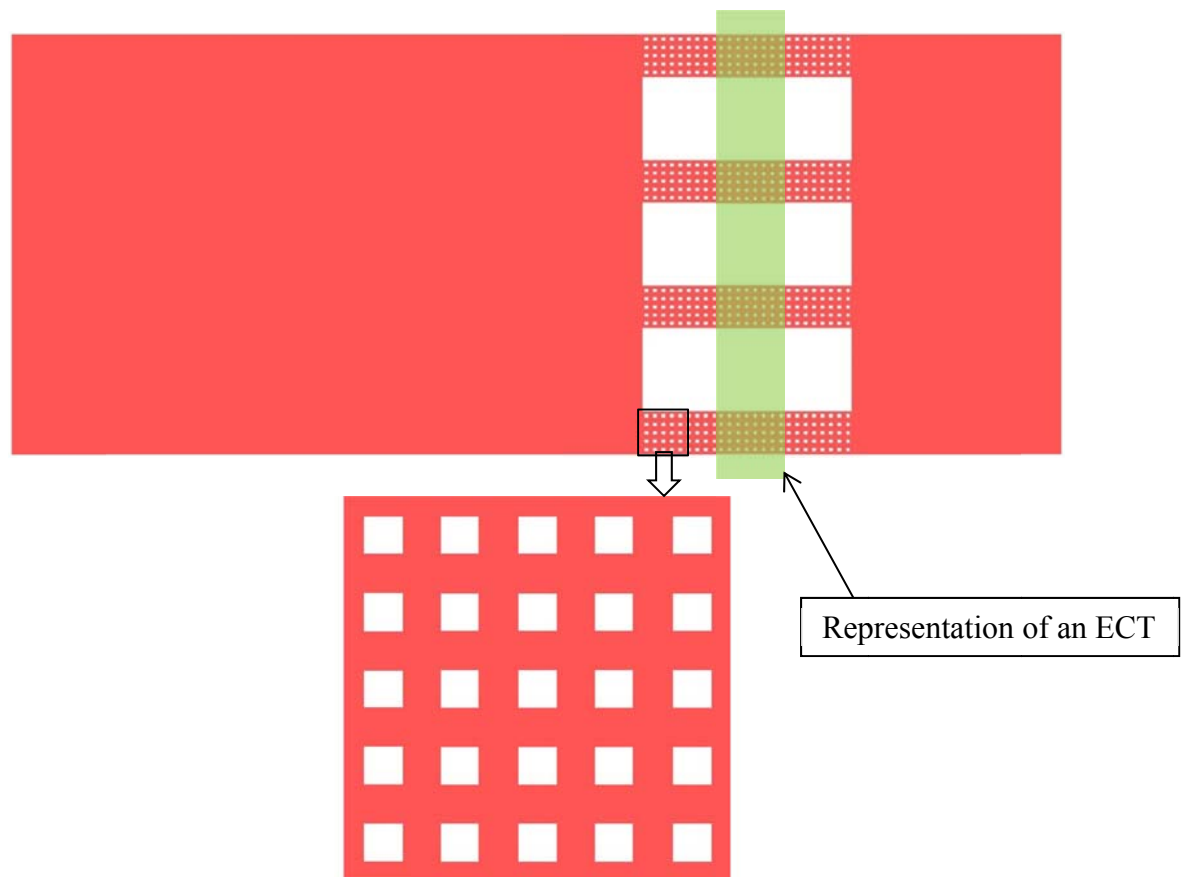


Figure 2.2: P-MEA device, version 1. A section of the porous feature is shown in the blow-up. The ‘rectangle’ denotes the placement of the ECT.

The devices were fabricated and used in pilot experiments to judge the physical effects of the device on ECTs. The primary drawback of this initial prototype version was the width of the device; at a width of 20mm this version of the device proved to be highly disruptive of the tissue structure. Moreover, the number of porous openings in the mesh structure spread out the tissue during ECT creation and resulted in a very thin, spread out and shapeless 3-dimensional structures. The results of the pilot trials were used to determine the changes necessary for the next version of the device.

## 2.2 Version 2

From the pilot trials it was evident that the device had to be narrower than initially imagined. version 2 of the device was created by reducing the width of the device by 50% to 10mm. The number of electrodes in each arm was also decreased by 50% to two, for a total of eight electrodes. Version 2 of the design is shown in Figure 2.3. This device features three layers: a conductor of thin-film metal sandwiched between two layers of insulating polymer material.



Figure 2.3: P-MEA device, version 2. Thin-film metal conductor sandwiched between two layers of insulating polymer material.

Figure 2.3 shows the device design for each layer. The blue layer represents the insulating polymer while the conducting material is represented in red. The top polymer layer is windowed to allow electrode contact with the cardiac tissue and for electrical connections.

The device is longer and narrower than version 1 of the P-MEA with dimensions of '82mm x 10mm'. There are four arms with porous features and two electrodes in each arm for a total of eight electrodes in each P-MEA device. The porous mesh structure comprises of 12 pores, each 100 $\mu$ m x 200 $\mu$ m in size (Figure 2.5). The metal electrodes (in red) are 70 $\mu$ m x 700 $\mu$ m and run the entire length of the device ending in large

connection pads. Each connection pad is 1mm x 4mm in size and they are designed to be used in conjunction with a spring probe connecting harness.



(a)



(b)

Figure 2.4: P-MEA, version 2 shown with separated layers. (a) Top insulating polymer layer. (b) Metal electrode layer running the entire length of the device. The label “Top” was included as only the top surface had exposed electrodes at the location of ECT embedding.

In addition, the design incorporated some convenience features for handling and placement. The metal electrode layer is used to layout characters to easily identify the exposed top surface. The polymer layer which provides structure and boundaries to the device has curved indented features (Figure 2.5) to prevent sharp corners and any resulting tearing and to aid the centering of the exposed electrodes within the ECT. The lower end of the device has an elongated section with an opening left in its tab to handle and secure the device during and after tissue embedding. The separation between the four arms of the device (above and below the mesh structure) allows movement of the individual device arms within the ECT. Figure 2.5 shows the (expanded) section of the porous mesh structure of device.

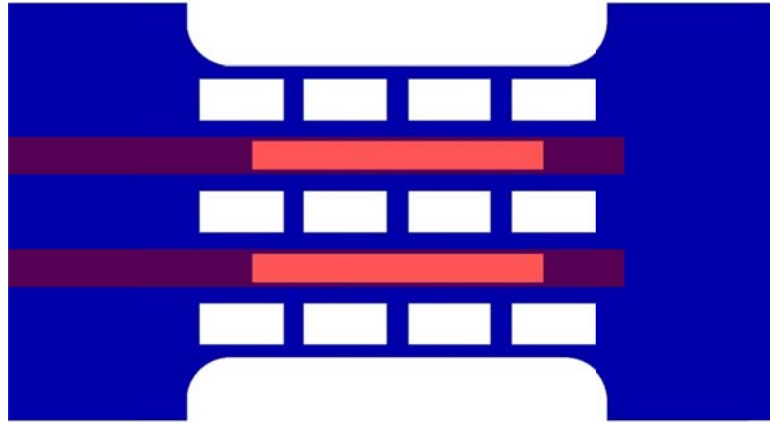


Figure 2.5: The porous mesh section of the device. This mesh section is embedded in the tissue; the exposed areas of the electrodes are noted by the brighter shade of red color.

The device was fabricated by a two-mask process and utilized polyimide as the insulator and gold as the metal electrode. The devices were embedded in the ECT while it is in gel form and the tissue forms when the gel polymerizes. The electrical stimulation of the tissue was accomplished by connecting an electrical stimulator to any two of the electrodes. Various experiments were conducted using version 2 of the device for acute and chronic electrical stimulation of ECT. During these experiments it was observed that the electrode material was corroding and deteriorating. The metal was reacting with the culture medium and releasing products into the culture tray resulting in cell death and consequently tissue damage. This was attributed to the higher amounts of voltage required to elicit a response from the ECT. The surface area of the pads was not sufficient to achieve electrical stimulation. Hence, a further change in the design of the device was required. The design was refined based on conducted experiments and observations. Several functional and convenience features were added to create version 3.

### 2.3 Version 3

Version 3 is the current and final version of the P-MEA device. Figure 2.6 presents the design layout of the P-MEA device with close-up views of key sections.

Unique design features of version 3 include:

- Width of 10 mm and length of 82 mm to allow electrical connections (2.6a).
- Four arms to allow movement of ECT between the individual device pads (2.6a).
- Total of four embedded electrodes in each device (2.6b).
- Four large pads on either side of the ECT which act as return electrodes during in-vitro testing (2.6b).
- Suture holes in each of the large pads to aid in-vivo suturing and contact (2.6b).
- The top polymer layer was windowed in specific locations (unshaded red areas) to allow electrode contact with the cardiac tissue and for external electrical connections (Fig 2.6a).
- Electrode dimensions are (0.09mm x 80mm); electrodes run the entire length of the device (2.6b).
- Each of the eight contact pads (2d) connect with one of eight small or large electrode pads (2.6b).
- Porosity: Each embedded electrode incorporates eight 100 $\mu$ m x 200 $\mu$ m rectangular openings surrounding an electrode pad which is 950 $\mu$ m x 340 $\mu$ m (2.6c).
- Curved indented markers for easy positioning of the exposed electrodes in the ECT (2.6c).

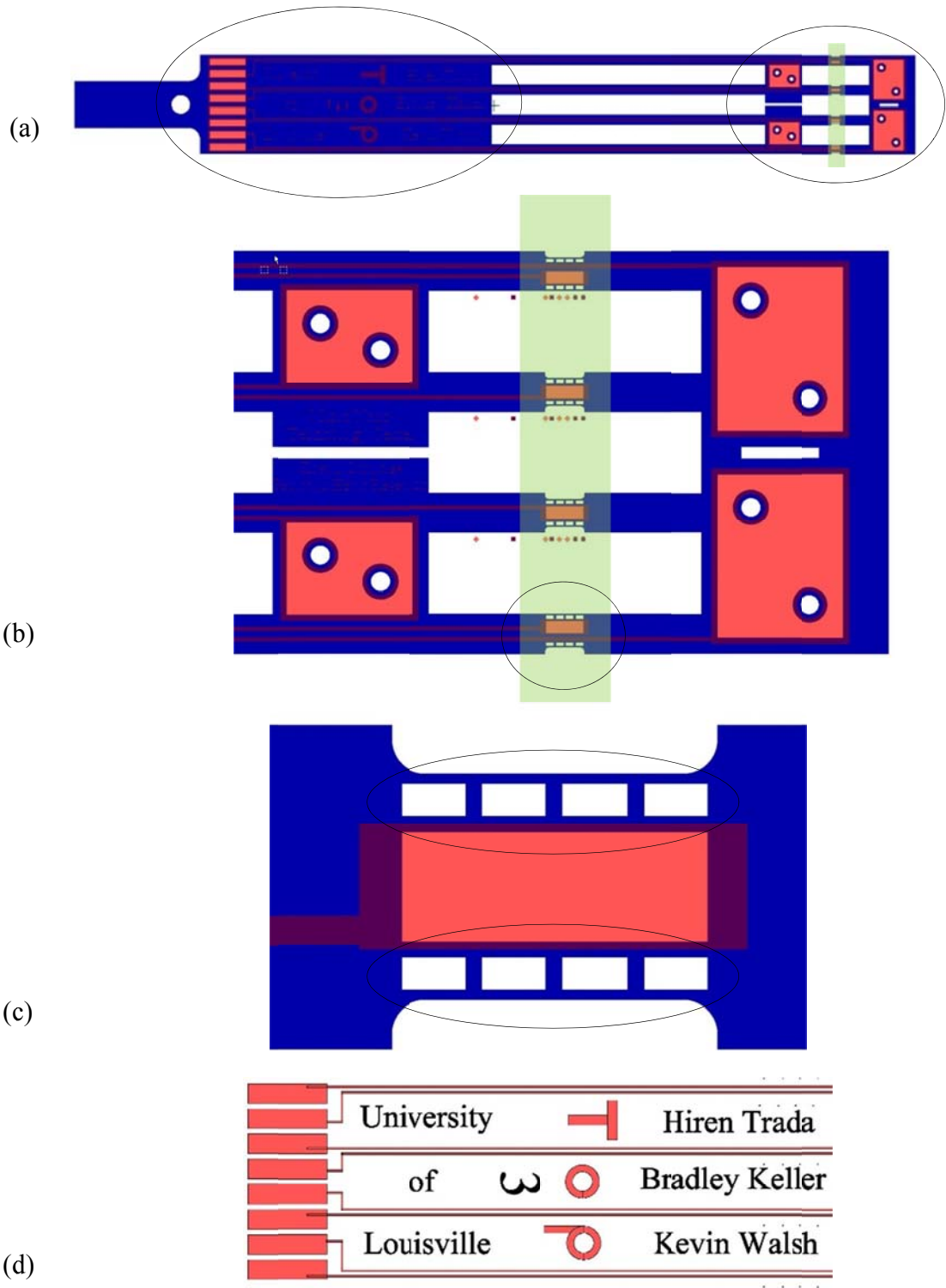


Figure 2.6 (a) Representative design of a P-MEA device. The red section represents the gold electrodes while the blue represents the polyimide layer. The feature in green is

representative of an embedded ECT. (b) Blown-up view of the main device area. The small pads were embedded inside the ECT, while the big pads are in the culture medium. (c) Close-up view of one of the embedded pads. The porous feature is highlighted by the 8 rectangular openings on either side of the small pad. The area in shaded red indicates the electrode portion covered by the polyimide. (d) Contact area with the connection pads.

For making external connections spring-probe connectors were used which were mounted on a custom board. The device was designed for use with a specific linear arrangement of spring probes and the contact areas were designed so alignment and interfacing are convenient. The circuit board was designed in CIRCAD and prototypes were created. After several pilot trials and modifications, the circuit board was outsourced for manufacturing 40 boards. The supporting board was made from 6mm thick acrylic sheets of 12"x12" dimensions. The design was created in L-EDIT and was used as an outline in a laser beam cutter and polisher. Figure 2.7 shows one setup of the supporting board along with two circuit boards. Each of the circuit boards has a spring-probe connector at the front end to make contact with the connecting pads on the P-MEA device. The other end has a custom wiring harness which takes the connections to larger board for multiple parallel connections.

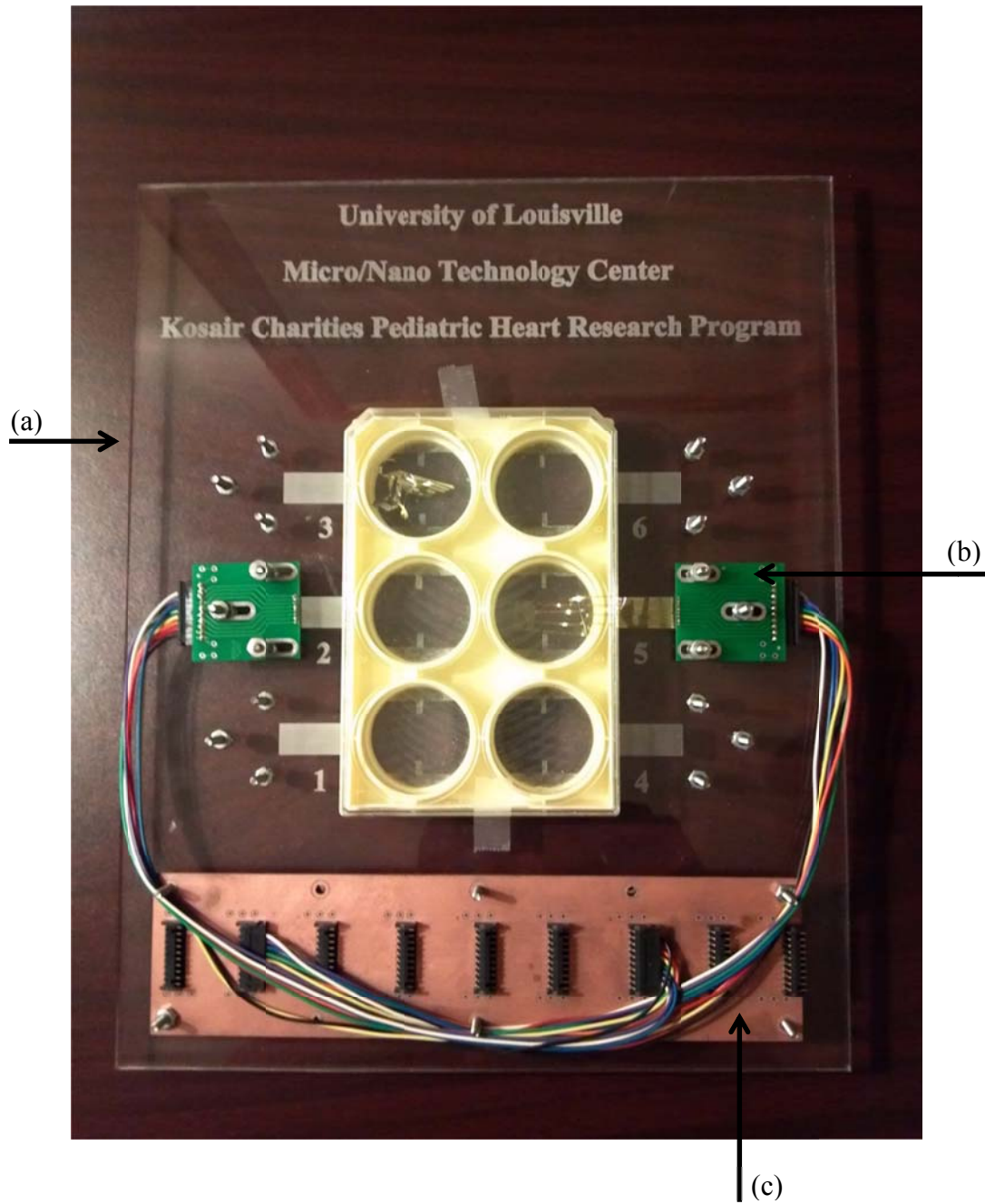


Figure 2.7: Supporting board and connecting circuit board for making connections to the P-MEA device. (a) laser-cut acrylic board, (b) circuit board with spring-probe connectors and custom wiring harness, (c) circuit board to run parallel connections to multiple devices at the same time.

## CHAPTER III

### FABRICATION

#### 3.1 Materials

The primary considerations in the choice of materials for the P-MEA devices were (1) bio-compatibility and (2) mechanical flexibility. Since the device is embedded inside tissue with living cells, the choice of materials had to be limited to biocompatible materials. Biocompatibility requires that all materials are both non-toxic and non-reactive. The usage scenarios include in-vitro and in-vivo applications where the device is required to be highly flexible while being strong enough to withstand bending and folding, but not break or damage the electrical conductor. Other considerations required the device design and material to be able to deliver sufficient voltage to elicit a response from the ECT at a safe level. This should be accomplished without causing any Faradaic reactions which could create and release unwanted compounds leading to material corrosion and deterioration which would further lead to tissue toxicity and cell death. [60]. In his review article, Merrill has compiled and listed an excellent table with materials that have been used by various researchers over the years [60, Table 1, Pg. 185]. The table primarily lists materials by their classification of biocompatibility and toxicity.

Among the insulators, polyimide is a polymer material which has both flexibility and bio-compatibility. Polyimide is available from HD MicroSystems in liquid form suitable

to be deposited and cured to achieve a desired thickness. The polyimide chosen for the P-MEA, PI-2611, is specifically designed for microelectronic applications and has excellent thin-film properties such as low stress, low coefficient of thermal expansion (3 ppm/°C), high tensile strength (350 MPa), and good ductility. The insulating material has to undergo metal deposition twice during the fabrication process and PI-2611 can withstand it without any evident damage to the film. Cured film thickness ranges from 3µm-9µm. The target thickness for the device, which includes a dual layer of the insulating polymer, was 15µm-18µm. This required the final cured thickness of one single layer to be approximately 8µm.

The most common and popular choices for thin-film metal electrodes are gold and platinum, both noble metals. They are highly desirable for their electrical properties as well as ductility and malleability. Platinum has been used extensively and is highly popular as a stimulating material, more so than gold. The choice between platinum and gold was simple logistics and economics; gold was less expensive and readily available (at MNTC, Louisville) for the fabrication of P-MEA prototypes. Gold does not corrode like other metals but it requires an adhesion layer because it does not adhere well to surfaces [79]. Chrome, nickel or titanium can be used as adhesion layers for thin-film gold depositions. In a theoretical study of metal-polyimide interfaces, Marta Ramos compared and contrasted bonding strength and adhesion energies of chrome and nickel to polyimide [68]. Although the calculations seem to suggest chrome as having higher adhesion energy than nickel, P-MEA experiments showed nickel as a better adhesion layer for gold on polyimide.

### 3.2 Process Flow

Because the minimum feature size of the P-MEA is in the micron scale MEMS-based microfabrication techniques were utilized in the class 100 cleanroom of the MNTC at the University of Louisville (Louisville, KY) to manufacture these devices. The device fabrication involved a two-mask fabrication process, one to pattern the electrodes and then one to pattern the polymer layer and open up contact windows for the electrodes. A 4” silicon wafer was used as a support structure to build the devices.

The process flow can be summarized in three major steps: (1) depositing and curing the first layer of polymer, (2) depositing and patterning the metal electrodes and (3) depositing, curing and patterning the second (top) layer of polymer. The first layer of the insulating polymer material is not patterned; the device is designed such that both layers of the polymer are patterned simultaneously in the last step. The second layer of polymer is designed to cover the metal layer which acts as a natural stop during the polymer etch. The etch continues in other areas to result in the delineation of the device. Thus the device fabrication requires only two photomasks. Figure 3.1 (b) shows the cross-sectional view of the device fabrication process (the cross-section is taken at the approximate location shown by the green arrow lines in Figure 3.1 (a)). Figure 3.1 (c) shows the step-by-step flow-chart.



Figure 3.1 (a): P-MEA device. Green arrow lines show the approximate location of the cross-sectioning. The device design used for the example is version 3.

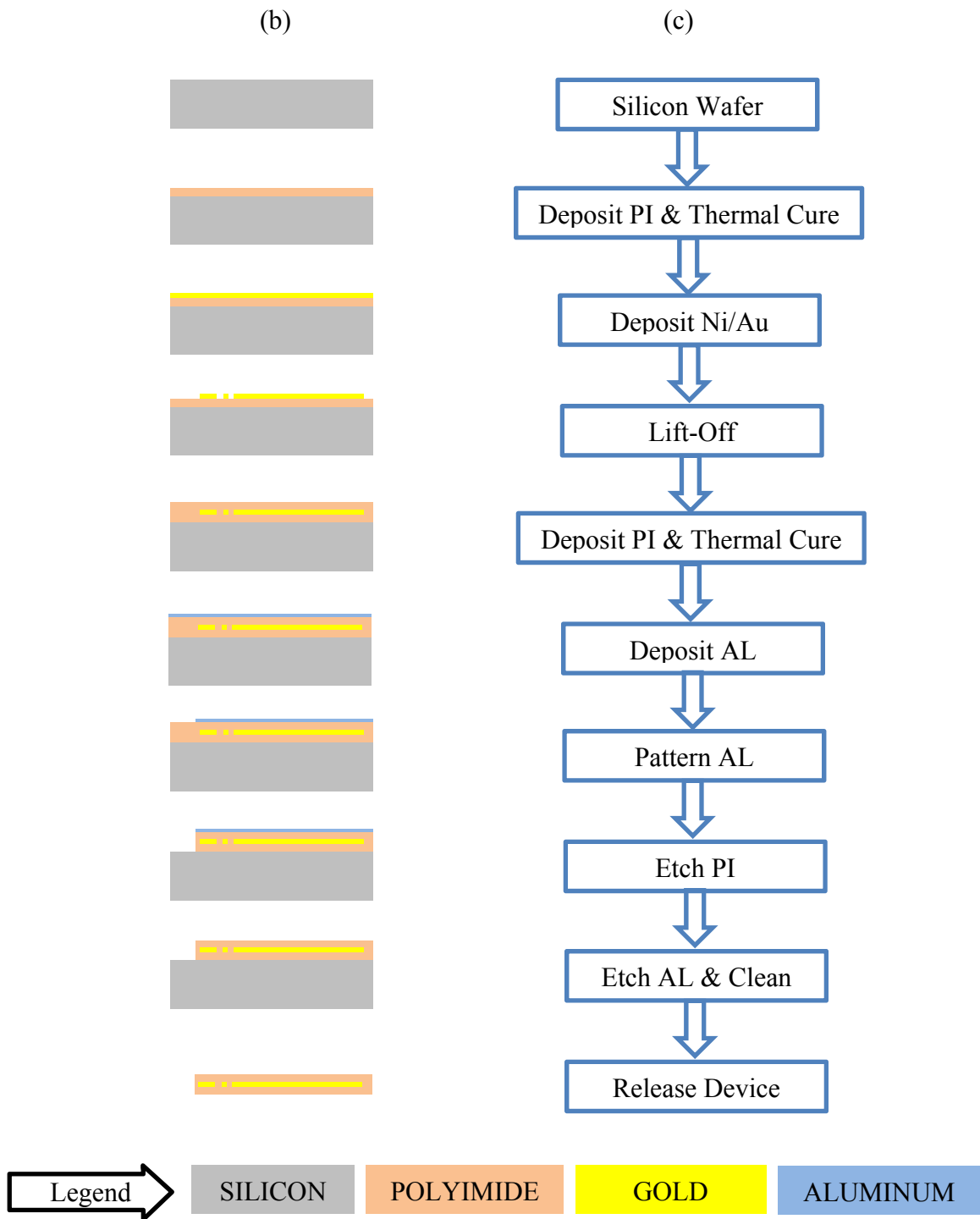


Figure 3.1: Fabrication process flow. (a) Left column shows the cross-sectional view of the (cut shown by the green arrow lines in 3.1 (a)) (b) Right column shows the flowchart for the processing steps.

### 3.3 Fabrication Process

#### 3.3.1 Silicon Wafer Cleaning

A 4" silicon wafer was used as a handle wafer to support device fabrication. Before commencing fabrication, the wafers were subject to a standard cleaning procedure known as RCA clean to remove organic, ionic and metallic contamination from the wafer surface [ref. Kern W.]. The wafers were subjected to a two-step immersion-cleaning process in which the silicon surface was first treated to a mixture of hydrogen peroxide ( $H_2O_2$ ) and ammonium hydroxide ( $NH_4OH$ ) heated to  $75^\circ C$  (removes organic particles and contamination). The second step involved a solution of hydrochloric acid (HCL) and  $H_2O_2$  to remove ionic and metallic contamination. The wafer was then rinsed with deionized (DI) water and blow-dried with nitrogen ( $N_2$ ). A dehydration bake was performed immediately following the RCA clean process on an open hotplate at  $115^\circ C$  for five minutes.

#### 3.3.2 Depositing Polyimide

The polyimide PI-2611 is a viscous liquid stored in the manufacturer's bottle at a recommended temperature of  $-18^\circ C$  to maximize its shelf life to two years [PI-2600 Series Product Bulletin, Figure 3.2 (a)]. It is taken out and stored in small quantities at room temperature at need. Room temperature PI-2611 was spin-coated on each wafer in four static-dispensing steps to allow an even coating of the polyimide. The silicon wafer was first placed on a wafer chuck in a spin-coater (Headway Research, Garland, TX). The material is deposited on to the center of the wafer by directly dropping from the

bottle to create a ‘five cent coin’ sized layer. The PI-2611 was then allowed to stabilize and flow on the wafer surface to eliminate any trapped air bubbles (Figure 3.2.(b)). The deposition was finalized by spinning the wafer according to the parameters shown in Table 3.1.

Table 3.1: Spin parameters for deposition of Polyimide PI-2611 on Si wafer. Two steps are used to spread the polyimide and evenly coat the surface.

Step	Speed (rpm)	Ramp Rate (rpm/s)	Duration (secs)
1	500	100	10
2	1500	150	20
3	3000	1000	20
4	0	500	0



Figure 3.2: (a) PI2611 bottle stored in refrigerator. (b) Spin-coating PI-2611 on a silicon wafer.

### 3.3.3 Thermal Curing

A soft bake was performed at 115°C for three minutes on an open hotplate immediately following the spin-coating. This step removes all residual moisture from the coated layer of polyimide. Following the soft bake, the polyimide-coated wafers were thermally cured in a high temperature vacuum oven (YES-PB 6-2P-CP, Yield Engineering Systems, Livermore, California) at 350°C for one hour (Figure 3.3). The curing process starting temperature was 50°C with heating and cooling ramp times of 100°C /hour and a total curing time of 7 hours (Figure 3.4). The vacuum environment was subject to dehydration cycles to remove oxygen and moisture. Nitrogen gas was continuously supplied across the surface of the wafer to maintain an inert environment.



Figure 3.3: PI cure vacuum oven from Yield Engineering Systems. Wafers (up to 6” in diameter) are loaded vertically and nitrogen gas flows in a perpendicular direction (to the chamber), across the surface of the wafer. (Image source: company website).

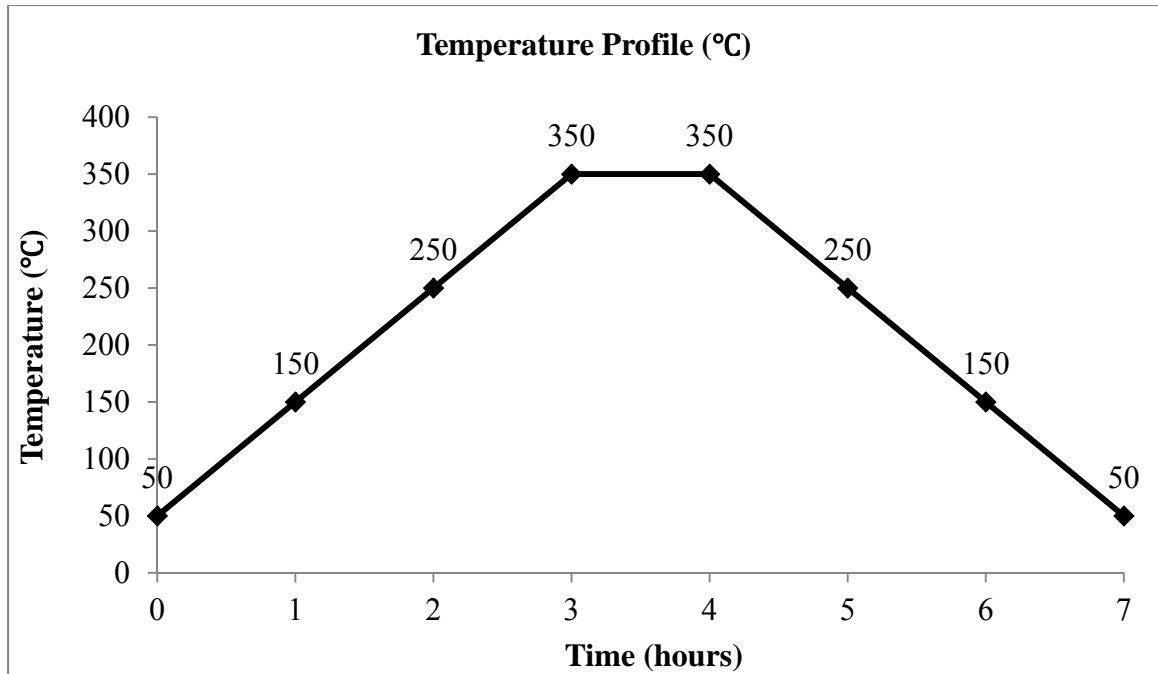


Figure 3.4: Temperature profile of a seven hour thermal curing process for the polyimide PI-2611 in a YES vacuum oven with heating and cooling ramp rates of 100°C/hour.

### 3.3.4 Photolithography (Mask 1)

A pattern for the electrodes was created on the polyimide surface using a photomask and photoresist. A photomask is a glass plate with a coating of chromium created in a laser patterning system (Heidelberg DWL 66FS) based on the design developed in L-Edit software (Tanner EDA, Monrovia, CA). The pattern was transferred from the mask to the wafer in a light sensitive resist via exposure to ultraviolet (UV) light. The resist was coated on to the surface and then UV exposure (partially blocked by the mask) enables an identical imprint to be created in the photoresist layer. This was accomplished by loading the mask and the wafer in a mask aligner (MA/BA6, SÜSS MicroTec AG, Garching, Germany; Figure 3.5).



Figure 3.5: Mask aligner model MA/BA6 from SÜSS MicroTec AG. The mask is upside down and the wafer is in contact or close proximity to the surface. The alignment is performed using the optics and computer system. (Image source: company website).

The pattern for the photoresist was used to create the gold electrodes by using a lift-off process. Usually a metal pattern creation follows the path of metal deposition, photoresist application/development and finally metal etch. A lift-off process reverses the order of metal deposition and photoresist patterning. The photoresist is first coated and developed, followed by the metal deposition. It enables the patterning of materials without using powerful etchants. Gold etch requires the use of strong chemical etchants

such as aqua regia (hydrochloric acid + nitric acid) or AU-5 (potassium iodide). Moreover these are dark in color and make the submerged sample nearly impossible to observe. A lift-off process eliminates the etching step by creating a hanging retro edge profile in the patterned photoresist layer. The metal is deposited on the resist; the unwanted resist is soaked in a solvent and removed along with the unwanted metal. The lift-off process used for the P-MEA fabrication is listed in Figure 3.6.

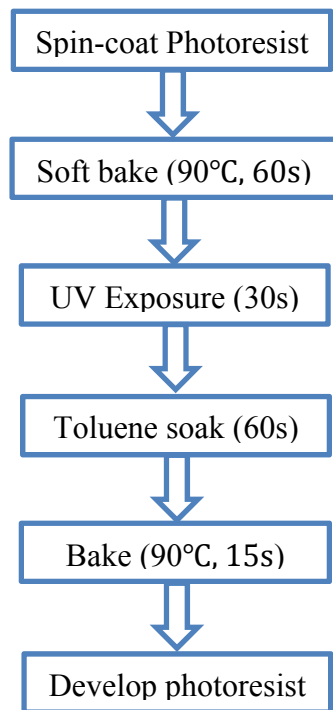


Figure 3.6: Photoresist lift-off process flow. The toluene soak hardens the top of the resist, leaving overhanging edges at the sidewalls of the resist.

A G-line photo resist S1827 (Microposit S1800 series, MicroChem Corp., Newton, MA) was used to first create the pattern (using Mask 1) over which the metal was deposited. The photoresist is spin-coated on the polyimide-coated wafer surface using the parameters listed in Table 3.2. A resist coating of  $2.7\mu\text{m}$  was obtained using

these parameters. A soft bake was performed on a hotplate at 90°C for 60 seconds. Wafer and mask were loaded on to the mask aligner and exposed to UV light at a power density of 4.5 mW/cm<sup>2</sup> for 20 seconds. The resist was subjected to a 60-second toluene soak (Avantor Performance Materials, Center Valley, PA) to harden the top layer of resist. Development of the exposed resist was performed in MF-319 (Avantor Performance Materials, Center Valley, PA) to create the desired pattern.

Table 3.2: Spin parameters for coating photoresist S1827; total time was 18.7 seconds

Step	Speed (rpm)	Ramp Rate (rpm/s)	Duration (secs)
1	500	500	0.2
2	4000	1000	10
3	0	1000	0

Table 3.2: Spin parameters for coating photoresist S1827; total time was 18.7 seconds.

### 3.3.5 Sputter Deposition

Sputter deposition or sputtering is a physical vapor deposition (PVD) process in which material from a target is removed and deposited on a wafer. In sputtering, the wafer and the target material are positioned across from one another in a vacuum environment and a high voltage is applied across them to create a negative potential at the target. The transport of material takes place in argon plasma where the Ar<sup>+</sup> ions strike the target with energy to dislodge individual atoms from the target surface which in turn are transported on to the wafer surface. A magnet is held behind the source target to control

the energy field which effectively increases the sputter path length and improves sputter rates. This process is also known as magnetron sputtering [ref. Introduction to Microfabrication (2010) - Sami Franssila]. Metal depositions for the P-MEA were performed using a DC sputtering process in argon plasma in PVD 75 (Kurt J. Lesker Company, Pittsburgh, PA, Figure 3.7).



Figure 3.7: PVD 75 sputter deposition system from KJL. The double doors hide the main process chamber on the left while the controlling computer and power supplies are on the right. The process chamber usually contains four 3” targets but can be customized to

unique needs (MNTC PVD75 has two 3" and one 4" targets). (Image source: company website).

The wafer was held upside down above the targets in a revolving holder at a speed of 5 rpm. This rotation allowed an even coating of the metal during deposition. A vacuum is created before the argon gas is released into the chamber at a base pressure of  $5 \times 10^{-5}$  Torr. The sputter pressure was set at 3mT and sputter power was 300W using a DC power source. Nickel was deposited for 2 minutes followed by 10 minutes of gold deposition (Figure 3.8). Nickel was used as an adhesion layer to ensure good adherence between the gold and polyimide layers. Before each deposition the target is subjected to a sputter clean process by merely turning on the power source for 30 seconds while shielding the wafer with a shutter.

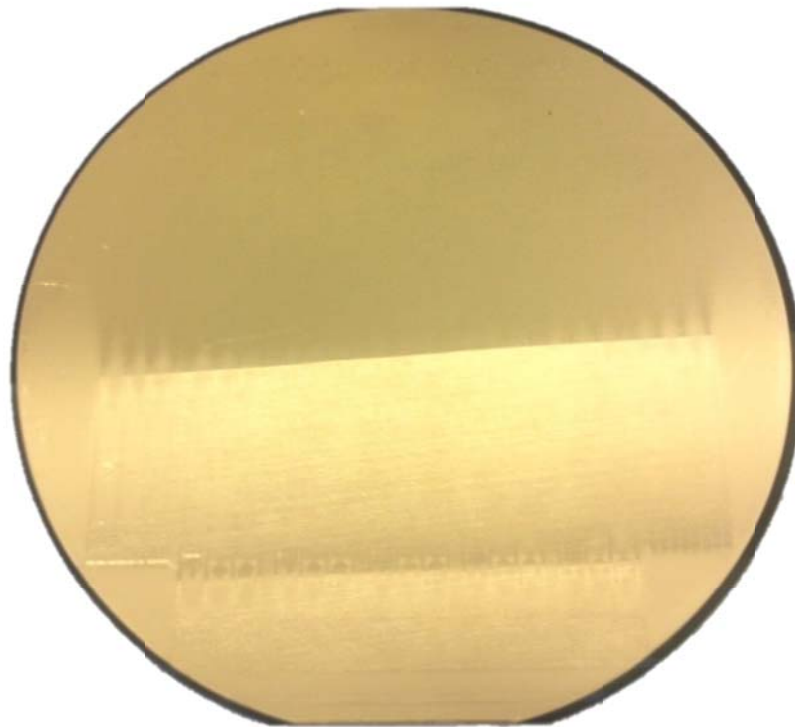


Figure 3.8: A 4" silicon wafer with a sputter-coated layer of Ni/Au on a polyimide layer. Note the faint lines visible under the surface; they are the electrodes etched in photoresist.

### 3.3.6 Lift-Off Process

Following deposition the wafer was then subjected to a 44.1 KHz ultrasonic agitation in acetone. The resist ‘lifted off’ leaving behind the gold layer in the pattern of the Fdevice electrodes and traces (Figure 3.9).

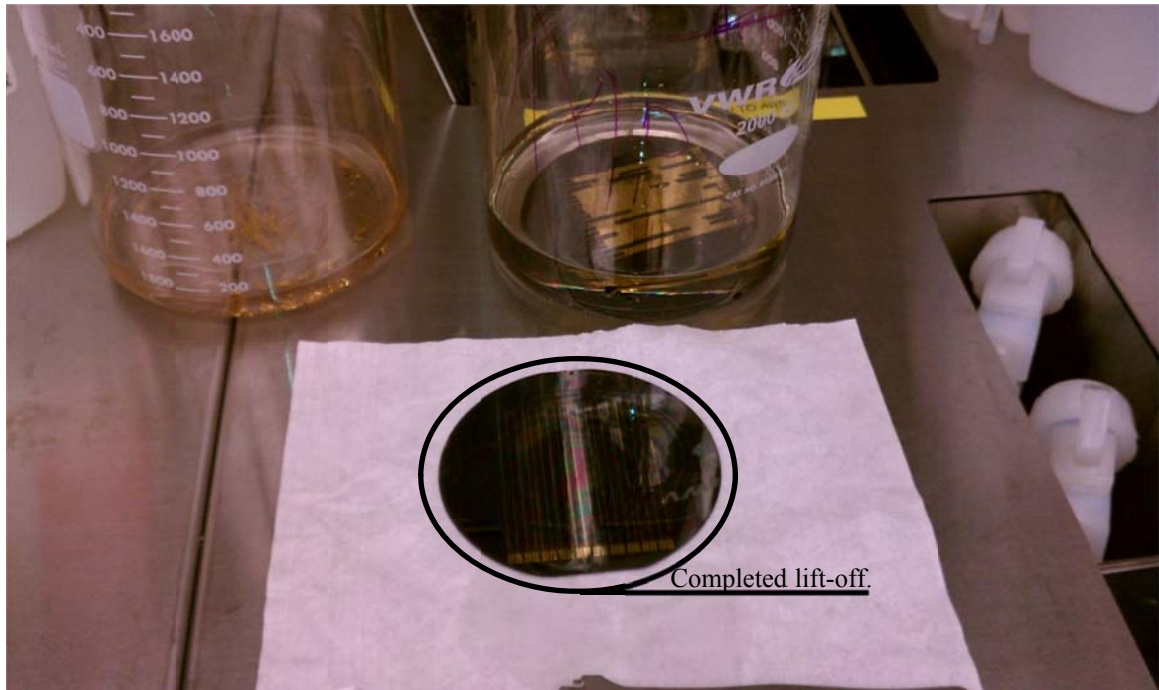


Figure 3.9: Acetone solvent soak for the lift-off process. Photoresist dissolves readily in acetone and the patterned photoresist was removed along with the metal on top of it. Note the gold particles floating in the acetone in the left beaker. The right beaker shows a lift-off process in progress with the Ni/Au layer partially removed.

A wafer with a completed lift-off process is shown in Figure 3.10; it shows the gold electrodes formed on the first polyimide layer (version 2 of the device).

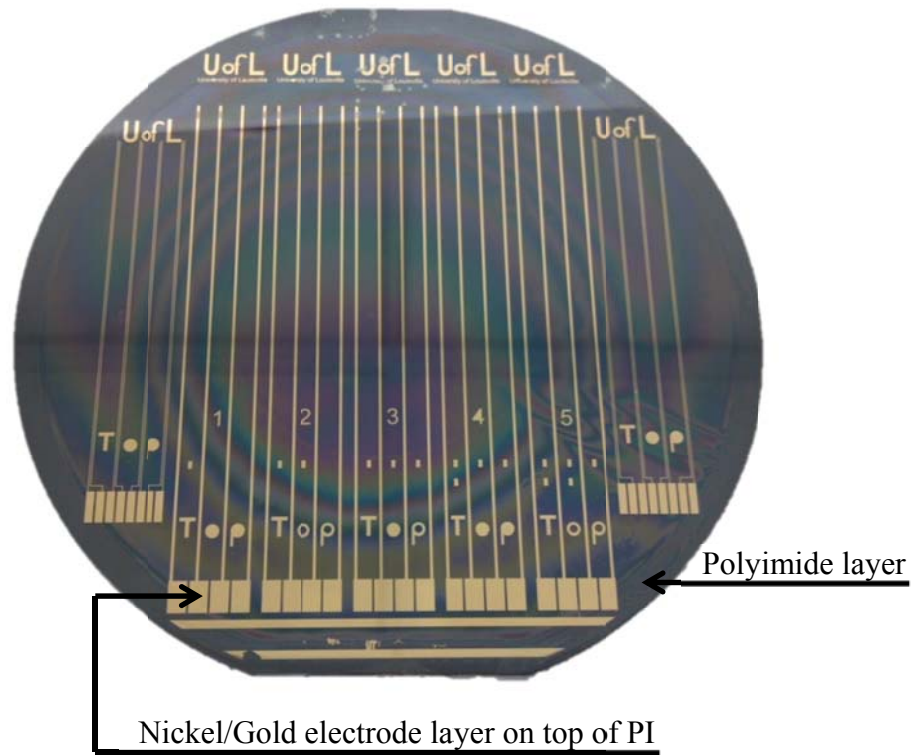


Figure 3.10: Wafer with completed gold electrodes after a lift-off process and DI water rinse cleaning. (version 2 of the P-MEA shown in fabrication).



Figure 3.11: Second layer of polyimide – soft bake on hotplate prior to vacuum curing.

The second layer of polyimide was then deposited on top of the gold layer and cured using the same parameters as before. Figure 3.11 shows a soft bake being performed on an open hot plate prior to thermal curing in the YES oven.

### 3.3.7 Aluminum Sputtering

After the second layer of PI was cured, aluminum was sputter-deposited on top of the cured surface. Sputtering was performed using the PVD75 sputter deposition system; sputter pressure was 3mTorr, power was 300W and length of deposition was 10 minutes. The final thickness of the aluminum layer was approximately 0.2 $\mu$ m (shown in Figure 3.12). This aluminum layer was used as a hard mask to protect the polyimide during etching.

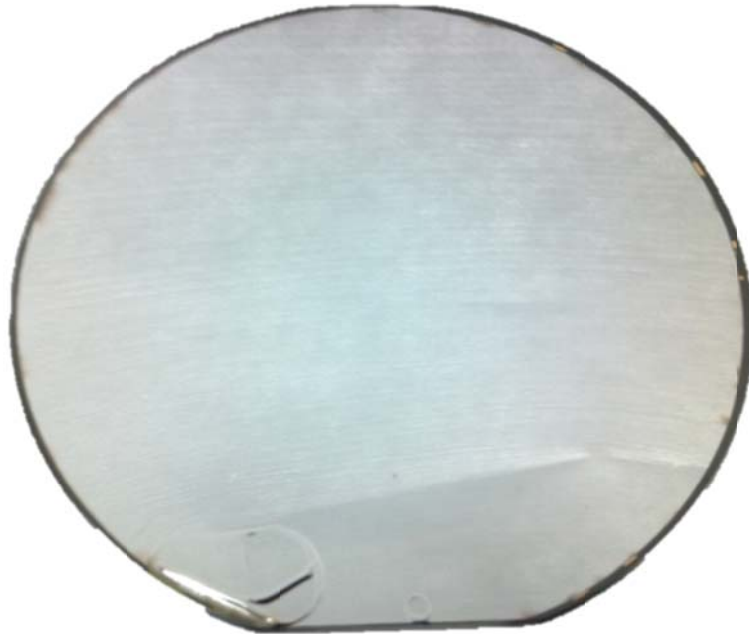


Figure 3.12: Aluminum coating on top of the cured polyimide layer. The aluminum film was used as a mask for the polyimide etch.

### 3.3.8 Photolithography (Mask 2)

The second lithography step was similar to the first one (section 3.3.4) in terms of materials and processing. The photoresist S1827 was spin-coated on the aluminum surface using the same parameters and patterned using Mask 2. After processing the wafer looks as shown in Figure 3.13.

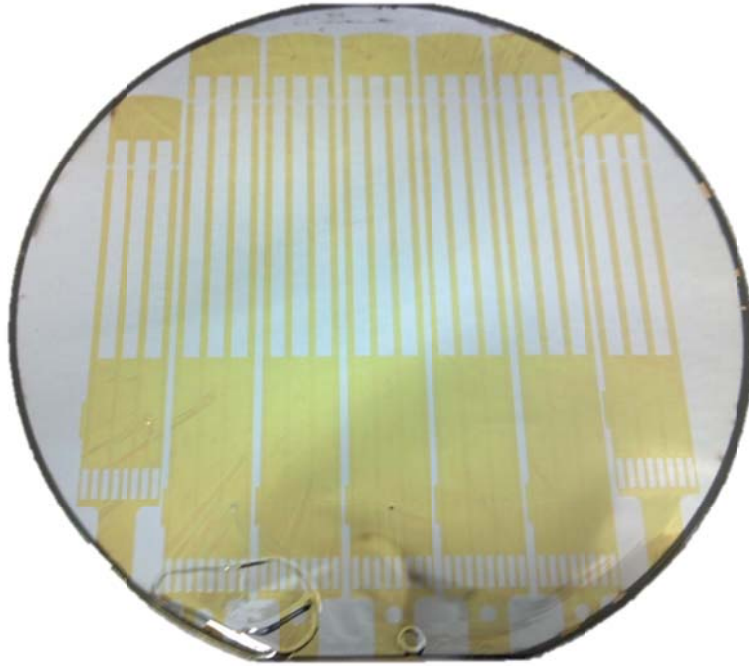


Figure 3.13: P-MEA device pattern in photoresist S1827 layer; the resist is seen in the yellow colored pattern over the shiny aluminum coating. The PI layer is visible around the periphery of the wafer under the aluminum layer.

The patterned photoresist was used as a mask to etch the aluminum film. The etch was performed using the wet chemical etchant, aluminum etch (Avantor Performance Materials, Center Valley, PA). It comprised of 2% nitric acid, 3% acetic acid, 80% phosphoric acid and 15% water. The etchant was heated to a temperature of 45°C in a beaker on an open hotplate. The post-etch cleaned wafer is shown in Figure 3.14.

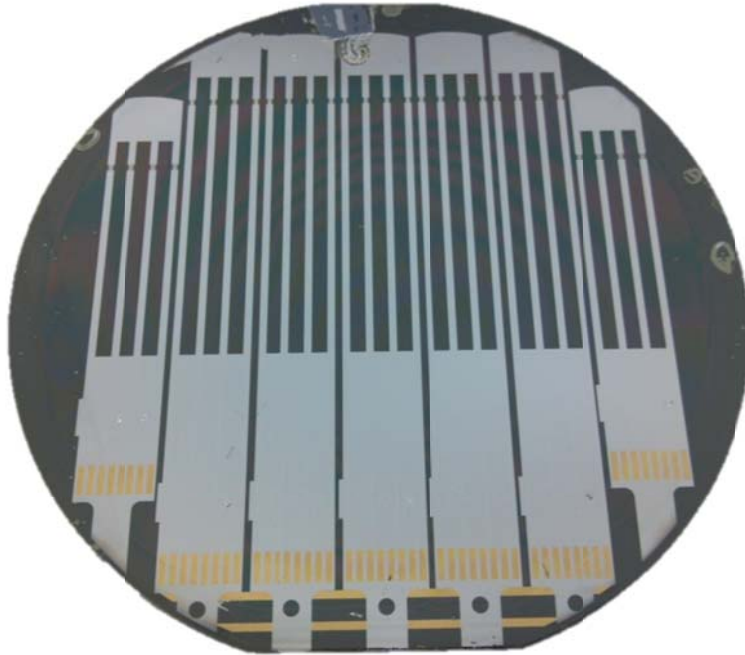


Figure 3.14: The wafer with the etched aluminum layer. This aluminum layer now has the pattern from Mask 2.

### 3.3.9 Polyimide Etch

The polyimide was etched in a Reactive Ion Etch (RIE) system (CS-1701, Nordson MARCH, Concord, CA) process using oxygen gas plasma at a pressure of 50mT and power of 300W for 20-30 minutes. The RIE process served a dual purpose; opening up the electrode areas on the top surface of the device required to make contact with the ECT and the electrical connections, as well as patterning and cutting out the device. The oxygen plasma etched the polyimide layer and stopped on the metal surface (gold). However, the etch continued along the device perimeter to define the overall design and separate the individual devices. The aluminum mask was stripped after the RIE process was completed; the wafer with the patterned devices is shown in Figure 3.15.

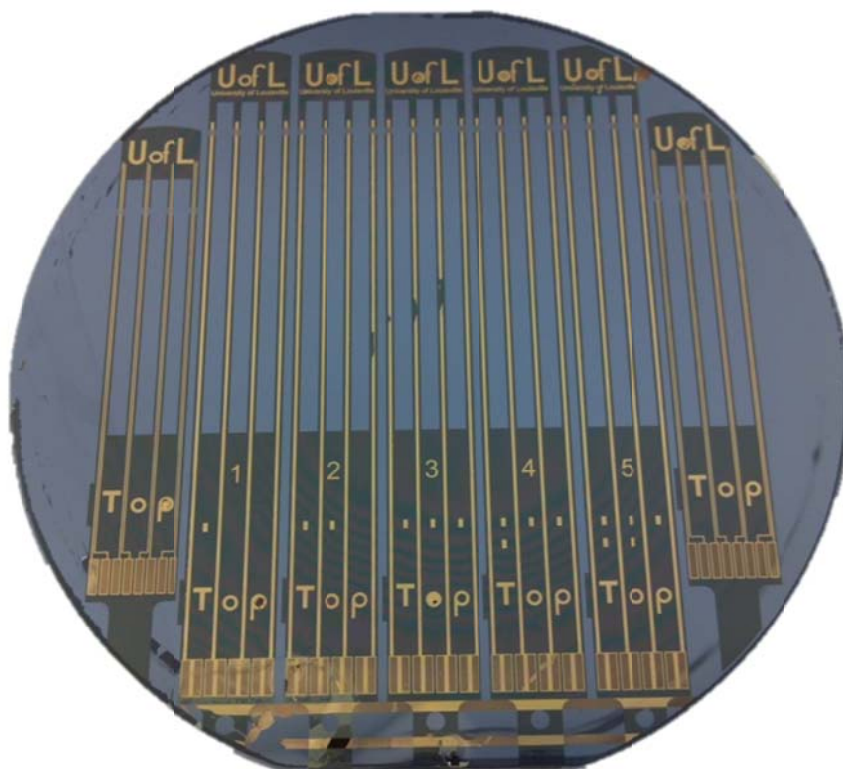


Figure 3.15: The silicon wafer containing the P-MEA devices (version 2) after the completed etch process. Note the residue on the exposed gold pads; the shinier traces of the metal are sandwiched between the two polyimide layers.

Devices were cleaned using an acetone soaked soft wipe followed by methanol (Avantor Performance Materials, Center Valley, PA). Deionized water was used for a final clean. Figure 3.16 shows the cleaned P-MEA devices (version 3) on a silicon wafer. Each device was then tested on a probe station (MPS150, Cascade Microtech, Beaverton, OR) for electrode integrity and resistance between the proximal contact pad and the distal electrodes. These values as well as thicknesses for the deposited layers are reported in the results section.

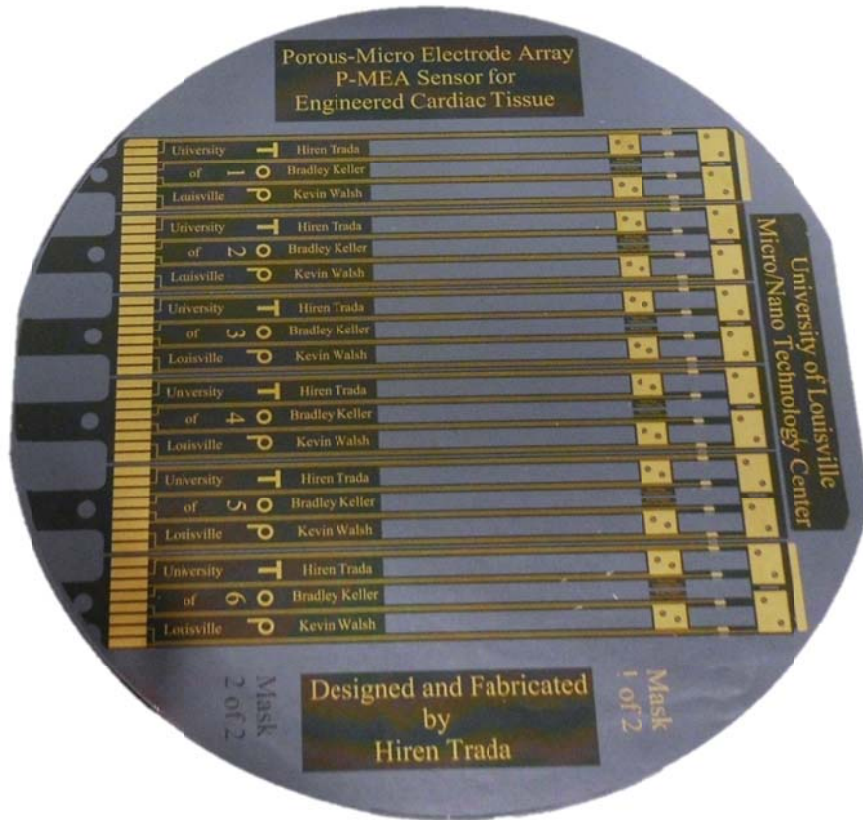


Figure 3.16: version 3 of the P-MEA devices on a 4” silicon wafer. The devices were squeezed together to increase the number of devices to six (from five in version 2).

The devices were removed from the wafer by sliding a razor blade underneath the end tab near the connection pads. Once a small corner lifts off, it was relatively easy to grab hold of the tab with a pair of tweezers and gently peel off the entire device. No special chemicals or processing were required to remove the P-MEA devices.

## CHAPTER IV

### ELECTRICAL AND ELECTROCHEMICAL TESTING

#### 4.1 Device Integrity Testing

The devices were tested for electrical integrity on a wafer probe station (MPS150, Cascade Microtech, Beaverton, OR) after fabrication. Each electrode trace was tested for continuity since the electrode was long and narrow; a tiny imperfection during fabrication could render the electrode line useless. Resistance measurements were taken for each electrode during the test by connecting the meter between the proximal embedded pads and the distal connection pads (shown in Figure 4.1).

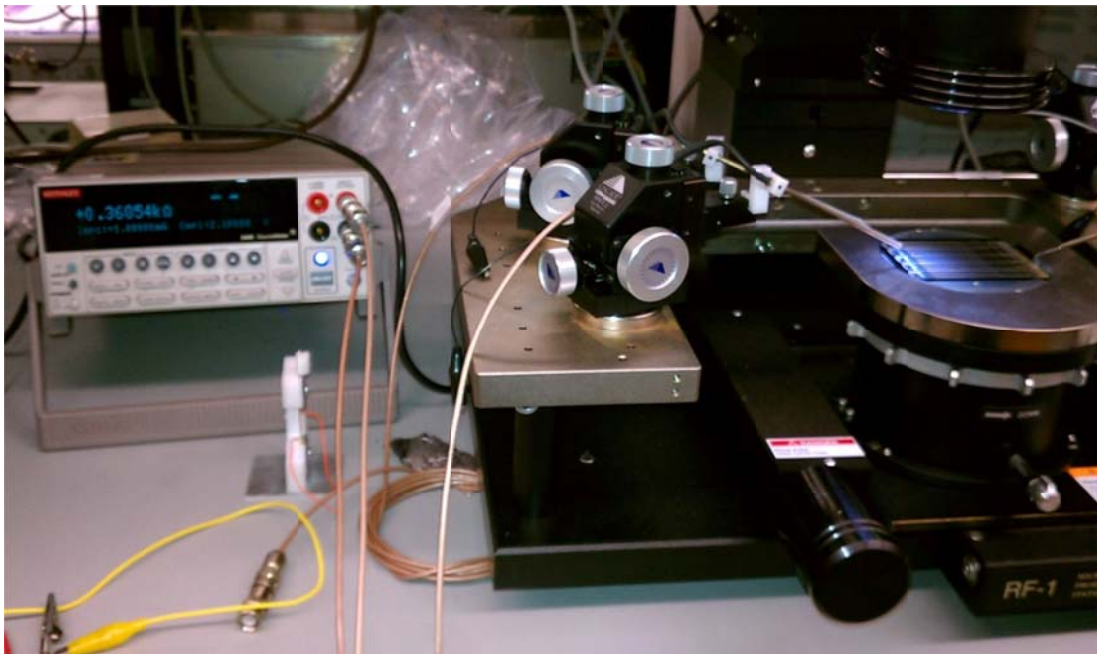


Figure 4.1: Cascade probe station for testing device electrode integrity and resistance.

The wafer was placed on the probe station wafer chuck with the small embedded pads visible through the lens optics. One probe was maneuvered into position and placed on the gold surface of the embedded pad. The optical assembly of the probe station had limited travel and could not be positioned to view the distal pad. Hence the second probe was positioned without any optical aid (Figure 4.2).

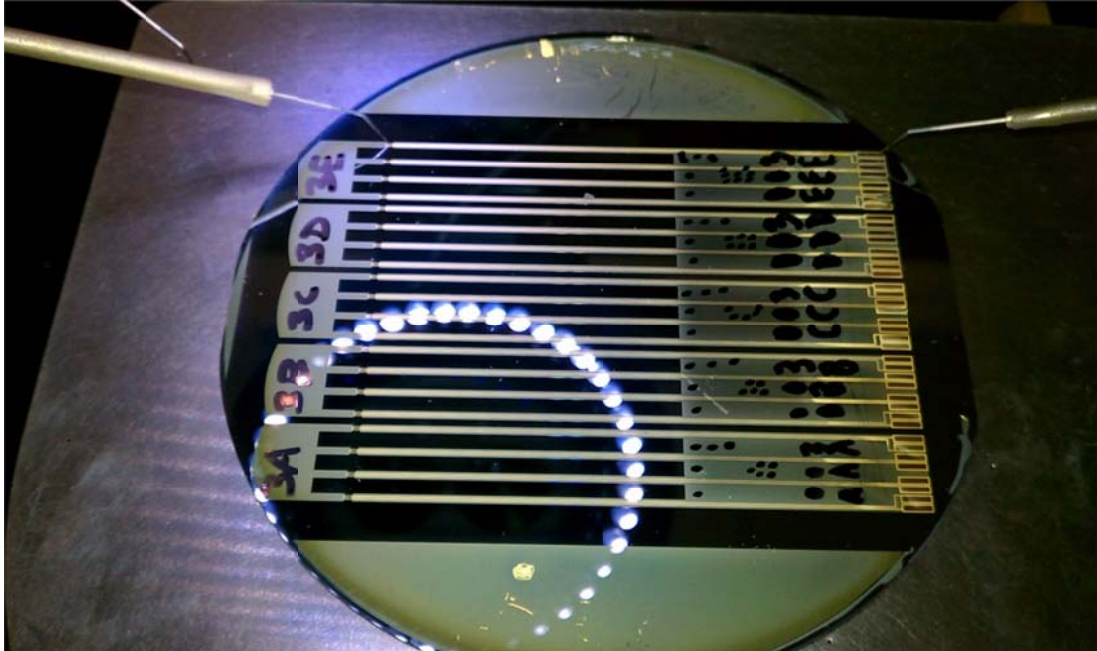


Figure 4.2: Probe testing the electrodes. Probe on the left is on the embedded pad and was positioned underneath the lens, while the probe on the right is on the connecting pad.

Average resistance measurements across the lengths of the electrodes ranged from  $69.45\Omega$  to  $78.52\Omega$ . In addition, the thickness of the Ni/Au electrodes of five (randomly chosen) devices was measured using a Dektak profilometer. This resulted in an average thickness of 20nm of nickel and 400nm of gold. An average thickness of  $0.4\mu\text{m}\pm 0.02\mu\text{m}$  was obtained for the electrode films. The thermal curing results in a polyimide layer of  $8\mu\text{m}$  thickness and the double polyimide layer was approximately  $16\mu\text{m}$  thick.

## 4.2 Equivalent Electrode Model

Further evaluation of the P-MEA device was done by performing electrochemical experiments using the same scenario as the actual application. This involved the device transporting electrical signals from a stimulator to the ECT immersed in culture medium (Dulbecco's Modified Eagle Medium (DMEM), 11965-092 (high glucose), Gibco by Life Technologies, Grand Island, NY), which acts like an electrolyte. Since charge transfer takes place between the electrons in the electrode and ions in the electrolyte it was necessary to evaluate the performance of the electrodes while immersed in the culture medium. The four small exposed electrode pads embedded within the ECT were electrically coupled to form one common connection while the four large electrode pads in the culture medium were coupled to form the common return connection. To evaluate the electrochemical interface a representative equivalent circuit model needs to be used. Several models have been proposed to approximate the electrode-electrolyte interface. The most widely used model is a two-element model, which has resistance representing the electrode's polarization resistance or impedance and a capacitance in parallel with the resistance [60-62]. The capacitance represents the charged layer at the electrode-electrolyte interface which is caused due to the presence of a layer of charge at the electrode surface and an equal and opposite layer of charge in the electrolyte. This double layer of charge at the interface behaves akin to a capacitor and hence is called as the double-layer capacitance. Each parallel combination of the resistance and capacitance represents one set of electrodes. For the P-MEA device, the four small embedded electrodes were referred to as the 'Working Electrode' (WE) and the four large electrodes as the 'Counter Electrode' (CE). For the equivalent circuit model (Figure 4.3), R1 and C1

model the WE, and R2 and C2 model the CE. In addition to these components there was a resistance RS which represents the solution (electrolyte) resistance.

4.3 (a)

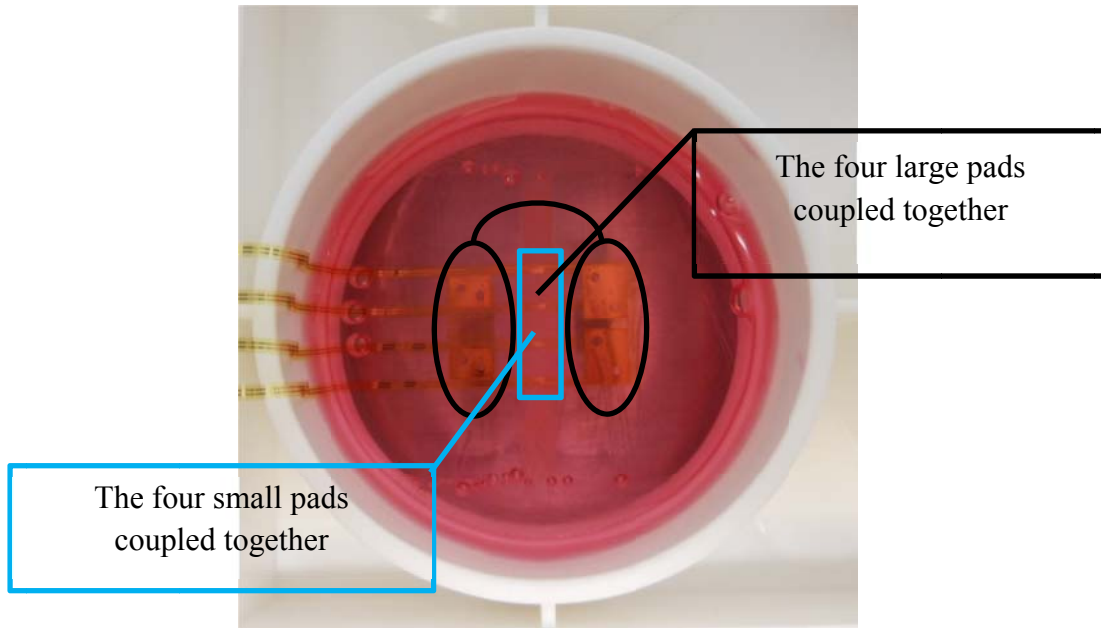


Figure 4.3 (b)

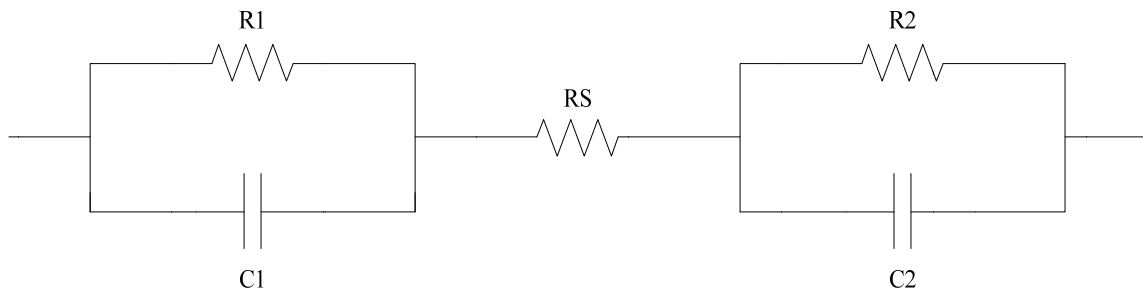


Figure 4.3: (a) An ECT embedded with a P-MEA device. The four large pads were electrically coupled together (externally) and the four small embedded pads were coupled together. (b) Equivalent circuit model for the P-MEA device in culture medium (DMEM). R1 & C1 represent the interface between the embedded pads & DMEM; R2 & C2 represent the interface at the large pads & DME, and RS represents the solution resistance.

Charge transfer between the electrode and electrolyte can occur in three primary ways, non-faradaic charging and discharging, reversible faradaic reactions, and irreversible faradaic reactions. Of the three mechanisms, the first two are highly desirable while irreversible faradaic reactions are not due to the risk of electrode corrosion and tissue damage [60].

#### 4.3 Electrochemical Impedance Spectroscopy (EIS)

A safe operating limit for the device-electrolyte interface can be determined by assessing the performance of the electrodes in culture medium (DMEM) using Electrochemical Impedance Spectroscopy (EIS). EIS is an excellent tool for analyzing electrode performance in an electrolyte and can be used to determine presence or absence of irreversible reactions [24-27]. Impedance Spectroscopy, as the name suggests is the measurement of impedance of an electrical circuit over a range or spectrum of frequencies [70-72]. Electrochemical Impedance Spectroscopy is an analysis tool wherein a sinusoidal signal is applied to an electrochemical system or cell, and the current flowing through the cell is measured. The amplitude of the signal is kept very small; between 1mV-10mV, to ensure a pseudo-linear response from the cell. The frequency range is typically varied from 1mHz to 1MHz. Due to the very small input signal frequencies, the EIS tests often take hours to complete the entire spectrum. To evaluate the performance and to determine operating limits, a DC component is applied with the AC signal and the voltage is varied over a desired testing range [70-73].

The input voltage and current response can be represented by the following equations:

$$v(t) = v_0 \sin(\omega t) \quad \text{Eq. 4.1}$$

$$i(t) = i_0 \sin(\omega t + \theta) \quad \text{Eq. 4.2}$$

where  $\theta$  is the phase shift of the signal. Using Ohm's law, the impedance can be written as;

$$Z = \frac{v(t)}{i(t)} = \frac{v_0 \sin(\omega t)}{i_0 \sin(\omega t + \theta)} \quad \text{Eq. 4.3}$$

$$\therefore Z = z_0 \frac{\sin(\omega t)}{\sin(\omega t + \theta)} \quad \text{Eq. 4.4}$$

In the complex plane this equation can be represented as;

$$Z(\omega) = Z_0(\cos\theta + j\sin\theta) \quad \text{Eq. 4.5}$$

Equation 4.5 for the impedance contains real ( $Z'$ ) and imaginary ( $Z''$ ) components. The imaginary component is due to the capacitive-like behavior at the electrode-electrolyte interface. Plotting both values in a chart gives us a Nyquist plot for the system. For a simple equivalent circuit, similar to the one shown in figure 4.3 (b), this results in a semi-circle (shown in Figure 4.4). This circuit is also called as a single time constant circuit, as is evident from the one semi-circle in the plot. Multiple interfaces would result in multiple time constants and multiple semi-circles. Bode plots are used to view frequency and phase angle information. In a typical Bode plot, the magnitude and phase angle of the impedance vector is plotted against the frequency input. The phase plot indicates the behavior of the double layer capacitance at the interface. At low frequencies the ions in the electrolyte diffuse to the interface at a finite rate hence the

Nyquist plot has a linear response at low  $\omega$ .  $R_P$  shown in the figure indicates the polarization resistance of the electrode under investigation. It can be simply defined as the ability of the electrode to resist current flow. The higher the resistance, the lower the rate of corrosion and deterioration. So a semi-circle with a higher radius is always desirable in the Nyquist plot.

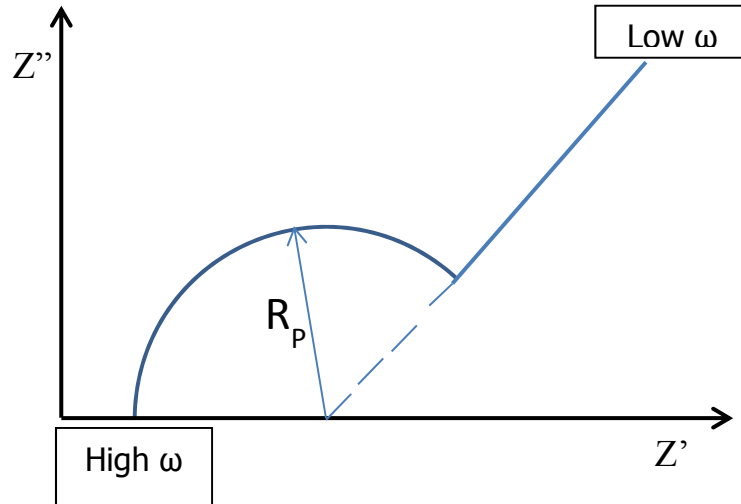


Figure 4.4: Representative Nyquist plot for a single time constant interface. Nyquist plots don't contain any frequency information, they can only represent impedances.

The results from EIS are collected and used in a software simulator to generate values for the components in the equivalent circuit. The relationship between the impedance and the circuit components can be given by;

$$Z(\omega) = R_S + \frac{R_P}{1+j\omega CR_P} \quad \text{Eq 4.6}$$

Potentiostat/Galvanostat Model 273A (Princeton Applied Research, Oak Ridge, TN) was used to collect EIS data and ‘EIS Spectrum Analyser’ (freeware, Belarusian State University, Minsk, Belarus) to analyze and simulate the performance of the P-MEA-S electrodes in DMEM. Experimental setup is shown in Figure 4.7.



Figure 4.5: Model 273A, Potentiostat/Galvanostat (Princeton Applied Research, Oak Ridge, TN); used for the EIS experiments and measurements.

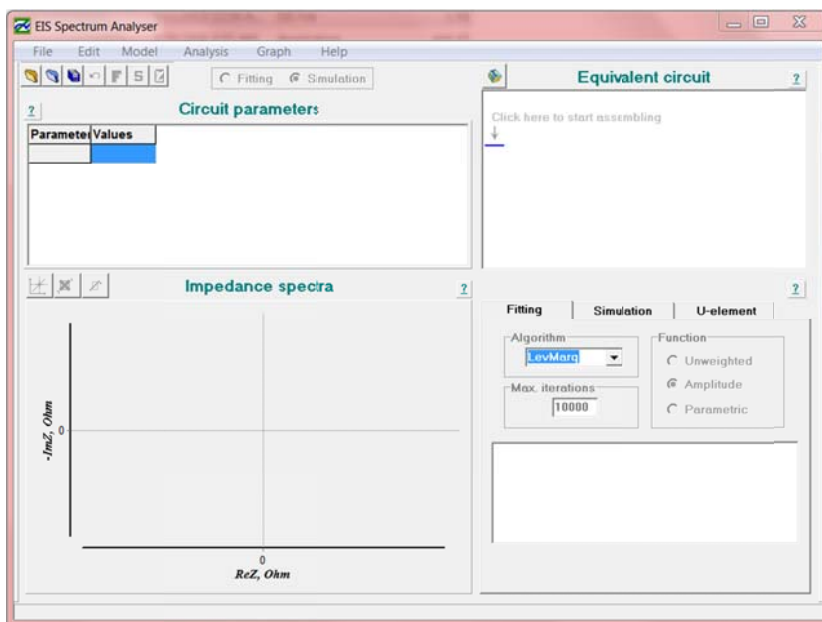


Figure 4.6: ‘EIS Spectrum Analyser’ is a free software available from Belarusian State University for EIS analysis.

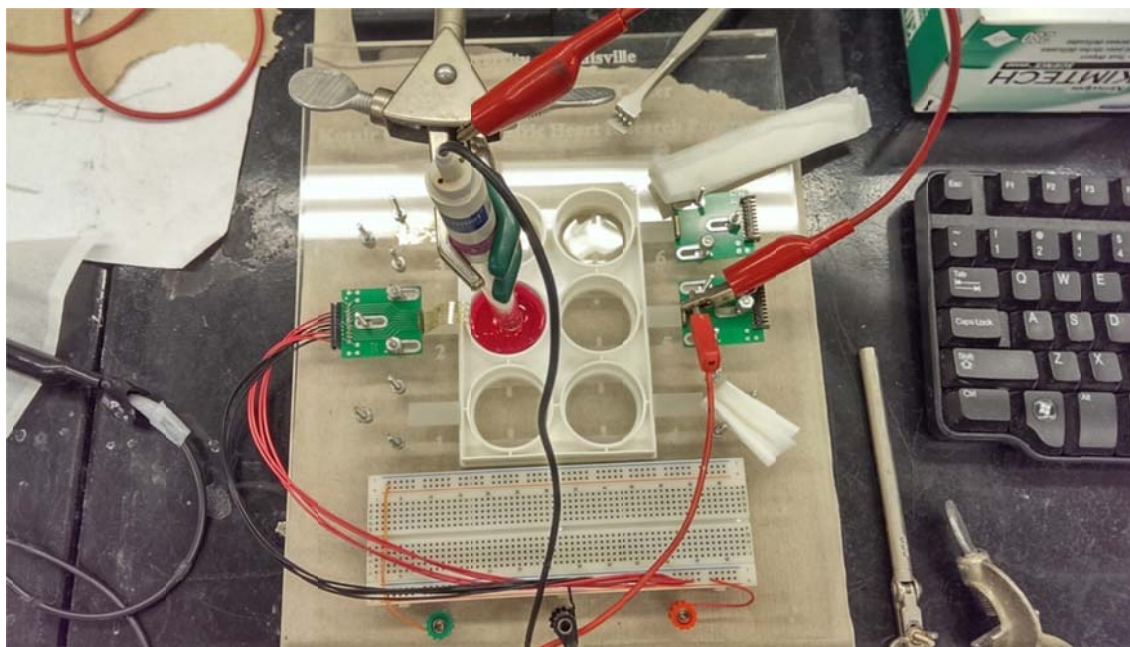


Figure 4.7: Experimental setup for EIS and other electrochemical tests. The P-MEA is being tested for electrochemical performance in culture medium.

Figure 4.8 (a) shows the Nyquist plot for the EIS analysis of the individual P-MEA-S electrodes in DMEM. This Nyquist chart plots the real impedance component ( $Z'$ ) against the imaginary impedance ( $Z''$ ). These curves can be used to predict the presence or absence of irreversible reactions. Electrode impedance comes from the resistance and capacitance comprising the electrode-electrolyte interface. The imaginary component is contributed by the capacitance which has a frequency dependent impedance defined by:

$$Z_C = \frac{1}{j\omega C} \quad \text{Eq 4.7}$$

where  $Z_C$  is the capacitive impedance ( $\Omega$ ),  $C$  is the value of the capacitance (F), and  $\omega$  is the angular frequency defined as:

$$\omega = 2\pi f \quad \text{Eq 4.8}$$

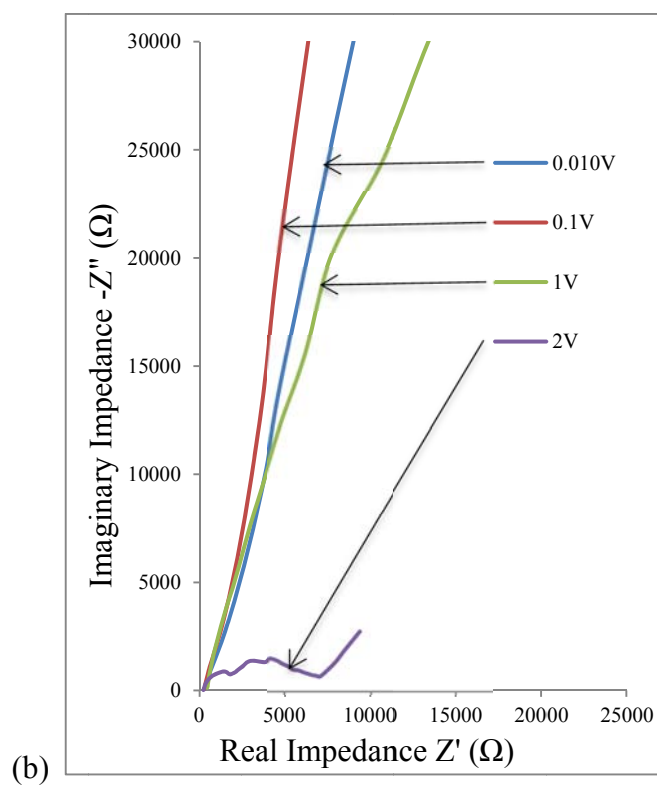
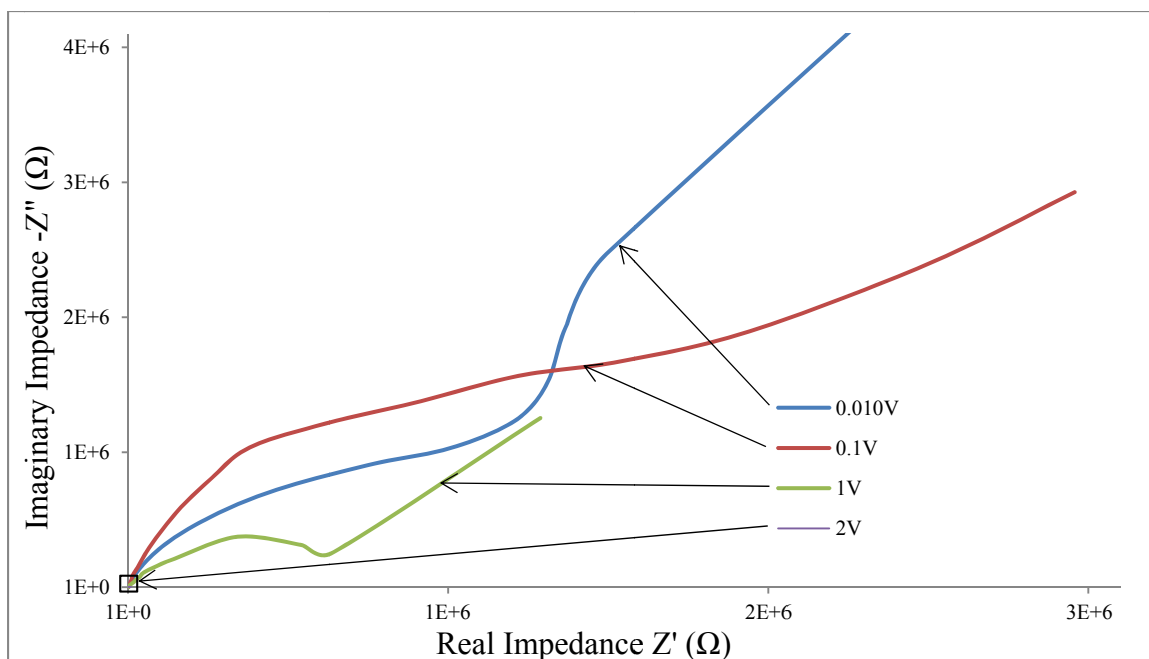


Figure 4.8 (a): Nyquist plots for individual EIS tests on P-MEA-S in DMEM media at 0.01, 0.1, 1, and 2 volts. Note the downward shift in the EIS plot at 2 volts consistent with irreversible reactions. (b) Expanded scale of the individual EIS plot at 2 volts.

From eq. 4.7 it can be seen that as frequency increases the impedance decreases and vice-versa. Plotting the impedance values in the Nyquist Plot results in the curve resembling an incomplete semi-circle. The greater the radius of the semi-circle, the higher the charge-transfer resistance. The semi-circle is the consequence of a single time-constant circuit. This kind of circuit can be represented by the equivalent model (Figure 4.3 (b)).

For P-MEA voltage ranges of 0.01V, 0.1V and 1V, the imaginary component value was high which is attributable to the capacitive behavior of the double layer. The closer the interface behaves akin to a capacitor, the higher the value of the  $Z''$ . The impedance values obtained for the 2V signal are so extremely small compared to the other voltages. Figure 4.8 (b) shows the high frequency range of the Nyquist plots wherein the low performance of the electrodes at 2V is evident. These are indicative of the presence of faradaic reactions that may result in electrode corrosion and cause damage to the tissue [24, 63-67].

In capacitors, there is a phase difference between voltage and current where voltage lags current. In an ideal capacitor, this phase shift is  $90^\circ$ . The phase plots of the EIS analysis are shown in Figure 4.9. For input voltages of 0.01V & 0.1V the electrodes displayed behavior very close to an ideal capacitor for frequencies between 1Hz to 1KHz. For the 1V signal the low frequency phase shift angle was initially lower. However, the 2V phase plot displayed a non-ideal, small phase shift. The phase plots indicate that the electrode-electrolyte interface behaved akin to a capacitor at the desired operating frequencies. Thus it can be concluded that during electrical stimulation the charge transfer takes place due to capacitive/non-faradaic reactions.

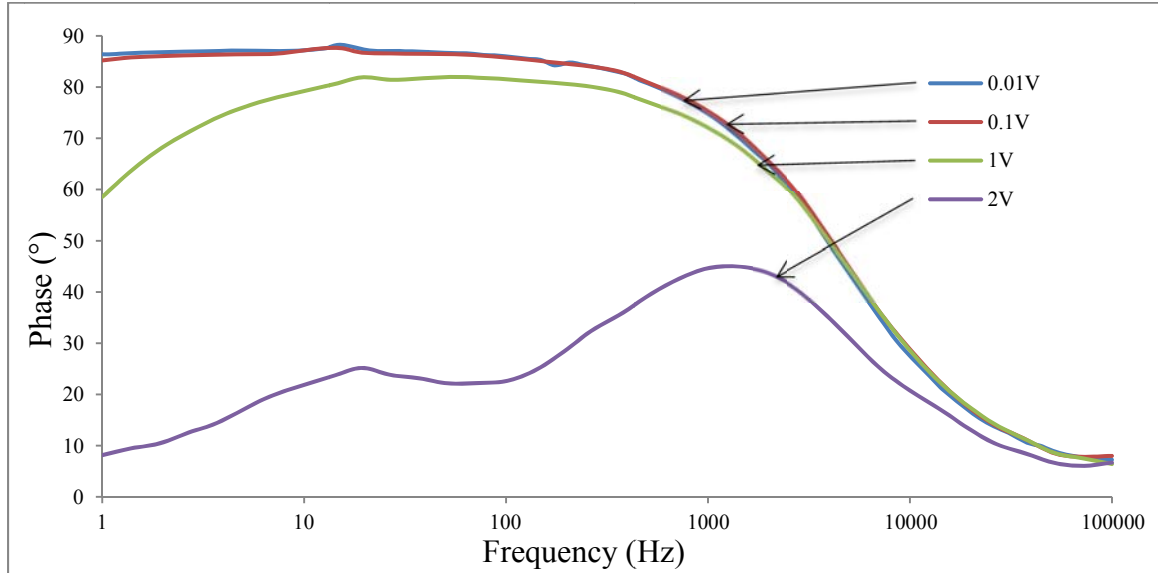


Figure 4.9: Individual EIS phase plots for P-MEA-S in DMEM media at 0.01, 0.1, 1, and 2 volts. Note the downward shift in the phase plot at 2 volts consistent with the loss of capacitive performance.

The EIS data was analyzed and fitted to the chosen model using an ‘EIS Spectrum Analyzer’ (Table 4.1). The elements R1 and C1 represent the WE, R2 and C2 represent the CE, and ‘ $\eta$ ’ is a correction factor which displays how closely the interface resembles a capacitor. R1 also represents the electrode polarization resistance ‘ $R_p$ ’, which indicates the electrode’s ability to resist degradation [57]. Ideally, the value of R1 should be as high as possible. For input voltages of 0.01V, 0.1V & 1V, values of R1 were consistently high, representing favorable device performance. However, data at 2V was consistent with electrode deterioration due to the low polarization resistance value. R2 and C2 were consistent across all voltage ranges.

The EIS data and fitted model values indicate that the P-MEA electrodes should be able to function within the range of 1V without causing cell or tissue damage.

Table 4.1: Equivalent circuit parameters for an idealized P-MEA. R1 & C1 form the working electrode (small pads), R2 & C2 form the counter electrode (large pads) and Rs is the solution resistance.

V <sub>in</sub>	RS	R1	R2	C1	η <sub>1</sub>	C2	η <sub>2</sub>
(V)	(Ω)	(Ω)	(Ω)	(F)	(%)	(F)	(%)
0.01	2.46E+02	2.22E+06	1.21E+03	3.14E-07	0.88	2.27E-06	0.73
0.1	2.59E+02	4.30E+06	1.10 E+03	3.28E-07	0.88	1.01E-06	0.81
1	2.95E+02	1.57E+06	1.86 E+03	2.57E-07	0.93	7.73E-06	0.88
2	2.13E+02	5.37E+03	1.01 E+03	2.31E-07	0.67	2.14E-05	0.60

## CHAPTER V

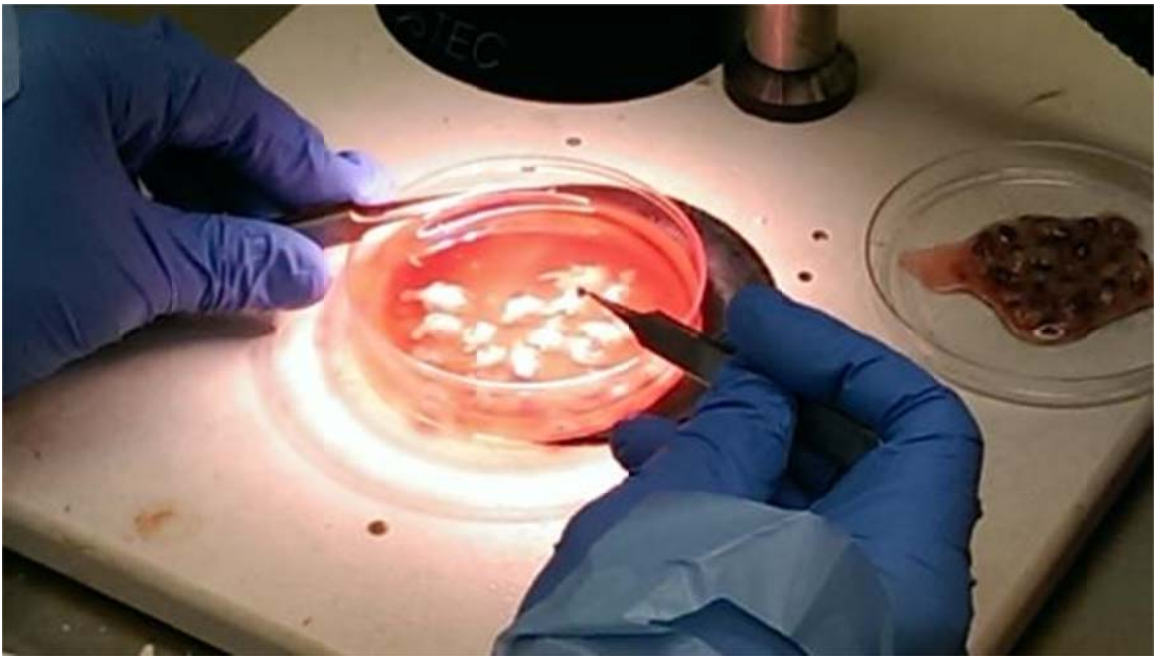
### ENGINEERED CARDIAC TISSUE

#### 5.1 Cell Isolation and Implant Creation

Engineered Cardiac Tissue (ECT) was created from cardiac cells isolated from embryonic chick hearts. Cells were derived from embryonic chick ventricles to construct each ECT as previously published by Tobita [40]. Fertile White Leghorn chicken eggs were incubated in a forced-draft, constant-humidity incubator until Hamburger-Hamilton (HH) stage 31 (day 7 of a 21-day incubation period). The embryos were removed from the eggs and the heart was separated to excise the ventricles (Figure 5.1). Excised embryonic ventricles were enzymatically digested by using 2mg/ml of collagenase type II followed by 0.05% trypsin-EDTA solution (Invitrogen, Carlsbad, CA). Isolated cells were preplated (filtering process) for 1 hour to reduce the non-cardiac cell population, large debris, and red blood cells. The isolated cells were then cultured on a gyratory shaker (60–70 rotations/min) for 24h to re-aggregate viable CMs. Approximately ( $3 \times 10^6$ ) cells/ml were mixed with acid-soluble rat-tail collagen type I (Sigma, St. Louis, MO) and matrix factors (Matrigel, BD Science, Franklin Lakes, NJ).



(a)



(b)

Figure 5.1: (a) Embryos being removed from fertile day-7 incubated chick eggs. (b) Heart excised from day-7 embryos.

The following cell/matrix mixture was made:

- 1) Isolated cells were suspended within a standard culture medium (Modified Dulbecco's Essential Medium, Invitrogen) containing 20% FBS (Invitrogen).
- 2) Acid-soluble collagen type I solution (pH 3) was neutralized with alkali buffer (0.2 M NaHCO<sub>3</sub>, 0.2 M HEPES, 0.1 M NaOH) on ice.
- 3) Matrigel (17% of total volume, BD Sciences) was added to the neutralized collagen solution.
- 4) Cell suspension and matrix solution were gently mixed. The final concentration of collagen type I was 0.67 mg/ml.

Cylindrical-shaped ECT were constructed using a collagen type I-coated silicone membrane culture plate (Tissue Train, Flexcell International, Hillsborough, NC) and FX-4000TT system (Flexcell International). The center of the Tissue Train culture plate silicone membrane was deformed by vacuum pressure to form a 20mm x 2mm trough using a cylindrical loading post (Tissue Train and FX-4000TT). The P-MEA device was then positioned across the vacuum-formed trough with the small exposed electrodes located directly above the trough (Figure 5.2 (a&b)). Approximately 200  $\mu$ l of cell/matrix mixture was poured into the trough (Figure 5.2 (b)) and the composite structure was then incubated for 120 minutes in a standard CO<sub>2</sub> incubator (37°C, 5% CO<sub>2</sub>) to form a cylindrical-shaped construct. Both ends of the construct were held by anchors attached to the Tissue Train culture plate (Figure 5.2 (c)). Once the ECT containing the P-MEA device solidified, the vacuum pressure was gradually released (Figure 5.2 (d)). The culture plate well was then filled with a growth medium containing 10% FBS and 1% chick embryo extract (SLI, Horsted Keynes, UK), and the ECT construct floated within

the growth medium with end attachments to the Tissue Train plate (Figure 5.2 (e)). Culture medium was changed every other day for the duration of in vitro culture.

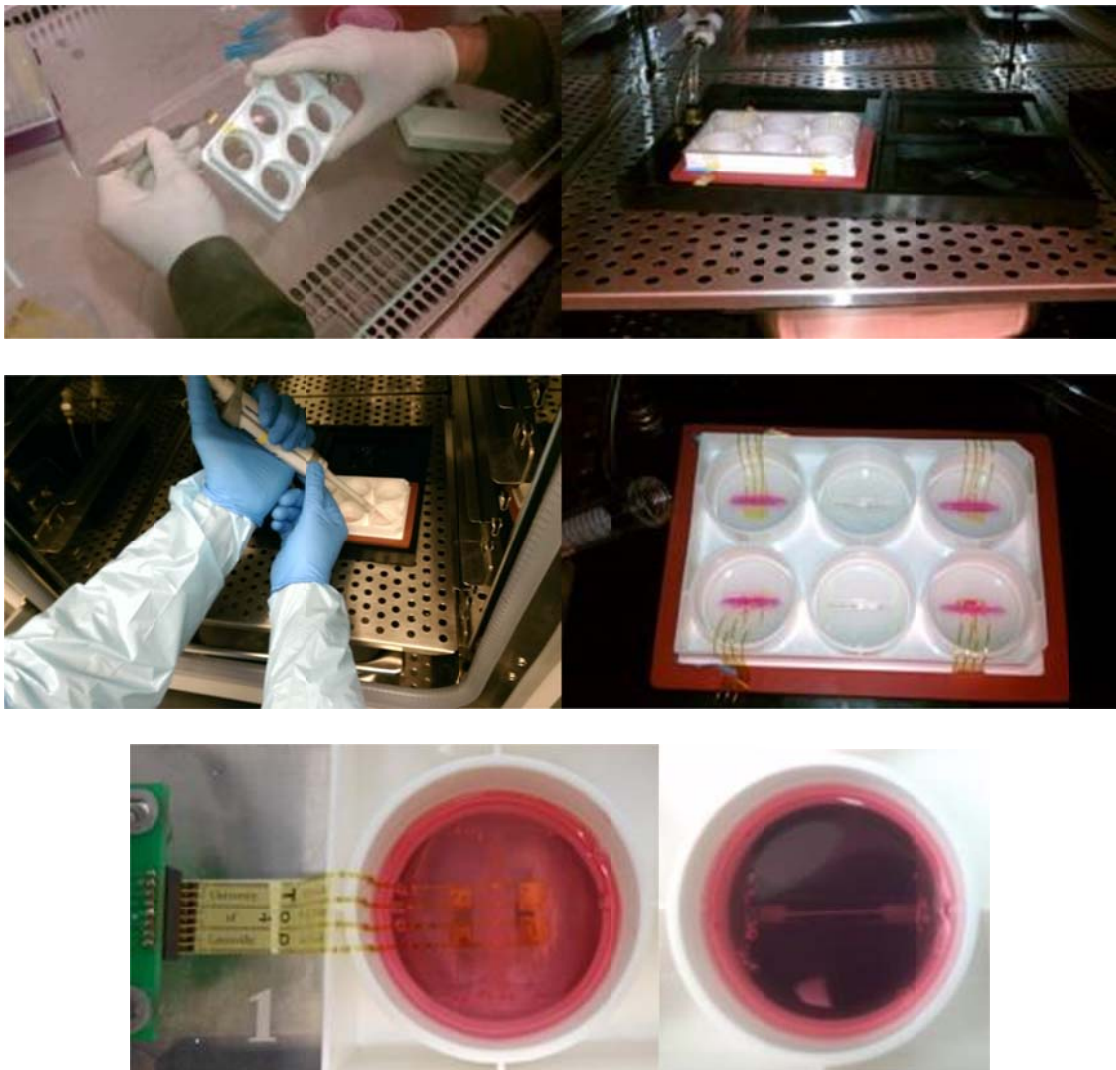


Figure 5.2: (a-d) (clockwise from top left): (a) Positioning the P-MEA device (version 2) in a tissue culture plate. (b) Culture plate on the tissue train base plate. (c) Depositing the chick cardiac cell derived ECT gel construct. (d) The chick ECTs after polymerization, note the vacuum-created trough in the empty wells. (e) (Version 3) P-MEA embedded ECT filled with culture medium and an ECT without an embedded P-MEA.

## 5.2 Electrical Stimulation

The ECT samples were divided into three groups and named accordingly;

[1] Control (had no embedded P-MEA)

[2] Sham (were embedded with P-MEA, no chronic electrical stimulation)

[3] P-MEA-Paced (embedded with P-MEA, chronic electrical stimulation).

The electrical stimulation experiments consisted of two separate but related protocols; chronic pacing and acute pacing. An isolated programmable stimulator from Coulbourn Instruments (model A13-65, Lehigh Valley, PA) was used to generate 1V amplitude, biphasic pacing pulses with a pulse width of 1ms duration for both, positive and negative pulses (Figure 5.3). The acute pacing protocol was used to determine maximum pacing rates and minimum threshold capture voltages on days 3, 5, 7 & 10 of culture. The applied input frequency was 2Hz, which translated to 120 beats per minute (bpm). The minimum threshold voltage was determined as the lowest voltage required to elicit a response of 120BPM from the ECT. Then the input voltage was fixed at 1V and the frequency was increased in small steps above 2Hz. The tissue response was noted for every stimulus until the tissue was no longer able to capture the external stimulus to determine the maximum capture rate. Chronic pacing was initiated on day 3 of culture using a 1V, 2Hz, biphasic stimulus and applied continuously from culture day 3 to day 10. The P-MEA-paced ECTs were subject to both, chronic as well as acute pacing while the sham ECTs were only subject to acute pacing on the same culture days. Intrinsic beat rates for all three groups were observed and recorded on days 3, 5, 7 & 10. A total of 60 samples were tested, including 25 P-MEA-paced, 25 controls and 10 shams. ECTs which had diminished contraction capability (due to cell-cell coupling or other factors) were

discarded and not included in the report. ECTs that did not have data for all four days were not included as well. In addition, some ECTs suffered from contamination which resulted in cell death and tissue necrosis; these were not included in the data reported.

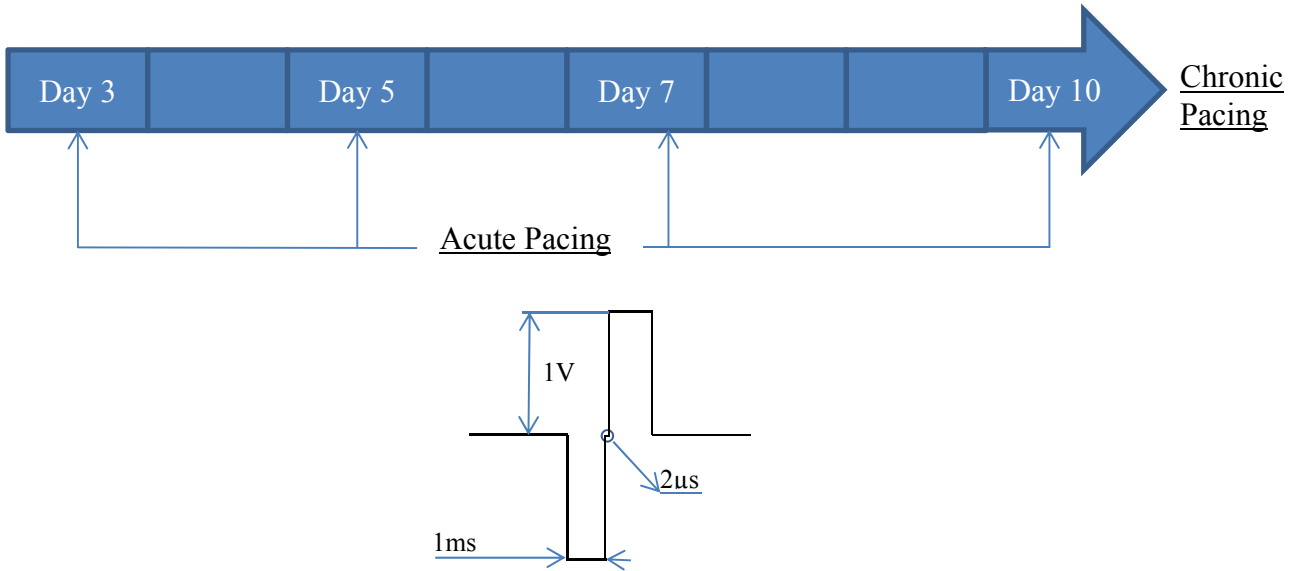


Figure 5.3: The pacing protocol and the electrical stimulus applied across the ECT. Biphasic pulse of 1ms (negative and positive each) with a 2 $\mu$ s pulse gap. Initial stimulation frequency was 2Hz and was varied depending on the experiment.

Table 5.1 (a): Intrinsic beat rates for Control ECTs (all values in bpm).

Sample No.	Day 3	Day 5	Day 7	Day 10
1	56.00	46.00	48.00	48.00
2	40.00	56.00	50.00	80.00
3	34.00	36.00	36.00	36.00
4	48.00	64.00	58.00	58.00
5	50.00	56.00	36.00	34.00
6	58.00	68.00	60.00	44.00
Average	47.67	54.33	48.00	50.00
Std. Dev.	9.24	11.76	10.35	17.06
Std. Error	$\pm 3.77$	$\pm 4.80$	$\pm 4.23$	$\pm 6.97$

Table 5.1 (b): Intrinsic beat rates for Sham ECTs (all values in bpm).

Sample No.	Day 3	Day 5	Day 7	Day 10
1	16.00	56.00	56.00	54.00
2	68.00	68.00	52.00	62.00
3	46.00	36.00	44.00	42.00
4	72.00	52.00	32.00	76.00
5	38.00	86.00	50.00	44.00
6	68.00	68.00	50.00	54.00
Average	51.33	61.00	47.33	55.33
Std. Dev.	22.08	17.05	8.45	12.50
Std. Error	±9.01	±6.96	±3.45	±5.10

Table 5.1 (c): Intrinsic beat rates for P-MEA-paced ECTs (all values in bpm).

Sample No.	Day 3	Day 5	Day 7	Day 10
1	72.00	66.00	88.00	92.00
2	30.00	48.00	46.00	72.00
3	68.00	74.00	88.00	74.00
4	68.00	34.00	38.00	8.00
5	68.00	20.00	52.00	12.00
6	58.00	60.00	58.00	10.00
7	74.00	64.00	66.00	64.00
8	30.00	54.00	70.00	66.00
9	24.00	68.00	74.00	82.00
10	72.00	58.00	62.00	60.00
11	74.00	64.00	66.00	66.00
12	22.00	36.00	76.00	74.00
13	48.00	42.00	72.00	74.00
Average	54.46	52.92	65.85	58.00
Std. Dev.	20.74	15.91	14.84	28.55
Std. Error	±5.75	±4.41	±4.12	±7.92

Table 5.1 lists the intrinsic beat rates for control (n=6), sham (n=6) and P-MEA-paced (n=13) ECTs. Comparing the data from the table, it was evident that embedment of the P-MEA device does not cause any adverse effects in the contraction of the ECT. In fact, the reverse was true, since the intrinsic beat rates were higher in nearly all cases. The intrinsic beat rates obtained were higher for sham and P-MEA-paced ECTs compared to control ECT by an average value of 8bpm (Figure 5.4). This could be attributed to the increased stiffness as a result of the tissue encapsulation around the P-MEA. The values of control and sham ECTs were similar with the shams having higher values. The P-MEA-paced ECTs varied significantly on day 7, an effect that can be attributed to the chronic electrical stimulus being applied to the tissue.

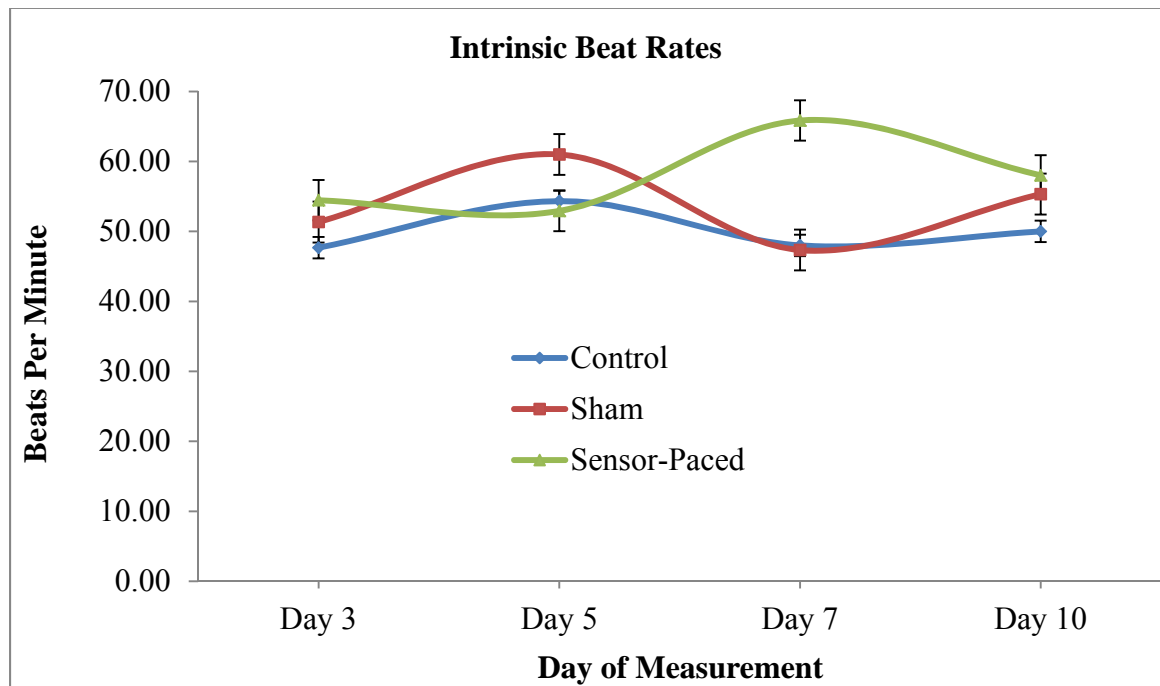


Figure 5.4: Chart comparing intrinsic beat rates for all three groups. P-MEA embedded ECTs have higher beat rates than control ECTs.

Table 5.2: Maximum pacing rates for P-MEA-paced ECTs (all values in bpm).

Sample No.	Day 3	Day 5	Day 7	Day 10
1	272.00	352.00	428.00	286.00
2	316.00	286.00	222.00	250.00
3	240.00	316.00	352.00	300.00
4	286.00	334.00	352.00	375.00
5	352.00	352.00	352.00	333.00
6	232.00	210.00	274.00	232.00
7	180.00	300.00	274.00	274.00
8	300.00	261.00	262.00	250.00
9	180.00	316.00	316.00	261.00
10	300.00	316.00	316.00	286.00
11	300.00	316.00	316.00	286.00
12	274.00	334.00	354.00	316.00
13	274.00	376.00	354.00	316.00
Average	269.69	313.00	320.92	289.62
Std. Dev.	50.31	42.95	53.45	38.98
Std. Error	±13.95	±11.91	±14.82	±10.81

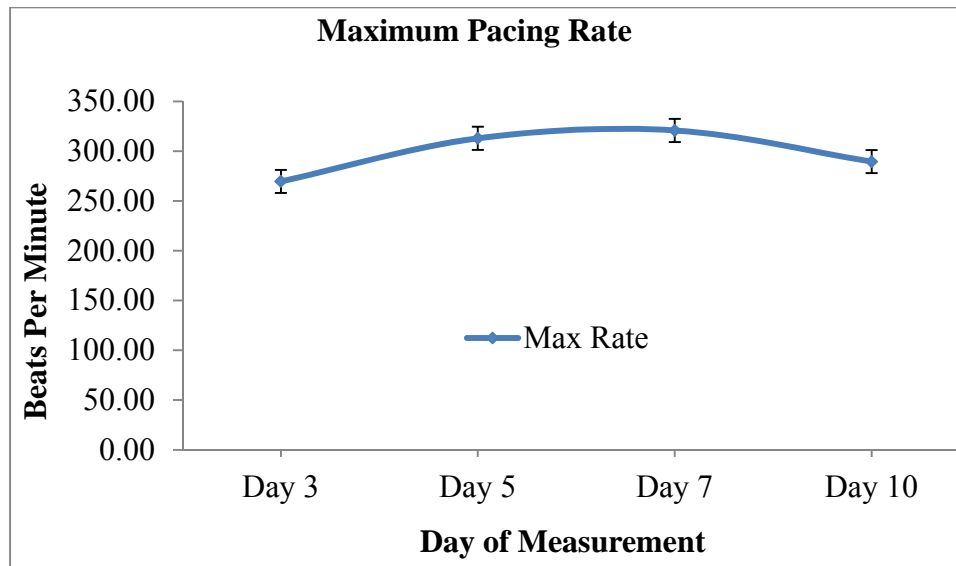


Figure 5.5: Chart showing maximum pacing rates of chronically stimulated ECTs. Max rates peak at day 7 and decline thereafter.

Table 5.3: Minimum threshold voltages (in volts) for P-MEA-paced ECTs at 120bpm.

Sample No.	Day 3	Day 5	Day 7	Day 10
1	0.60	0.60	0.50	0.70
2	0.40	0.50	0.50	0.60
3	0.40	0.30	0.35	0.50
4	0.30	0.25	0.35	0.45
5	0.25	0.40	0.35	0.35
6	0.30	0.30	0.35	0.40
7	0.50	0.30	0.25	0.30
8	0.25	0.40	0.40	0.30
9	0.30	0.40	0.35	0.30
10	0.40	0.40	0.40	0.50
11	0.30	0.30	0.35	0.40
12	0.30	0.50	0.40	0.40
13	0.20	0.50	0.30	0.30
Average	0.35	0.40	0.37	0.42
Std. Dev.	0.11	0.11	0.07	0.13
Std. Error	0.03	0.03	0.02	0.03

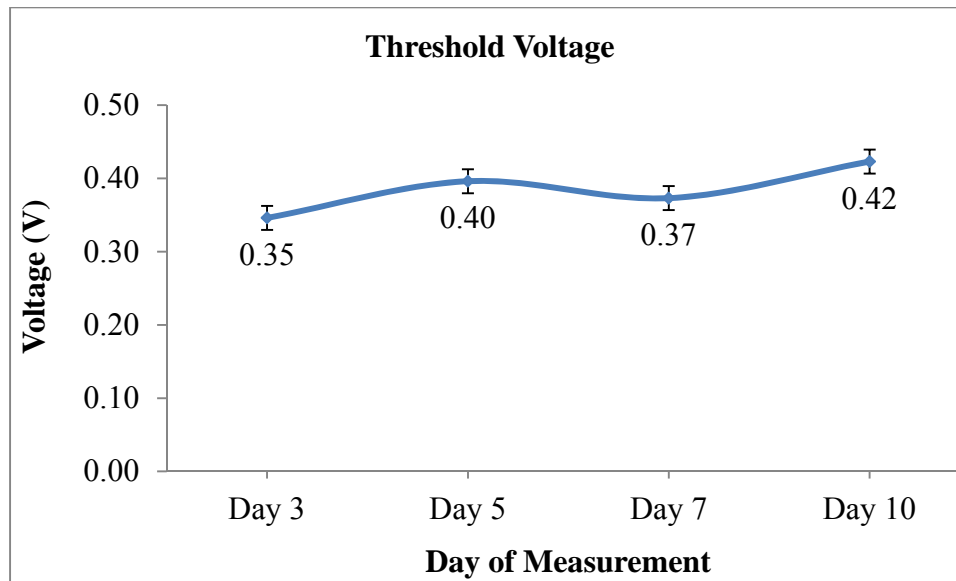


Figure 5.6: Minimum threshold voltage for ECT capture at 120bpm; well below 0.5V.

The conclusive evidence of functionality of the P-MEA can only be determined from the ability of the device to stimulate, pace, and capture live tissues. Successful and consistent stimulation of tissues was accomplished using the P-MEA device with voltages ranging from 0.35V to 0.42V. Compared to voltages used by other research groups [], the obtained average threshold voltage of 0.4V (using the P-MEA) was much lower than the water electrolysis voltage and much lower than the target of 1V (Table 5.3 & Figure 5.6). This results in a huge advantage over existing methods in terms of stability of the culture medium and tissue contamination due to byproducts because of higher voltages. Maximum pacing capture rates follow an increasing trend with the highest values reached on day 7, which align well with the highest rates of intrinsic contraction also recorded on day 7. The tissue seems to be maturing and reaching a peak at or around day 7 of tissue culture.

### 5.3 Histological and Immunofluorescence Staining

Histological staining and analysis was performed on ECT samples after the end of the 10-day culture period. Day 10 ECT samples were fixed with 4% paraformaldehyde at room temperature for 15 minutes and embedded in paraffin blocks. 4 $\mu$ m serial sections were cut longitudinally for histological staining. Hematoxylin-Eosin (HE) staining was performed and light micrographs were taken using Nikon Eclipse E600 microscope. The images were captured by SPOT color camera operated by Spot Advance software. ECT slides were treated with 0.1 M Glycine and 0.5% Triton X-100 for 30 minutes at room temperature after slides were de-waxed, hydrated and rinsed in 1xPBS for three times. 5-Ethynyl-2'-Deoxyridine (EdU) (a marker for cell proliferation) staining was performed

according to Click-iT EdU Imaging Kits protocol (Invitrogen, C10339), then mouse monoclonal anti-Troponin T (Thermo, Cat# Ms-295-p0) 1:400 in 1%BSA was applied to the tissue sections overnight, followed by Alexa Fluor 488-conjugated donkey anti mouse 1:400 (Life Technologies). Slides were mounted with ProLong® Gold Antifade Reagent (Life Technologies). Immunofluorescent images were collected using (1) a Nikon Eclipse E800M microscope with dry 10x, 20x, 40x Plan Fluor objective lens with 0.75 NA and Qlympus DP72 camera to generate images with a 1360x1024 pixel density, or (2) a Nikon Eclipse Ti Confocal System attached to a Nikon Ti-E inverted microscope platform and Nikon Plan Apo 60x oil DICH objective lens with 1.4 NA to capture images with a 2048x2048 pixel density. 10 regions per section were imaged in a blinded fashion and analyzed using NIH 'Image J' software to count TnT and EdU positive cells to assess cell number, identity, and proliferation rates. The software was used to perform manual counting of cell nuclei, identify cardiomyocytes and proliferating cells. In addition, counting was performed using an algorithm written by Will J. Kowalski [originally published by Xu, F., Beyazoglu, T., Hefner, E., Gurkan, U.A., and Demirci, U. (2011)].

Figure 5.7 (a-i) shows representative histologic samples. 'Control' ECTs did not have embedded P-MEAs, 'Sham' ECTs (P-MEA Non-Paced) had non-stimulated embedded devices, and 'P-MEA Paced' had stimulated P-MEA. The physical shape of the control ECT was cylindrical with the ends being splayed and nearly flat as they grab hold of the tabs. ECTs were cylindrical between the device arms and splayed and flat immediately adjacent to the embedded pads. The tissue was sliced longitudinally and 10 random areas of each section were examined. The control samples had myocardial tissue with cardiomyocytes (CM) predominantly aligned along the longitudinal axis. The sham and

P-MEA-paced ECT cardiomyocytes were aligned according to the preferential electric field generated by the applied electrical stimulus. Since there were four embedded pads and four external pads for the return electrode the electric fields are varied. Cardiac Troponin-T (TnT) staining identified myofibers in the tissue aligned along the longitudinal tissue axis in all three groups. DAPI images showed the total cell nuclei (blue color) and the merged image shows TnT with DAPI and 5-Ethynyl-2'-Deoxyridine (EdU). Cell counts indicated that an average of  $76 \pm 2\%$  of the cells were cardiac vs.  $24 \pm 2\%$  non-cardiac. Cardiac cell proliferation was found to be very low; Control  $2 \pm 1\%$  (n=4), Sham  $5 \pm 2\%$  (SE) (n=4), and P-MEA Paced  $1 \pm 0\%$  (SE) (n=8). Electrical stimulation of ECT (created from embryonic cells) had negligible effect on cell proliferation in the tissue.

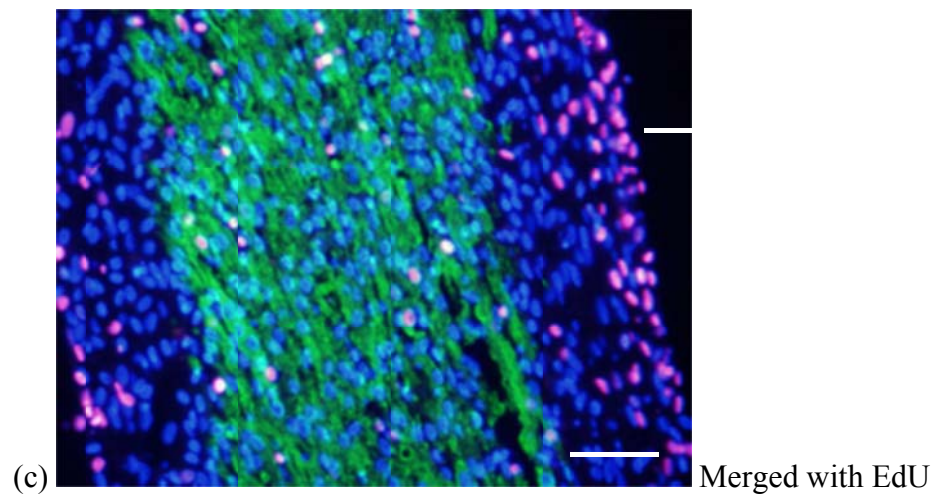
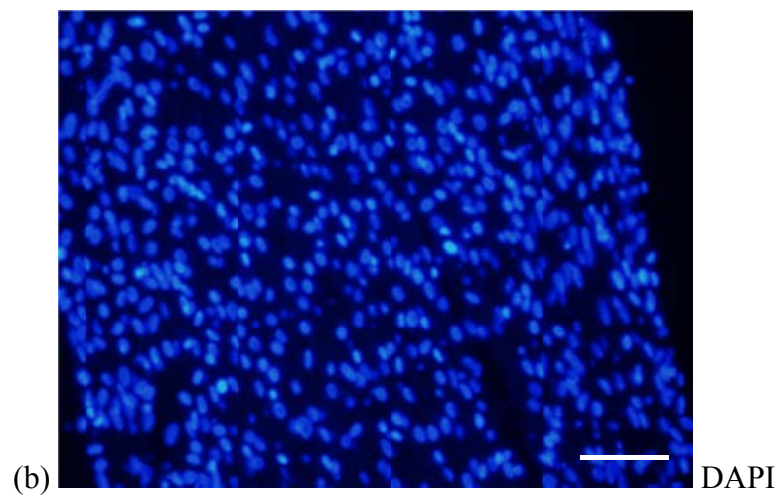
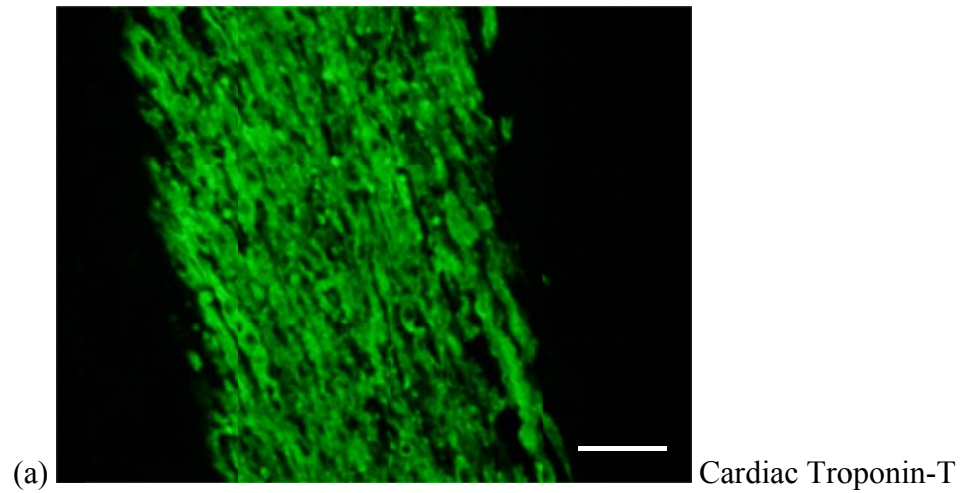


Figure 5.7 (a-c): ECT myofiber cellular distribution for Control ECT at day 10. Cardiac Troponin-T (TnT-Green). Nuclei (DAPI-blue). Proliferating cells (EdU – red). (all images at 40x magnification, scale bar represents 50 $\mu$ m).

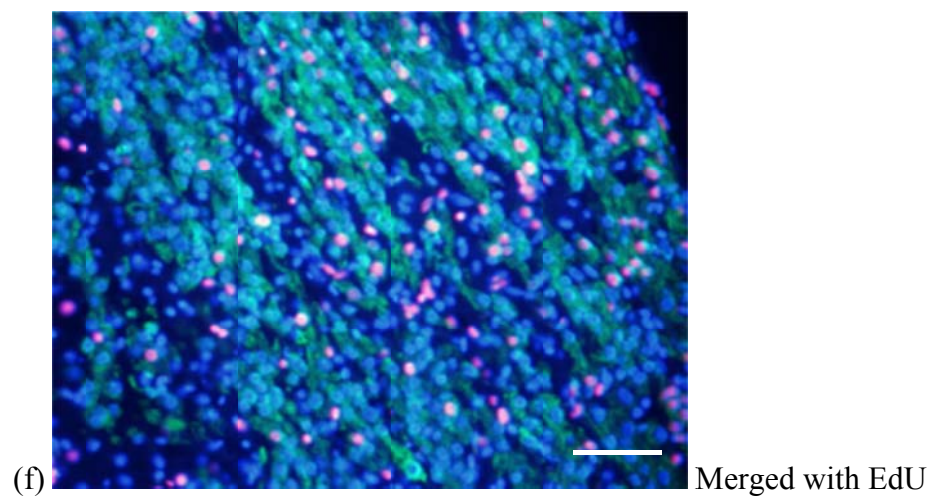
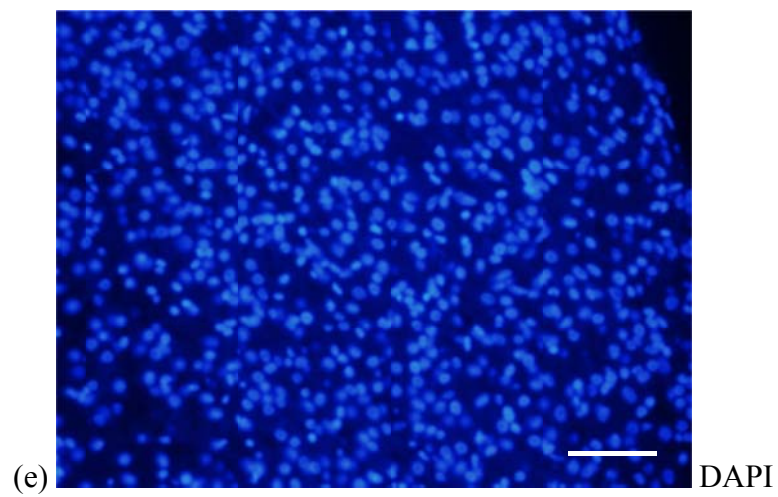
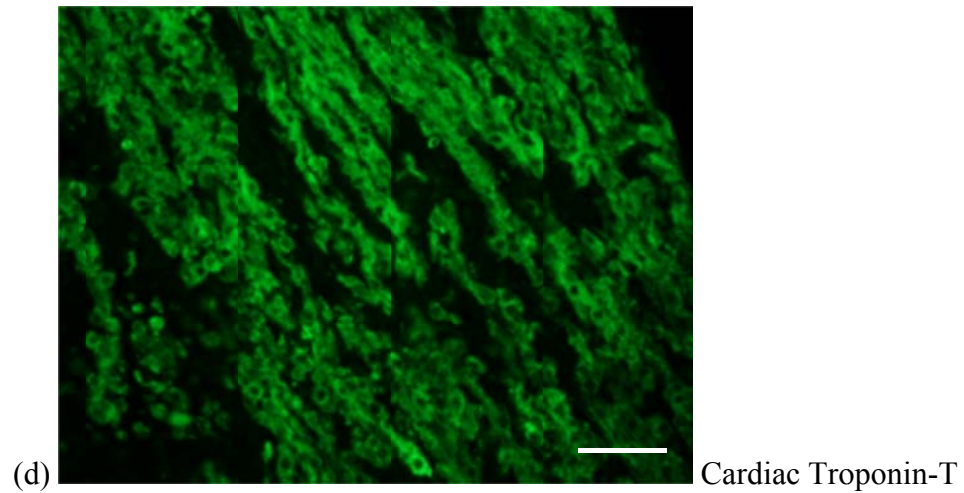


Figure 5.7 (d-f): ECT myofiber cellular distribution for Sham ECT at day 10. Cardiac Troponin-T (TnT-Green). Nuclei (DAPI-blue). Proliferating cells (EdU – red). (all images at 40x magnification, scale bar represents 50 $\mu$ m).

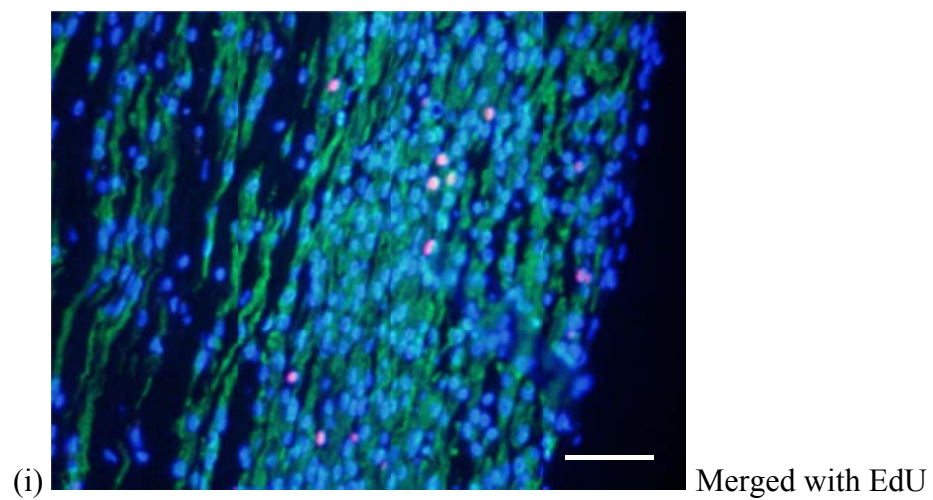
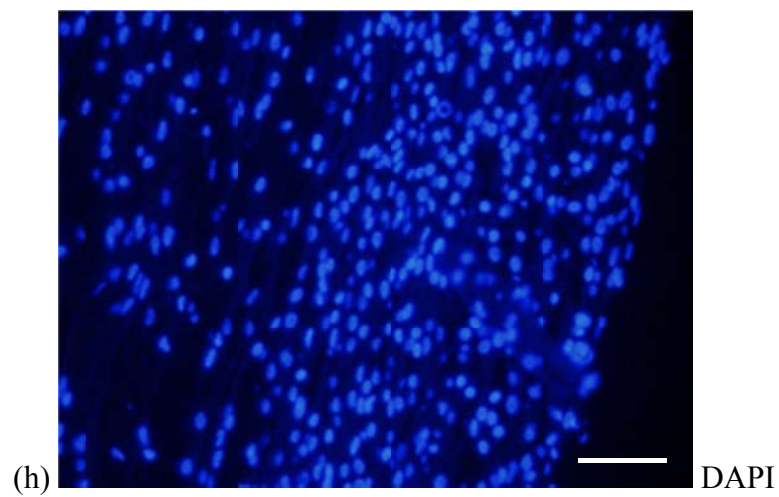
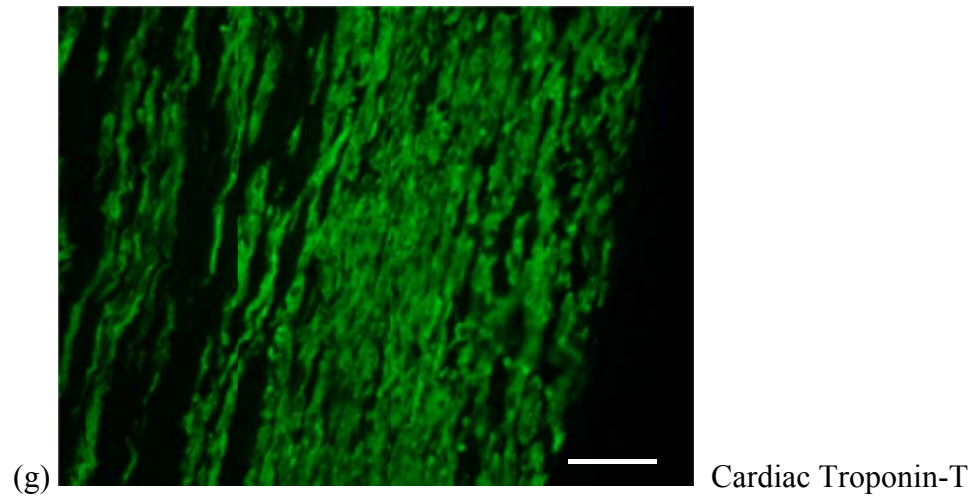


Figure 5.7 (g-i): ECT myofiber cellular distribution for P-MEA-paced ECT at day 10. Cardiac Troponin-T (TnT-Green). Nuclei (DAPI-blue). Proliferating cells (EdU – red). (all images at 40x magnification, scale bar represents 50 $\mu$ m).

#### 5.4 Contractile Force Measurement

Beating and contraction in a tissue generates force that can be measured and used as an evaluation marker for tissue maturation. Contractile force measurements were performed on the ECT using previously published methods []. The specimen was transferred to a dissection chamber filled with Tyrode solution containing (in mM) 119.8 NaCl, 5.4 KCl, 2.5 CaCl<sub>2</sub>, 1.05 MgCl<sub>2</sub>, 22.6 NaHCO<sub>3</sub>, 0.42 NaH<sub>2</sub>PO<sub>4</sub>, 0.05 Na<sub>2</sub>EDTA, 0.28 ascorbic acid, 5.0 glucose, and 30 2,3-butanedione monoxime (BDM), gassed with 95% O<sub>2</sub>-5% CO<sub>2</sub> (pH 7.4). The ECT was excised by severing the P-MEA where it exited the ECT, leaving only the embedded pads in the ECT (Figure 5.8). During a 30 minute equilibration period, the construct was field-stimulated with a signal frequency of 2 Hz at 5V (Aurora Scientific). The segment length of the tissue was gradually increased until total force reached maximum ( $L_{max}$ ). The external diameters of the tissue at each stretch increment were recorded by using a video microscopy system (SM-3T, Single Arm Boom Stand Trinocular Microscope, Amscope, Irvine, CA). At each pacing frequency measurements were taken for active force at  $L_{max}$  and passive force at  $L_{max}$ . Data is reported as mean  $\pm$  SE (standard error).



Figure 5.8: A P-MEA embedded ECT under force measurement. The remnants of the P-MEA can be seen in the still-embedded pads in the ECT. The left hook is attached to a force transducer and the right anchor is movable to stretch the ECT.

Figure 5.9 shows the active and total force generated by the ECT paced at 2Hz and 4Hz. Active stress can be calculated by dividing the recorded values with the Cross-Sectional Area (CSA) of the tissue as long as the geometry of the ECT is cylindrical. However, deformation of the ECTs was noted at the sites of P-MEA implantation such that CSA cannot be accurately determined (Figure 5.8). Higher total force was recorded, but similar active force generated by the sham and P-MEA-paced ECTs versus control ECTs. Average total force generated by control, sham and P-MEA-paced ECTs was [ $1.78\text{mN} \pm 0.22\text{mN}$  (SE) for 2Hz,  $1.70\text{mN} \pm 0.22\text{mN}$  (SE) for 4Hz]; [ $2.45\text{mN} \pm 0.31\text{mN}$  (SE) for 2Hz,  $2.38\text{mN} \pm 0.31\text{mN}$  (SE) for 4Hz]; [ $2.48\text{mN} \pm 0.27\text{mN}$  (SE) for 2Hz,  $2.40\text{mN} \pm 0.27\text{mN}$  (SE) for 4Hz] respectively. The higher total force in the P-MEA embedded ECTs may be due to increased ECT stiffness due to the presence of the P-MEA or to changes in the ECT material properties in response to chronic pacing. Electrical stimulation seems to have had a negligible effect on the force generation by the ECT. Additional experiments are required with variations in the number of embedded P-MEA arms and distance between P-MEA arms to determine a direct effect of embedded P-MEAs on ECT material properties.

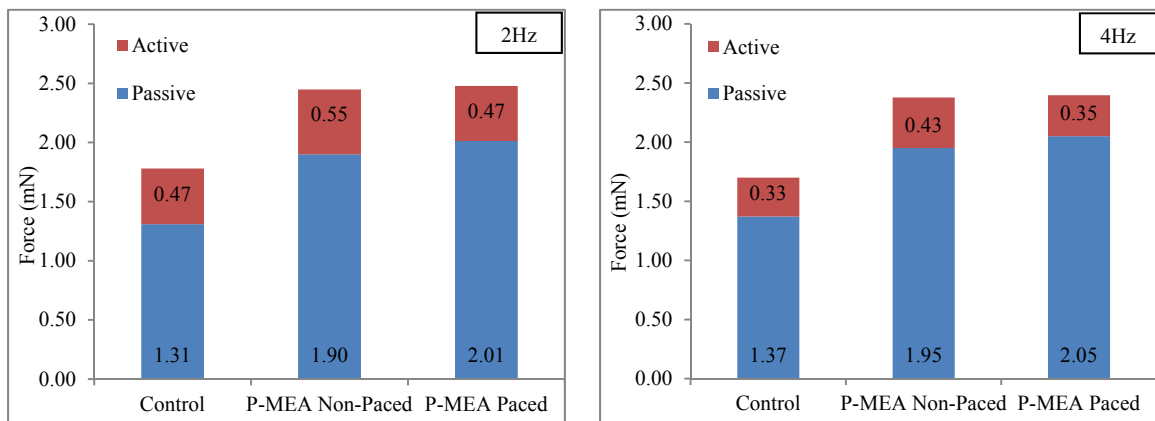


Figure 5.9: ECT force recordings. Passive and active total force generated by the ECT paced at 2 and 4 Hz (all force values in mN).

## CHAPTER VI

### CONCLUSION

#### 6.1 Device success and shortcomings

A novel device capable of low-voltage electrical stimulation of engineered cardiac tissue has been designed, fabricated, and validated. The primary advantage of this device is the ability to successfully stimulate ECT at a voltage of 0.5V, which is 10 times lower than current methods. The low voltage minimizes any undesirable oxidative by-products in the culture environment or cell injury. In addition, a number of features relevant to in vitro as well as in vivo applications have been incorporated. The device was shown to be thin and flexible enough for embedment and robust enough to accomplish tissue capture over a period of several days (*primary hypothesis proven, corollary 1 & 2*).

The P-MEA device has undergone three major transitions during its development (Figure 6.1). version 1 was used to determine physical dimensions and drawbacks and contained no electrodes; version 2 was designed with electrodes and used for embedment and stimulation. One major flaw with version 2 was its inability to stimulate at a low voltage. This was due to the method of stimulus application. The two outer arms (two electrodes each) were used as the working and return electrodes for delivering the stimulus. The higher voltages (3V) required to elicit a response caused electrode deterioration and resulted in undesirable byproducts being released into the culture medium, which in turn resulted in cell death and tissue damage as shown in Figure 6.2.

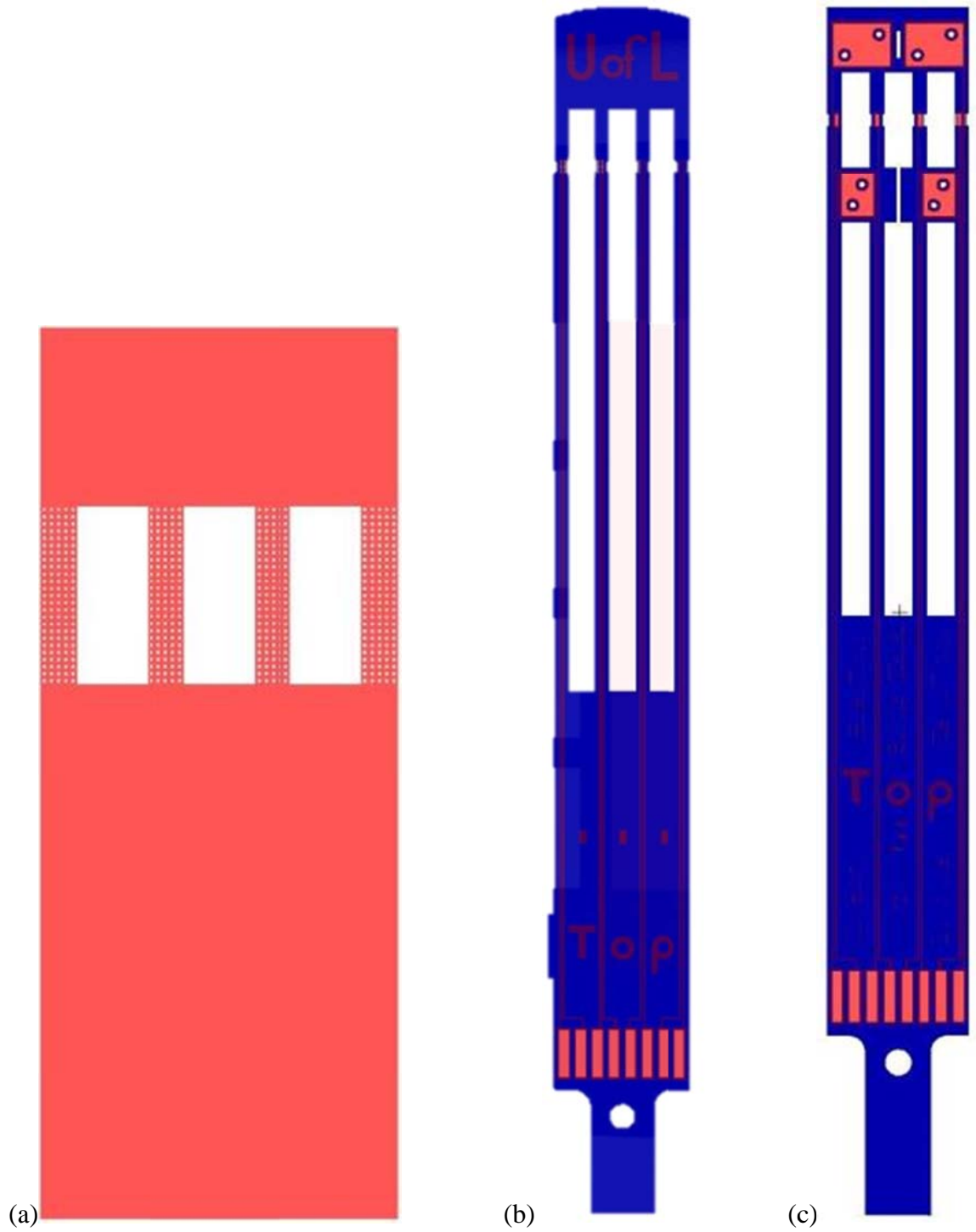


Figure 6.1: Evolution of the P-MEA design over three major iterations (not to scale);  
(a) version 1, (b) version 2, (c) version 3.

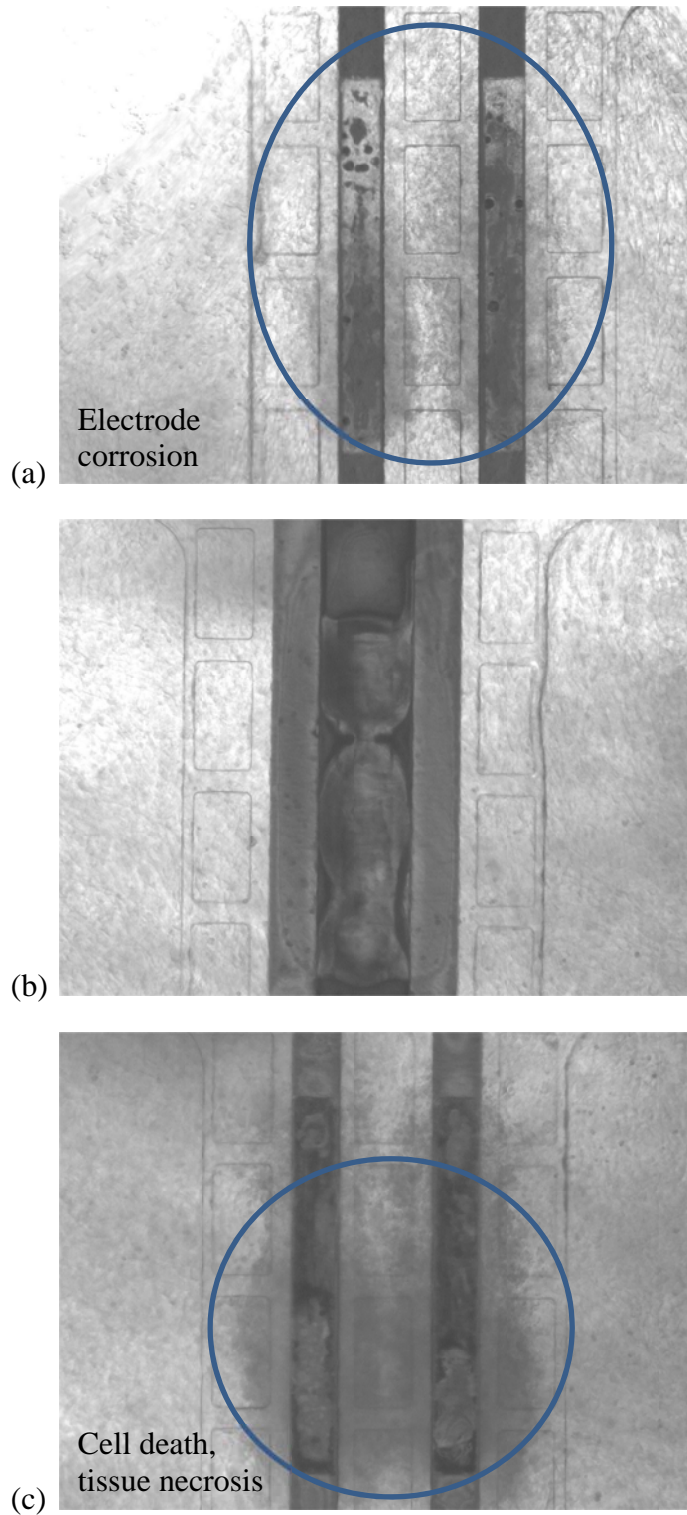


Figure 6.2: Electrode deterioration in version 2 of P-MEA; undesirable byproducts released into the medium leading to cell death and tissue necrosis (encircled dark/shadowed region).

Version 3 of the P-MEA was developed to overcome the problems caused by version 2. This included a change in the design as well as the stimulation philosophy. Instead of using the embedded pads as return electrodes, a change was made to separate and reposition the return electrodes outside the ECT. This major change allowed an increase in the area of the electrodes which resulted in a decrease in the required voltage. version 3 of the P-MEA has lasted for a duration of 2 weeks continuous in-vitro application without any corrosive effects (*specific aim 1 accomplished*).

The fabrication process flow was developed and refined over the evolution of the design to obtain a high yield of devices. This process is now transferred to a manufacturing foundry (MNTC, Louisville) (*specific aim 2 accomplished*).

Electrochemical characterization was performed on the P-MEA by conducting electrochemical impedance spectroscopy experiments. The data generated during these experiments was analyzed and computed using a simulation software to generate element values for an equivalent electrical model (*specific aim 3 accomplished*).

Histological staining and force measurements did not reveal any substantial differences between the paced ECT and non-stimulated controls. Cardiac cell proliferation was found to be very low in stimulated ECT. Force measurements for embedded ECT were higher than control ECT but with negligible differences between stimulated and non-stimulated. Thus the conclusion is that electrical stimulation did not have any appreciable effect on the functional maturation of embryonic cell cardiac tissue. (*corollary 3 disproven/negative*).

One of the drawbacks of the P-MEA is that its embedded nature caused minor changes in ECT form and structure. Since the ECT was separated by the P-MEA device arms, it caused a 'splayed' effect between each pair of the arms. Without a disruption, the ECT compacts physically to result in a cylindrical structure. The embedment resulted in a thinning of the ECT; instead of a circular cross-section it caused a flatter and wider physical layout. In several ECT, thinning associated with P-MEA embedding resulted in the inadvertent removal of the P-MEA out of the ECT (Figure 6.3).

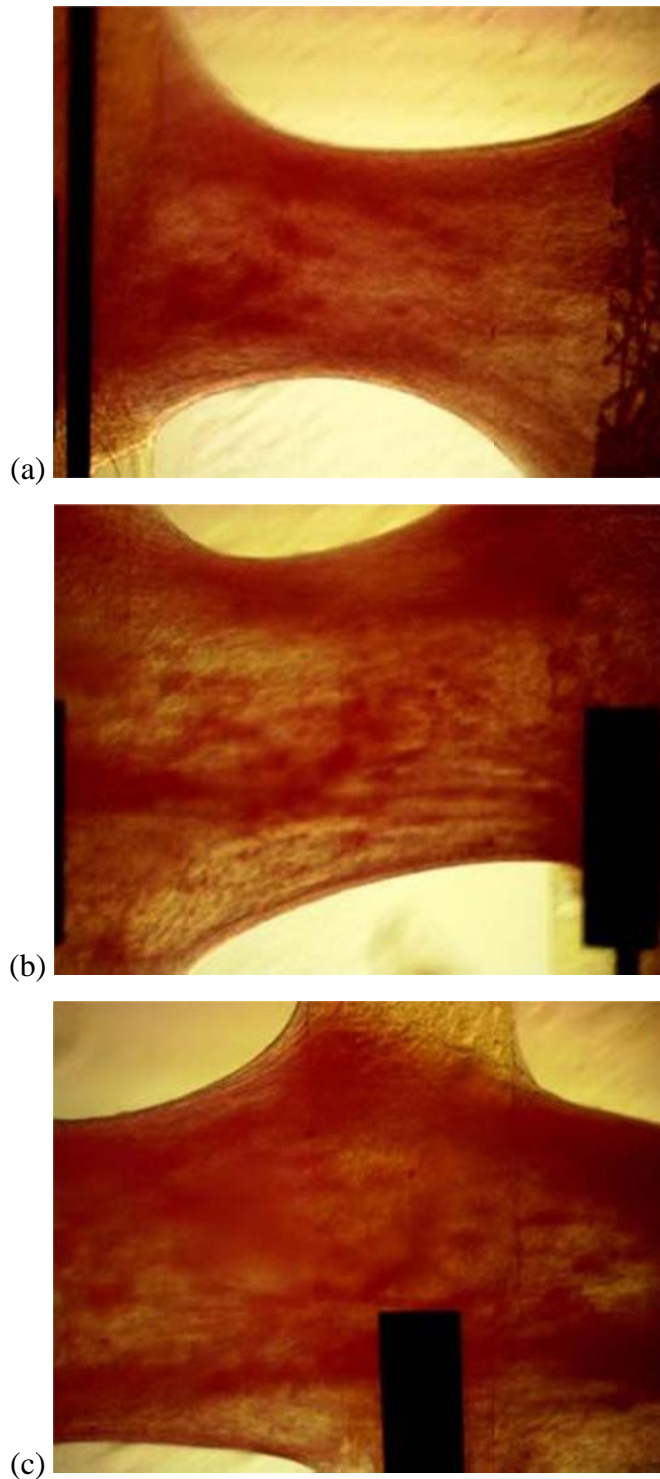


Figure 6.3: (a) Splayed effect caused by embedment of the P-MEA (b) Thinning of ECT resulted in the ECT being separated from the pad (c) ECT encapsulated around one arm of the P-MEA.

## 6.2 Current and Future Work

Ongoing applications of the P-MEA include using the P-MEA to stimulate cardiomyocyte (CM) maturation in stem cell derived ECT where CM maturation is known to be delayed. Some research groups have shown maturation of stem cell derived tissue using electrical stimulation. Currently, the P-MEA is being used for in-vitro stimulation of two types of stem cell ECT; (1) Human Induced Pluripotent Stem (IPS) cells and (2) Mouse Adipose Stem Cells (ASC). Observed stimulation voltages range from 0.9V-3V for the IPS ECT and 0.5V-1V for ASC ECT.

Current and future work involves implantation of P-MEA embedded ECT onto the rat epicardium to test the ability to electrically couple implanted ECTs to the recipient myocardium. Once the P-MEA device embedded within the ECT becomes electrically coupled to the underlying epicardial tissues, the device should facilitate electrical pacing, mapping, and recording experiments. Pilot in vivo P-MEA embedded ECT implantation trials have been carried onto the surface of the adult rat myocardium similar to previously published method for ECT mediated cardiac repair [28] with the P-MEA device sutured on to the surface of a rat heart for a period of three weeks (Figure 6.4). High resolution ultrasound imaging during pacing protocols confirmed the electrical coupling of the P-MEA to the recipient heart. Pilot trials have shown the ability of the P-MEA to survive implantation in vivo for the duration of the three week experiment, though additional experiments are required to fully assess P-MEA biocompatibility and functional coupling. These data will be valuable in guiding the pre-clinical translation of this approach.



Figure 6.4: A P-MEA device implanted onto the surface of an adult rat heart. This particular device was sutured on the infarcted myocardium and placed for three weeks.

One of the additional benefits of having an embedded device like the P-MEA is the ability to make physical contact with the cells. This allows for capture and recording of signals from the tissue. Future work utilizing the P-MEA could potentially utilize this benefit to record and measure depolarization, beat rates and conduction velocity. A National Instruments (hardware) system and LabVIEW (software) based interface is recommended for signal capture. A signal conditioning system at the front end would be required due to the expected small size of the signals.

### 6.3 Pending Outcomes

1. The following manuscript is in revision after a favorable review:

Trada H, Vendra V, Tinney JP, Yuan, FP, Jackson D, Walsh K, Keller BB. Implantable thin-film porous microelectrode array sensor (P-MEA-S) for electrical stimulation of engineered cardiac tissues. *BioChip Journal* (in revision, Dec. 2014).

2. Ongoing experiments are utilizing the P-MEA to evaluate the effect of chronic electrical stimulation on the structural and functional maturation of ECTs generated from human-iPS derived CM and murine-ASC derived CM. These studies will lead to additional publications where I will be a contributing author.
3. A provisional patent has been filed by UofL related to the reduction to practice of the P-MEA device.

## REFERENCES

1. A. Go et. al.; *Heart disease and stroke statistics—2014 update: a report from the American Heart Association. Circ.* 2014.
2. A. Guyton, J. Hall; *Textbook of Medical Physiology, 12<sup>th</sup> ed.* (2010), pgs. 101-113.
3. L. Sherwood; *Human Physiology From Cells to Systems, 7<sup>th</sup> ed.* (2010), pgs. 303-341.
4. N. Severs, The cardiac muscle cell. *Bioessays*, 2002, 22, 2.
5. P. Zammaretti, M. Jaconi; Cardiac tissue engineering: regeneration of the wounded heart. *Current Opinion in Biotechnology Current Opinion in Biotechnology*, 15(5), 430–434. (2004).
6. S. Dimmeler, A. Zeiher, and M. Schneider, Unchain my heart: the scientific foundations of cardiac repair. *Journal of Clinical Investigation*, 2005, 115, 3.
7. K. Ye, & L. Black, Strategies for Tissue Engineering Cardiac Constructs to Affect Functional Repair Following Myocardial Infarction. *Journal of Cardiovascular Translational Research*, 2011, 4, 5, 575-591.
8. B.B. Keller, L.J. Liu, J.P. Tinney, K. Tobita. Cardiovascular developmental insights from embryos. *Ann N Y Acad Sci.* 2007, 1101:377-88.
9. K. Clause, J. Tinney, L. Liu, B. Keller, K. Tobita, Engineered early embryonic cardiac tissue increases cardiomyocyte proliferation by cyclic mechanical stretch via p38-MAP kinase phosphorylation. *Tissue Eng. Part A Tissue Engineering - Part A.* 2009, 15(6), 1373–1380.
10. M. Radisic, H. Park, H. Shing, T. Consi, F. Schoen, R. Langer, L. Freed, G. Vunjak-Novakovic, Functional assembly of engineered myocardium by electrical stimulation of cardiac myocytes cultured on scaffolds. *Proc Natl Acad Sci.* 2004, 101(52), 18129–18134.
11. S. Nunes, J. Miklas, J. Liu, R. Aschar-Sobbi, Y. Xiao, B. Zhang, J. Jiang, S. Massé, M. Gagliardi, A. Hsieh, N. Thavandiran, M. Laflamme, K. Nanthakumar, G. Gross, P. Backx, G. Keller & M. Radisic, Biowire: a platform for maturation

- of human pluripotent stem cell-derived cardiomyocytes. *Nature Methods*. 2013, 10(8), 781–7.
12. H. Jawad, N. Ali, A. Lyon, Q. Chen, S. Harding and A. Boccaccini; Myocardial tissue engineering: a review. *Journal of Tissue Engineering and Regenerative Medicine* 2007; 1: 327–342.
  13. Y. Haraguchi, T. Shimizu, M. Yamato, and T. Okano; Concise review: cell therapy and tissue engineering for cardiovascular disease. *Stem Cells Translational Medicine*, 2012, 1 (2): 136-41.
  14. L. Lu, M. Mende, X. Yang, H-F Körber, H-J Schnittler, S. Weinert, J. Heubach, U. Ravens; Design and Validation of a Bioreactor for Simulating the Cardiac Niche: A System Incorporating Cyclic Stretch, Electrical Stimulation, and Constant Perfusion. *Tissue Engineering Part A*, 2013, 19, 403-414.
  15. G. Vunjak-Novakovic, N. Tandon, A. Godier, R. Maidhof, A. Marsano, T. Martens, and M. Radisic, Challenges in Cardiac Tissue Engineering. *Tissue Engineering, Part B: Reviews*. 2010, 16 (2): 169-187.
  16. M. Hirose, O. Kwon, M. Yamato, A. Kikuchi, and T. Okano; Creation of designed shape cell sheets that are noninvasively harvested and moved onto another surface. *Biomacromolecules*, 2000, 1 (3): 377-81.
  17. T. Shimizu, T. Okano; Tissue engineering for ischemic heart disease. *Nippon Rinsho*, 2003, 61 (4):710-715.
  18. T. Shimizu, M. Yamato, A. Kikuchi, T. Okano; Cell sheet engineering for myocardial tissue reconstruction. *Biomaterials*, 2003, (24):2309-2316.
  19. T. Shimizu, M. Yamato, Y. Isoi, T. Akutsu, T. Setomaru, K. Abe, A. Kikuchi, M. Umezu, T. Okano; Fabrication of pulsatile cardiac tissue grafts using a novel 3-dimensional cell sheet manipulation technique and temperature-responsive cell culture surfaces. *Circulation Research* 2002, 90:e40.
  20. T. Shimizu, M. Yamato, T. Akutsu, T. Shibata, Y. Isoi, A. Kikuchi, M. Umezu, T. Okano; Electrically communicating three dimensional cardiac tissue mimic fabricated by layered cultured cardiomyocyte sheets. *Journal of Biomedical Material Research* 2002, 60:110-117.
  21. M. Radisic and K. Christman; Materials science and tissue engineering: Repairing the heart. *Mayo Clinic Proceedings*. 2013, 88 (8): 884-898.
  22. L. Chiu, R. Iyer, J-P King, M. Radisic, Biphasic electrical field stimulation aids in tissue engineering of multicell-type cardiac organoids. *Tissue Engineering. Part A*. 2011, 17(11-12), 1465–77.

23. N. Tandon; *Biomimetic Electrical Stimulation for Cardiac Tissue Engineering*. Thesis--Massachusetts Institute of Technology, Dept. of Electrical Engineering and Computer Science, 2006.
24. N. Tandon, C. Cannizzaro, P-H Chao, R. Maidhof, A. Marsano, H. Au, M. Radisic, G. Vunjak-Novakovic, Electrical stimulation systems for cardiac tissue engineering. *Nature Protocols*. 2009, 4(2), 155–173.
25. N. Tandon, A. Marsano, C. Cannizzaro, J. Voldman, and G. Vunjak-Novakovic. Design of electrical stimulation bioreactors for cardiac tissue engineering". *Annual International Conference of the IEEE Engineering in Medicine and Biology Society. IEEE Engineering in Medicine and Biology Society. Annual Conference*. 2008: 3594-7.
26. N. Tandon, A. Marsano, R. Maidhof, L. Wan, H. Park, and G. Vunjak-Novakovic. Optimization of Electrical Stimulation Parameters for Cardiac Tissue Engineering. *Journal of Tissue Engineering and Regenerative Medicine*. 2011, 5, no. 6: e115-e125.
27. C. Cannizzaro, N. Tandon, E. Figallo, H. Park, S. Gerecht, M. Radisic, G. Vunjak-Novakovic, Practical aspects of cardiac tissue engineering with electrical stimulation. *Methods in Molecular Medicine*, 2007.
28. N. Tandon, B. Goh, A. Marsano, P. Chao, C. Montouri-Sorrentino, J. Gimble, and G. Vunjak-Novakovic. Alignment and Elongation of Human Adipose-Derived Stem Cells in Response to Direct-Current Electrical Stimulation. *Annual International Conference of the IEEE Engineering in Medicine and Biology Society. IEEE Engineering in Medicine and Biology Society*. 2009: 6517-21.
29. Shiyun Meng, Mahmoud Rouabhia and Ze Zhang (2011). Electrical Stimulation in Tissue Regeneration, Applied Biomedical Engineering, Dr. Gaetano Gargiulo (Ed.), ISBN: 978-953-307-256-2, InTech, Available from: <http://www.intechopen.com/books/applied-biomedical-engineering/electrical-stimulation-in-tissueregeneration>
30. S.K. Mazloomi, N. Sulaiman, Influencing factors of water electrolysis electrical efficiency. *Renewable and Sustainable Energy Reviews*. 2012, 16(6), 4257–4263.
31. A. Kassim, C. Rice, A. Kuhn. (1981) Formation of sorbitol by cathodic reduction of glucose, *Journal of Applied Electrochemistry*. 1981, 11, 261–267.
32. M. Pasta, F. Mantia, Y. Cui, Mechanism of glucose electrochemical oxidation on gold surface. *Electrochimica Acta*. 2010, 55(20), 5561–5568.

33. H. G. de Wilt, Part I. Oxidation of Glucose to Gluconic Acid. Survey of Techniques. *Industrial & Engineering Chemistry Product Research and Development*. 1972, 11 (4): 370-373.
34. H. G. de Wilt, and H. S. van der Baan, Part II. Oxidation of Glucose to K-Gluconate. Platinum-Catalyzed Oxidation with Oxygen in Aqueous Alkaline Solutions. *Industrial & Engineering Chemistry Product Research and Development*. 1972, 11 (4): 374-378.
35. M. Stecker, T. Patterson, and B. Netherton; Mechanisms of Electrode Induced Injury. Part 1: Theory. *American Journal of Electroneurodiagnostic Technology*. 2006, 46, no. 4.
36. G. Koh, M. Soonpaa, M. Klug, L. Field; Strategies for Myocardial Repair. *Journal of Interventional Cardiology*. (1995) 8, 387-393.
37. T. Eschenhagen, A. Eder, I. Vollert, A. Hansen, Physiological aspects of cardiac tissue engineering. *American Journal of Physiology. Heart and Circulatory Physiology*. 2012, 303(2), 133–143.
38. D.A Dunn, A.J. Hodge, E.A. Lipke. Biomimetic materials design for cardiac tissue regeneration. *Wiley Interdiscip Rev Nanomed Nanobiotechnol*. 2014, 6(1):15-39.
39. T. Eschenhagen, M. Didie', J. Heubach, U. Ravens, W-H Zimmermann, Cardiac tissue engineering. *Transplant Immunology*. 2002, 9(2-4), 315–321.
40. K. Tobita, L. Liu, A. Janczewski, J. Tinney, J. Nonemaker, S. Augustine, D. Stolz, S. Shroff, B. Keller, Engineered early embryonic cardiac tissue retains proliferative and contractile properties of developing embryonic myocardium. *American Journal of Physiology: Heart & Circulatory Physiology*. 2006, 60(4).
41. W.J. de Lange, L.F. Hegge, A.C. Grimes, C.W. Tong, T.M. Brost, R.L. Moss, J.C. Ralphe. Neonatal mouse-derived engineered cardiac tissue: a novel model system for studying genetic heart disease. *Circ Res*. 2011, 109(1):8-19.
42. S. Schaaf, A. Shibamiya, M. Mewe, A. Eder, A. Stöhr, M.N. Hirt, T. Rau, W.H. Zimmermann, L. Conradi, T. Eschenhagen, A. Hansen. Human engineered heart tissue as a versatile tool in basic research and preclinical toxicology. *PLoS One*. 2011, 6(10):e26397.
43. L. Chiu, M. Radisic, Cardiac tissue engineering, *Current Opinion in Chemical Engineering*. 2013, 2(1), 41–52.
44. I.C. Turnbull, I. Karakikes, G.W. Serrao, P. Backeris, J.j. Lee, C. Xie, G. Senyei, R.E. Gordon, R.A. Li, F.G Akar, R.J Hajjar, J.S. Hulot, K.D. Costa. Advancing

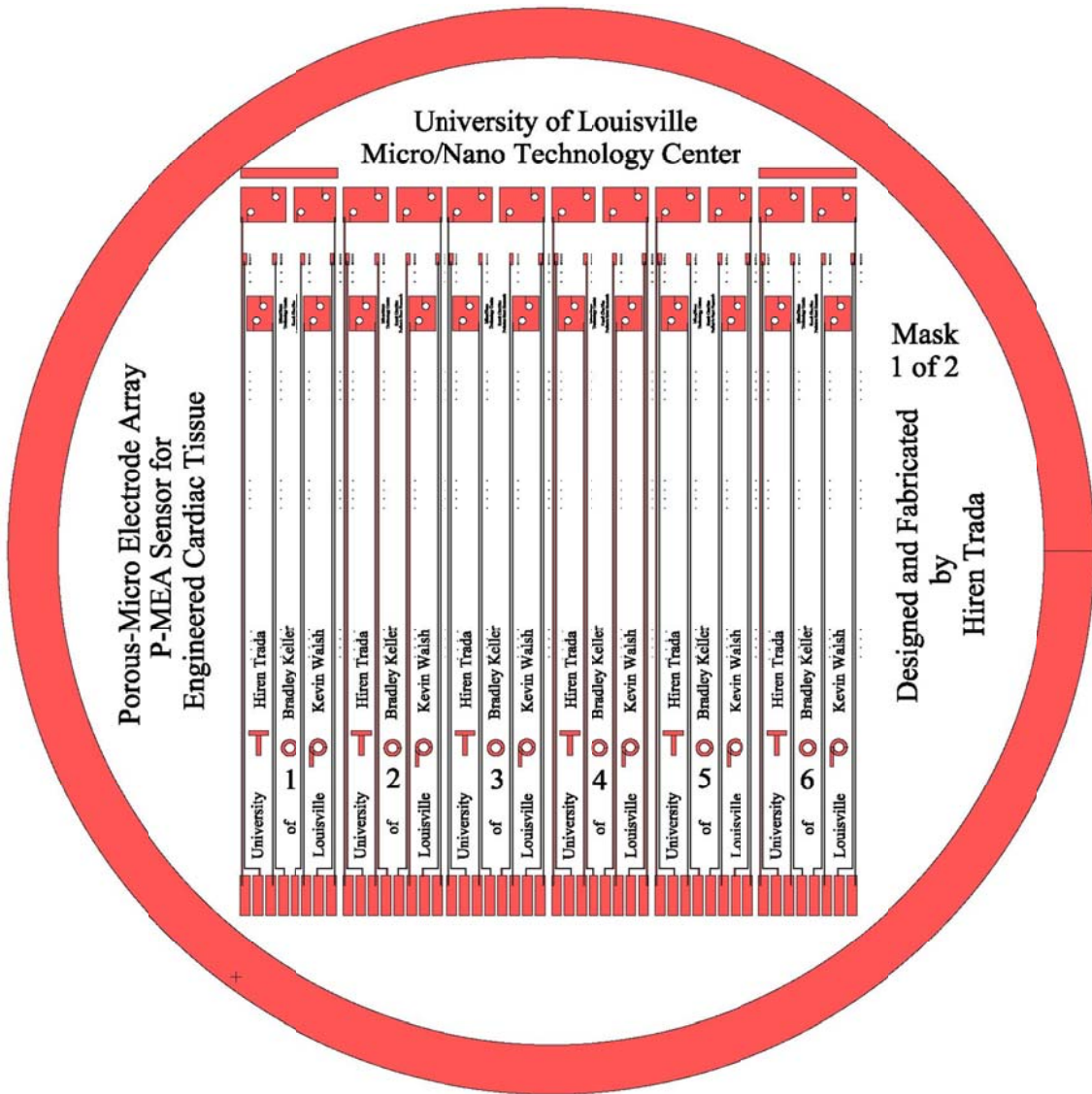
functional engineered cardiac tissues toward a preclinical model of human myocardium. *FASEB J.* 2014, 28(2):644-54.

45. T.C. McDevitt, K.A. Woodhouse, S.D. Hauschka, C.E. Murry, P.S. Stayton. Spatially organized layers of cardiomyocytes on biodegradable polyurethane films for myocardial repair. *J Biomed Mater Res A.* 2003, 66(3):586-95.
46. K.R. Stevens, L. Pabon, V. Muskheli, C.E. Murry. Scaffold-free human cardiac tissue patch created from embryonic stem cells. *Tissue Eng Part A.* 2009, 15(6):1211-22.
47. X. Guo, C. Wang, X. Tian, and X. Yang, Engineering cardiac tissue from embryonic stem cells. *Methods in Enzymology.* 2006, 420: 316-38.
48. L. Chiu, R. Iyer, L. Reis, S. Nunes, M. Radisic, Cardiac tissue engineering: Current state and perspectives. *Front. Biosci. Frontiers in Bioscience.* 2012, 17(4), 1533–1550.
49. K.L.Fujimoto, K.C. Clause, L.J., Liu, J.P. Tinney, S. Verma, W.R. Wagner, B.B. Keller, K. Tobita. Engineered fetal cardiac graft preserves its cardiomyocyte proliferation within postinfarcted myocardium and sustains cardiac function. *Tissue Eng Part A.* 2011, 17(5-6):585-96.
50. K.L. Kreutziger, V. Muskheli, P. Johnson, K. Braun, T.N. Wight, C.E. Murry. Developing vasculature and stroma in engineered human myocardium. *Tissue Eng Part A.* 2011, 17(9-10):1219-28.
51. S. Leontyev, F. Schlegel, C. Spath, R. Schmiedel, M. Nichtitz, A. Boldt, R. Rübsamen, A. Salameh, M. Kostelka, F.W. Mohr, S. Dhein, Transplantation of engineered heart tissue as a biological cardiac assist device for treatment of dilated cardiomyopathy. *Eur J Heart Fail.* 2013, 15(1):23-35.
52. B.B. Keller, L.J. Liu, J.P. Tinney, K. Tobita. Cardiovascular developmental insights from embryos. *Ann N Y Acad Sci.* 2007, 1101:377-88.
53. K. Clause, J. Tinney, L. Liu, B. Keller, K. Tobita, Engineered early embryonic cardiac tissue increases cardiomyocyte proliferation by cyclic mechanical stretch via p38-MAP kinase phosphorylation. *Tissue Eng. Part A Tissue Engineering - Part A.* 2009, 15(6), 1373–1380.
54. L. Chiu, R. Iyer, J-P King, M. Radisic, Biphasic electrical field stimulation aids in tissue engineering of multicell-type cardiac organoids. *Tissue Engineering. Part A.* 2011, 17(11-12), 1465–77.
55. N. Tandon, C. Cannizzaro, P-H Chao, R. Maidhof, A. Marsano, H. Au, M. Radisic, G. Vunjak-Novakovic, Electrical stimulation systems for cardiac tissue engineering. *Nature Protocols.* 2009, 4(2), 155–173.

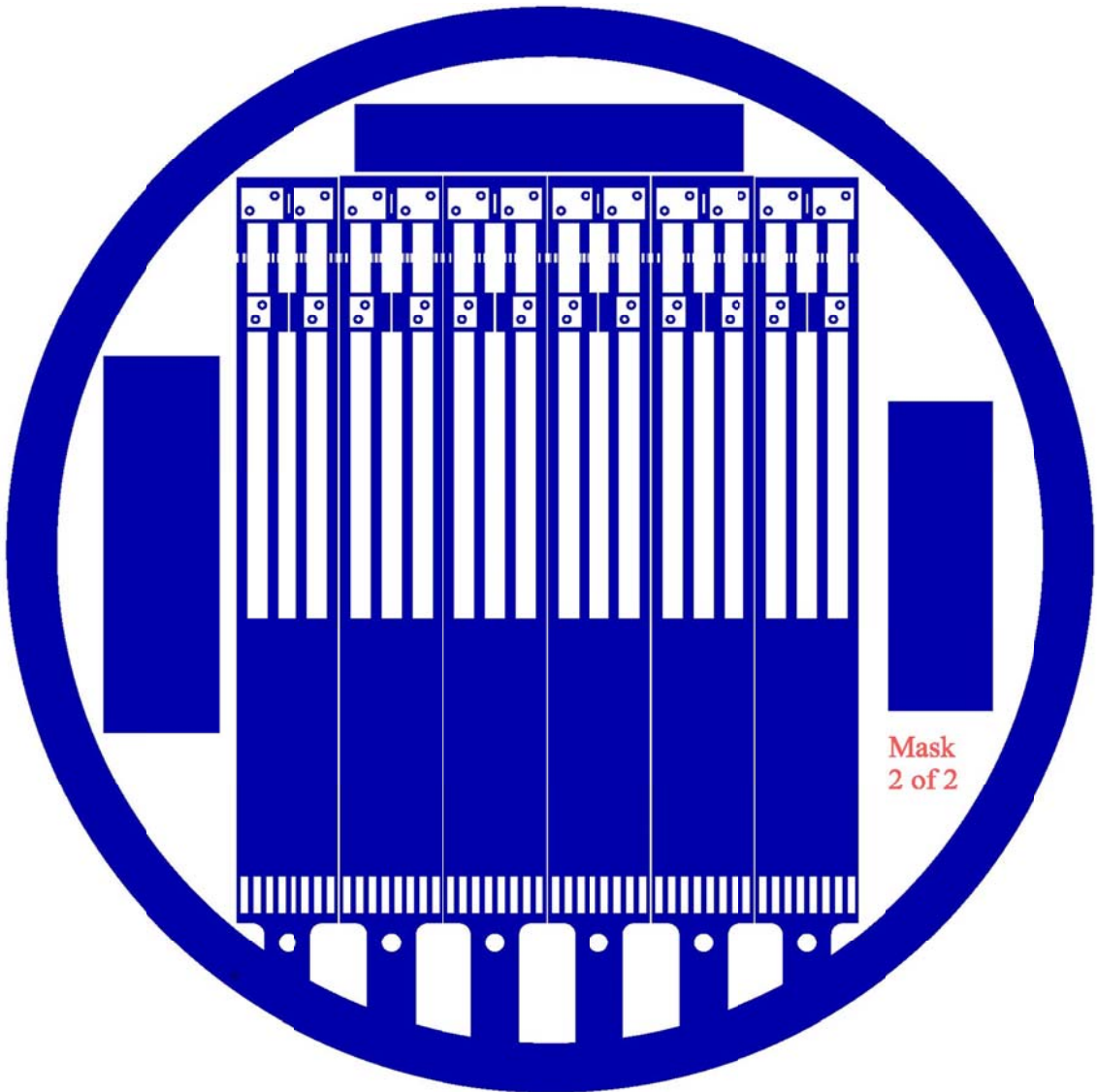
56. C. Cannizzaro, N. Tandon, E. Figallo, H. Park, S. Gerecht, M. Radisic, G. Vunjak-Novakovic, Practical aspects of cardiac tissue engineering with electrical stimulation. *Methods in Molecular Medicine*. 2007
57. N. Tandon, C. Cannizzaro, E. Figallo, J. Voldman, G. Vunjak-Novakovic, Characterization of electrical stimulation electrodes for cardiac tissue engineering. *Conf Proc IEEE Eng Med Biol Soc*. 2006, 1, 845–848.
58. S.K. Mazloomi, N. Sulaiman, Influencing factors of water electrolysis electrical efficiency. *Renewable and Sustainable Energy Reviews*. 2012, 16(6), 4257–4263.
59. A. Kassim, C. Rice, A. Kuhn. (1981) Formation of sorbitol by cathodic reduction of glucose, *Journal of Applied Electrochemistry*. 1981, 11, 261–267.
60. D. Merrill, M. Bikson, J. Jefferys, Electrical stimulation of excitable tissue: design of efficacious and safe protocols. *Journal of Neuroscience Methods*. 2005, 141(2), 171–98.
61. L. Geddes, Historical evolution of circuit models for the electrode-electrolyte interface. *Ann Biomed Eng Annals of Biomedical Engineering*. 1997, 25(1), 1–14.
62. E. McAdams, A. Lackermeier, J. Mclaughlin, D. Macken, The linear and non-linear electrical properties of the electrode-electrolyte interface, *Biosensors & Bioelectronics*. 1995, 10, 67–74.
63. E. Rouya, S. Cattarin, M. Reed, R. Kelly, G. Zangari, Electrochemical Characterization of the Surface Area of Nanoporous Gold Films. *Journal of The Electrochemical Society*. 2012, 159(4), K97.
64. B-Y. Chang, and S-M Park, Integrated Description of Electrode/Electrolyte Interfaces Based on Equivalent Circuits and Its Verification Using Impedance Measurements. *Analytical Chemistry*. 2006, 78, no. 4: 1052-60.
65. A. Norlin, J. Pan, & C. Leygraf, Investigation of Electrochemical Behavior of Stimulation/Sensing Materials for Pacemaker Electrode Applications I. Pt, Ti, and TiN Coated Electrodes. *Journal of the Electrochemical Society*. 2005, 152.2.
66. A. Norlin, J. Pan, & C. Leygraf, Investigation of Electrochemical Behavior of Stimulation/sensing Materials for Pacemaker Electrode Applications II. Conducting Oxide Electrodes." *Journal of the Electrochemical Society*. 2005, 152.7
67. A. Norlin, J. Pan, & C. Leygraf, Electrochemical Behavior of Stimulation/sensing Materials for Pacemaker Electrode Applications - Iii. Nanoporous and Smooth Carbon Electrodes." *Journal of the Electrochemical Society*. 2005, 152.9.

68. M. D. Ramos, Theoretical study of metal–polyimide interfacial properties. *Vacuum*, 2002, 64, 255-260.
69. H. Hieber, Aging Properties of Gold Layers with Different Adhesion Layers. *Thin Solid Films*. 37.3 (1976): 335-343.
70. E. Barsoukov, and J. Macdonald, *Impedance spectroscopy: Theory, Experiment, and Applications*. 2005
71. J. Scully, D. Silverman, and M. Kendig. *Electrochemical Impedance: Analysis and Interpretation*. Philadelphia: ASTM, 1993.
72. B-Y Chang, and S-M Park, Electrochemical impedance spectroscopy. *Annual Review of Analytical Chemistry*. 2010, 3: 207-29.
73. B. Ulgut, Basics of Electrochemical Impedance Spectroscopy, *Gamry Instruments*. <http://www.gamry.com/application-notes/basics-of-electrochemical-impedance-spectroscopy/>
74. G. Ruiz, and C. Felice, Non-linear Response of an Electrode-electrolyte Interface Impedance with the Frequency. *Chaos, Solitons & Fractals*. 2007, 31.2.
75. W. Franks, I. Schenker, P. Schmutz, & A. Hierlemann, Impedance Characterization and Modeling of Electrodes for Biomedical Applications. *Ieee Transactions on Biomedical Engineering*, 2005, 52, 7.
76. L. Burke, and P. Nugent, The Electrochemistry of Gold: I The redox behaviour of the metal in aqueous media". *Gold Bulletin*. 1997, 30 (2): 43-53.
77. L. Burke, and P. Nugent, The Electrochemistry of Gold: II The electrocatalytic behaviour of the metal in aqueous media. *Gold Bulletin World Gold Council*, 1998, 31 (2): 39-50.
78. T. Hambrecht, Functional Electrical Stimulation: An Overview. *Pacing and Clinical Electrophysiology*. 1989, 12 (5): 840-843.
79. K. Williams, K. Gupta, and M. Wasilik, Etch Rates for Micromachining Processing-Part II. *Journal of Microelectromechanical Systems*. 2003, 12 (6).
80. K. Kavanagh, H. Duff, R. Clark, K. Robinson, W. Giles, and D. Wyse. Monophasic versus Biphasic Cardiac Stimulation: Mechanism of Decreased Energy Requirements. *Pacing and Clinical Electrophysiology*. 1990, 13.10, 1268
81. X. Yang, L. Pabon, and C. Murry; Engineering Adolescence: Maturation of Human Pluripotent Stem Cell-Derived Cardiomyocytes, *Circulation Research*. 2014, 114 (3), 511-23.

APPENDIX



Mask 1 of P-MEA (version 3), (layout in L-Edit).



Mask 2 of P-MEA (version 3), (layout in L-Edit).

## CURRICULUM VITAE

Name: Hiren Vrajlal Trada

Address: Department of Electrical and Computer Engineering  
University of Louisville  
Louisville, Kentucky 40217

Education: Master of Science (M.S.), University of Louisville, Louisville, KY. 2004.  
Bachelor of Engineering (B.E.), University of Mumbai, India. 1999.  
Diploma of Engineering, Maharashtra State Board, India. 1996.

### Technical Expertise & Computer Skills:

- Semiconductor fabrication processes: Oxidation, DRIE, dry and wet silicon etching, lithography, photo-mask design and creation, and macro-micro interfacing (sensor-to-circuit board connections and wiring).
- Micro-level CAD modeling and simulation using CoventorWare (MEMCAD).
- Design layout using L-Edit & CoventorWare.
- Circuit Board (PCB) layout using CIRCAD.
- Computer maintenance & troubleshooting (hardware & software, PC & Mac).

### Awards, Honors & Activities

- ‘University Fellowship’ for Doctoral studies, UofL (Aug. 2003 – July 2007).
- ‘Who’s Who Among Students in American Universities & Colleges’, (nominated through) UofL (2007).
- ‘Certificate of Appreciation’ for ‘Outstanding Volunteerism & Community Service’, UofL (April 2006).
- ‘Champions for Children’, Jefferson County Public School District, Kentucky (May 2005).
- Volunteer Judge, Science Fair (Grades 6 & 8), Our Lady of Lourdes School, Louisville, KY (February 2006).
- Public Relations Officer (PRO) for the ‘Indian Student Association’, UofL (Jan. 2003 – Dec. 2003).
- Student Member of IEEE.

## Teaching Experience

- 20+ semesters of teaching experience for the Department of Electrical and Computer Engineering (ECE) at the University of Louisville (UofL).
- Teaching Assistant - ECE 544 – Introduction to Microfabrication & MEMS, UofL Aug. 2007 – April 2012  
Complete responsibility and charge of a graduate-level laboratory course in microfabrication & MEMS. Class meets in a state-of-the-art, class 100/1000 cleanroom at the University of Louisville. Students are provided with a hands-on cleanroom experience in various areas of microfabrication while fabricating a Silicon Piezoresistive Pressure Sensor.
- Instructor - ECE 252 – Introduction to Electrical Engineering (EE), UofL ‘May-to-July’ of 2008/10/11/12  
Undergraduate course for non-EE students. Work includes complete management of the class including course material, assignments, tests and examinations as well as guiding and managing the graders.
- Teaching Assistant - ECE 334 – Electronics-I & ECE 535 – Instrumentation Electronics. Jan. 2001 – Aug 2003  
Taught laboratory courses for eight semesters (at UofL). Work includes designing the experiments, grading assignments and providing students with hands-on experience in basic electronic circuits while co-ordinating with different instructors.

## Patents, Publications & Conferences

- *USPTO #61924408, Patent Pending (Jan. 2014):* Keller, B., Trada, H., Tinney, J., Walsh, K., and Jackson, D., “Porous Microelectrode Arrays Combined with Three-Dimensional Engineered Cardiac Tissue Constructs for Cardiac Repair and Regeneration”.
- Trada, H., Vendra, V., Tinney, J., Yuan, F., Jackson, D., Walsh, K., and Keller, B., “Implantable Thin-Film Porous-MicroElectrode Array Sensor (P-MEA-S) for Electrical Stimulation of Engineered Cardiac Tissues”. – (*Submitted, November 2014*).
- Trada, H., Tinney, J., Jackson, D., Walsh, K., Naber, J., and Keller, B., “Development of Porous MicroElectrode Array (P-MEA) for Electrical Stimulation and Pacing of Engineered Cardiac Tissue (ECT)”, *Fifth Annual Nanotechnology and Nanomedicine Symposium 2012*.
- Trada, H., Walsh, K., and Cambron, S., “Silicon Micro-Needle Arrays for Cardiomyopathy”, *UGIM 2008*.
- Trada, H., Walsh, K., Cambron, S., and Isham, A., “Out-of-plane Micro-Needle Arrays using Silicon Micromachining”, Abstract, *IEEE SoutheastCon 2007*.